



CHALMERS



Heavy Vehicle Braking using Friction Estimation for Controller Optimization

Master's thesis in Applied Mechanics

BERNHARD WESTERHOF
DIMITRIOS KALAKOS

MASTER'S THESIS IN APPLIED MECHANICS

Heavy Vehicle Braking using Friction Estimation for Controller Optimization

BERNHARD WESTERHOF
DIMITRIOS KALAKOS

Department of Applied Mechanics
Division of Vehicle Engineering and Autonomous Systems, Vehicle Dynamics group
CHALMERS UNIVERSITY OF TECHNOLOGY

Göteborg, Sweden 2017

Heavy Vehicle Braking using Friction Estimation for Controller Optimization
BERNHARD WESTERHOF
DIMITRIOS KALAKOS

© BERNHARD WESTERHOF , DIMITRIOS KALAKOS, 2017

Master's thesis 2017:69
ISSN 1652-8557
Department of Applied Mechanics
Division of Vehicle Engineering and Autonomous Systems, Vehicle Dynamics group
Chalmers University of Technology
SE-412 96 Göteborg
Sweden
Telephone: +46 (0)31-772 1000

Supervisor: Leon Henderson, Chalmers and Volvo GTT
Examiner: Bengt Jacobsson

Cover:
Volvo FMX 8x4 Tridem

Chalmers Reproservice
Göteborg, Sweden 2017

Heavy Vehicle Braking using Friction Estimation for Controller Optimization

Master's thesis in Applied Mechanics

BERNHARD WESTERHOF

DIMITRIOS KALAKOS

Department of Applied Mechanics

Division of Vehicle Engineering and Autonomous Systems, Vehicle Dynamics group

Chalmers University of Technology

ABSTRACT

In this thesis project, brake performance of heavy vehicles is improved by the development of new wheel-based functions for a longitudinal slip control braking system using novel Fast Acting Braking Valves (FABVs). To achieve this goal, Volvo Trucks' vehicle dynamics model has been extended to incorporate the FABV system. After validating the updated model with experimental data, a slip-slope based recursive least squares friction estimation algorithm has been implemented. Using information about the tire-road friction coefficient, the sliding mode slip controller has been made adaptive to different road surfaces by implementing a friction-dependent reference slip signal and switching gain for the sliding mode controller. This switching gain is further optimized by means of a novel on-line optimization algorithm. Simulations show that the on-line friction estimation converges close to the reference friction level within one second for hard braking. Furthermore, using this information for the optimized controller has resulted in reduction of braking distance on most road surfaces of up to 20 percent, as well as in most cases a reduction in air usage.

Keywords: Heavy Vehicles, Emergency Braking, Friction Estimation, Controller Optimization, Vehicle Validation, Slip Control Braking, Vehicle Testing

PREFACE

This thesis has been written by Dimitrios Kalakos from Kungliga Tekniska Högskolan (KTH) and Bernhard Westerhof from the Delft University of Technology (TU Delft), who is also registered for thesis work at Chalmers University of Technology via Erasmus. Supervision has been from KTH, Chalmers University of Technology and Volvo Group Trucks Technology (GTT). Volvo GTT has provided working places in the Braking & Suspension Control Systems department for the fulfillment of this thesis work.



CHALMERS
UNIVERSITY OF TECHNOLOGY




TU Delft

VOLVO

Volvo Group Trucks Technology

ACKNOWLEDGEMENTS

First and foremost the authors would like to thank Leon Henderson at Volvo Trucks for the great care he took in guiding us through the thesis work. With Leon's help, progress has been fast and the work was carried out with great efficiency, as he helped us with difficult decisions without delay. Furthermore, Leon's extensive knowledge about slip control methods has helped us understanding the finesses of the project.

Bengt Jacobson has proven invaluable with respect to vehicle dynamics and the academic quality of the work. Whenever Bengt was around, he would not hesitate helping the us out. Bengt has the quality of making time for students and we enjoyed that very much.

Mikael Nybacka's supervision and contribution from KTH kept us on the right academic path during the whole thesis project. His guidance and support helped us to meet successfully the expectations of the project.

We would furthermore like to thank Mats Sabelström for the introduction he gave us to braking systems on trucks and introducing us to Heavy Vehicles. Especially driving with Mats in an actual truck was an unforgettable experience.

Leo Laine has also helped a lot, getting us in touch with other thesis workers and arranging the presentations between the thesis workers, where Leo's advice was really beneficial. During the trip to the Volvo Museum, he was both an interesting and hilarious guide.

Also, we would like to thank Sachin Janardhanan for the help he gave us regarding the VTM and introducing us to the VTM. The same holds for Karthik Ramanan who has given us some great tips about VTM in the beginning of the thesis project.

Next to that, we would like to thank the other thesis workers at Volvo Trucks for giving new insights and spending some nice nights at Kings Head discussing work over a beer. Special mention goes out to Wouter van Unen, Martin Calleberg, Linus Hagvall and Patrick Volz.

NOMENCLATURE

List of Symbols

Symbol	Unit	Description
A	$[-]$	Slip slope proportionality constant
A_v	$[m^3]$	Cross-sectional area of the valve orifice
C	$[-]$	Slip slope bias constant
C_0	$[N]$	Longitudinal tire stiffness at zero slip
C_f	$[-]$	Valve discharge coefficient
C_s	$[N]$	Slip stiffness
F_x	$[N]$	Longitudinal force
F_z	$[N]$	Normal force or load
J_w	$[kgm^2]$	Wheel moment of inertia
K	$[-]$	Slip slope
K_{BR}	$[m^3]$	Brake gain
L_x	$[-]$	Fraction of the contact patch which is not sliding
P_c	$[Pa]$	Brake chamber pressure
P_d	$[Pa]$	Downstream pressure
P_{dem}	$[Pa]$	Pressure demand
P_{SMC}	$[Pa]$	Sliding mode controller pressure demand
P_{sup}	$[Pa]$	Supply pressure
P_u	$[Pa]$	Upstream pressure
R	$[Jkg^{-1}K^{-1}]$	Specific gas constant of air
R_{MS}	$[-]$	Mark-space ratio
R_r	$[m]$	Wheel rolling radius
S_v	$[-]$	Valve state
T	$[Nm]$	Torque
T_b	$[Nm]$	Braking torque
T_c	$[K]$	Temperature of the brake chamber
V_c	$[m^3]$	Volume of the brake chamber
V_f	$[-]$	Tyre model shaping factor
a_x	$[m/s^2]$	Longitudinal acceleration
c_{pl}	$[N/m^2]$	Longitudinal bristle stiffness per unit length
d_m	$[m/s^2]$	Mean fully developed deceleration
k_{press}	$[Pa^{-1}]$	Pressure controller proportional gain
k_s	$[Pa]$	Sliding mode controller switching gain
m	$[kg]$	Vehicle mass
\dot{m}_v	$[kg/s]$	Mass flow rate through the valve plant
m_s	$[kg]$	Sprung vehicle mass of the quarter car
m_u	$[kg]$	Unsprung vehicle mass of the quarter car
p_{cr}	$[-]$	Critical pressure ratio
r	$[m]$	Wheel radius
r_b	$[m]$	Wheel radius through which the braking force acts
s_c	$[m]$	Corrected braking distance
s_s	$[-]$	Sliding mode controller switching surface
s_x	$[-]$	Longitudinal wheel slip during acceleration
t	$[s]$	Time
u	$[m]$	Displacement
u_r	$[m/s]$	Relative moving velocity
v_x	$[m/s]$	Longitudinal vehicle velocity
z	$[m]$	Average deflection of the asperities
γ	$[-]$	Ratio of specific heats
δ_d	$[-]$	Hysteresis shape parameter

δ_s	$[-]$	Sliding mode controller switching surface boundary layer thickness
λ	$[-]$	Longitudinal wheel slip, Forgetting factor
λ_{ref}	$[-]$	Reference longitudinal wheel slip
μ	$[-]$	Friction coefficient
μ_0	$[-]$	Coefficient of static friction
μ_f	$[-]$	Coefficient of sliding friction
ρ	N	Normalized force
σ_0	$[N/m]$	Initial stiffness of the contact patch at velocity reversal
σ_1	$[Nm/s]$	Damping coefficient
σ_2	$[Nm/s]$	Coefficient for viscous friction
ω	$[rad/s]$	Wheel rotational velocity
Φ_s	$[Pa]$	Sliding mode controller proportional gain

List of Abbreviations

ABS	Anti-Lock Braking System
CAN	Controller Area Network
CoG	Center of Gravity
EBS	Electronic Brake System
ECU	Electronic Control Unit
EWB	Electronic Wedge Brake
FABV	Fast Actuating Braking Valve
HGV	Heavy Goods Vehicle
HV	Heavy Vehicle
HiL	Hardware in the Loop
LH	Left Hand side
MFDD	Mean Fully Developed Deceleration
PWM	Pulse Width Modulation
RH	Right Hand side
RLS	Recursive Least Squares
SMC	Sliding Mode Controller
UKF	Unscented Kalman Filter
VTM	Volvo Transportation Models

CONTENTS

Abstract	i
Preface	iii
Acknowledgements	iv
Nomenclature	v
Contents	vii
1 Introduction	1
1.1 Project Background	1
1.2 Motivations	1
1.3 Envisioned Solution	2
1.4 Objectives	2
1.5 Deliverables	2
1.6 Limitations	2
1.7 Approach	2
2 Literature Review and Background	4
2.1 Physics of Braking	4
2.2 Brake System Configurations for Heavy Vehicles	5
2.2.1 Advanced Braking Control Systems	8
2.2.2 Alternative Advanced Braking Control Systems	9
2.2.3 Advanced Brake Actuators on Heavy Vehicles	11
2.3 Tire modeling	12
2.3.1 Pacejka Tire Model (Magic Formula)	13
2.3.2 Brush Tire Model	13
2.3.3 Fancher Tire Model	15
2.3.4 Dahl Tire Model	15
2.3.5 LuGre Tire Model	15
2.4 Friction Estimation	16
2.5 Optimization Techniques	17
2.6 Validation	18
3 Volvo Transportation Model Integration and Validation	19
3.1 Quarter Car Model	19
3.1.1 Slip and Slip Error Calculation	20
3.1.2 Force Observer	20
3.1.3 Sliding Mode Controller	20
3.1.4 Pressure Controller	20
3.1.5 Valve and Brake Chamber Plant	21
3.2 Volvo Transportation Models	21
3.2.1 Vehicle Plant	22
3.2.2 Controllers and Actuators	22
3.3 Integration	23
3.3.1 Local Brake Controller	23
3.3.2 Parameter Changes	24
3.4 Validation	25
3.4.1 Partial Validation	25
3.4.2 Complete Model Validation Results	29
3.4.3 Discussion	47
3.5 Conclusions	48

4	Function Development	49
4.1	Online Friction Estimation	49
4.1.1	Method	49
4.1.2	Recursive Least-Squares (RLS) Identification	51
4.1.3	Parameter Initialization and Conditions for the RLS algorithms	53
4.1.4	Input and Output Signals of the Friction Estimator	54
4.2	Slip Controller Optimization	55
4.2.1	Reference Slip	55
4.2.2	Switching Gain	55
4.3	Updated Local Brake Controller	57
5	Results	59
5.1	Friction Estimator Testing	59
5.1.1	Testing Results	59
5.1.2	Discussion - Conclusion	62
5.2	Friction Estimation Model Integration	62
5.2.1	Surface with Constant Friction Level	63
5.2.2	Surface with Variable Friction Level	68
5.3	Gain optimization with friction estimation	72
5.4	Optimized System Results	73
6	Discussion	76
7	Conclusion	77
8	Future Work	78
	References	79
A	Vehicle Parameters	83
B	Model Modifications	83
C	Parameter Changes	83
D	Friction Estimation	83
E	Vehicle Testing Addendum	87
E.1	Results	88
E.2	Discussion and Conclusion	93

1 Introduction

1.1 Project Background

Heavy vehicles (such as trucks and buses) operate an electronically controlled, pneumatically actuated braking system. This type of system is commonly known as an electronic brake system (EBS). Recent work by Cambridge University has resulted in the development of a novel fast-acting EBS that enables stopping distances to be reduced by up to 17% in low friction conditions. Vehicle demonstrations of the prototype Fast-Acting Brake Valve (FABV) system were shown on the BBC [74]. The novel brake valve installation and the test vehicle (featured in the BBC footage) are shown in the following two figures.

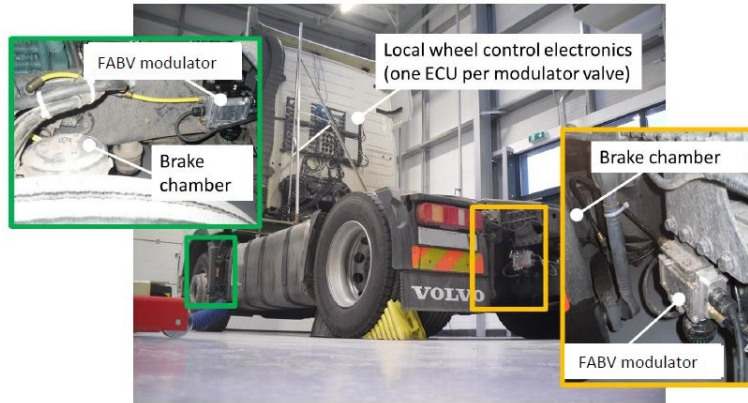


Figure 1.1: *Fast-acting brake valve (FABV) modulators installed on a Volvo FH12 tractor unit for vehicle testing*



Figure 1.2: *Test vehicle (fitted with FABVs) carrying out brake-in-turn test on wet basalt surface.*

Following on from this work, a next generation version of the FABV system has now been developed. Winter testing of this new system in extreme braking manoeuvres was carried out in the winter of 2016/2017.

1.2 Motivations

A slip controller has been developed utilizing the control bandwidth of the FABVS that is able to accurately track longitudinal wheel slip demands during extreme braking manoeuvres which improves greatly on braking performance of conventional heavy vehicle brakes. The local Electronic Control Units (ECUs), included with the new FABV design, have additional computing capacity that can be used to carry out other wheel-based braking functions. These are expected to include: tyre-road friction coefficient estimation, brake torque control, brake gain estimation and brake capability estimation. It is hoped that some of these functionalities can be designed and tuned in simulation before being implemented on the available test vehicles. In order to carry out

the above model based development, an accurate vehicle model including tyre and brake actuator dynamics need to be developed and validated against test data gathered during winter testing.

1.3 Envisioned Solution

To start, the abovementioned slip controller is to be implemented in Volvo Truck's existing vehicle models using MATLAB and Simulink. The test data gathered using the truck with the FABV during the 2016/2017 winter tests will be used to evaluate the truck model with the slip controller. Final validation will be done using straight line braking and brake-in-turn braking maneuvers. The validated vehicle model will be used to design novel wheel control systems to improve the active safety of the vehicle. More specifically, a friction estimation algorithm will be developed. With information about tire-road friction, both the slip controller and complete vehicle control algorithms can be further improved.

1.4 Objectives

The project objectives are:

- Incorporate the FABV brake actuator and its slip controller in the existing Volvo Truck models and validate this against test data of both straight-line braking and brake in-turn maneuvers
- Further development of wheel based control algorithms (and required estimation routines) in MATLAB and Simulink to improve the braking performance of heavy vehicles, potentially incorporating other vehicle actuators (e.g. steering) for driving scenarios with varying tyre-road friction.
- Design and/or develop friction estimation algorithms for wheel based application.

1.5 Deliverables

The project deliverables include:

- A validated MATLAB Simulink model of a heavy vehicle applicable for both straight-line braking and brake-in-turn maneuvers.
- Local brake control algorithms (implemented in Simulink) to improve the braking performance of heavy vehicle in extreme conditions, supplementing the existing slip control routines developed by Cambridge University.
- A friction estimation algorithm applicable for wheel based brake performance optimization.

1.6 Limitations

The truck used in this thesis project is the Volvo 8x4 FMX Tridem with a tag axle. The development of the wheel-based functions will be limited to this truck only, but the slip control architecture should be compatible with different truck configurations. For the validation, only straight-line braking and brake-in-turn maneuvers will be evaluated. More experiments could be devised in order to validate the truck behavior even further, especially for the lateral dynamics. To control the wheel slip, the sliding mode controller will be used and developed further, but no other control methods for will be investigated. The friction estimation will be limited to longitudinal friction estimation.

1.7 Approach

To achieve the objectives and obtain the deliverables, the following approach is followed. At first, extensive knowledge about all facets of the project has to be obtained. That includes, but is not limited to, braking physics and braking on heavy goods vehicles, tire modeling, friction estimation, optimization and vehicle model validation. An extensive literature review on these subjects is presented in chapter 2.

The next step is the incorporation of the FABV slip controller into the Volvo Trucks models. In chapter 3, it is described in detail what the models consist of and how integration of both models has been performed. Furthermore, the results of winter test data are compared to that of the new vehicle model with the incorporated FABV slip controller serving the purpose of model validation.

With a validated vehicle model, utilizing the FABV slip controller, vehicle wide function development can be commenced. Chapter 4 shows how an on-line friction estimation algorithm is developed and how the slip controller is optimized in order to improve vehicle safety and performance.

As a final contribution to this report, appendix E describes how the friction estimation algorithm with the adaptive reference slip was adapted for use on the real truck. Also, the performance of the friction estimation algorithm is shown.

2 Literature Review and Background

Commercial vehicles transport goods and passengers all over the world and they are essential to our way of living. In 2014, it has been estimated that approximately 330 million commercial vehicles had been in use worldwide [61]. Usage of trucks is also still increasing, according to the Bureau of Transportation Statistics (U.S.). More specifically, a total of 13,955 tonnes of goods has been transported in 2013 in the U.S., which is an increase of 10 percent with respect to 2007, and it contributes to roughly 70 percent of all transported goods by trucks, rail, water and other means of transportation [60]. In 2014, large trucks accounted for 8 percent of the vehicles being involved in fatal crashes in the U.S., while they only accounted for 2.7 percent of the total number of vehicles [59, 61].

It is suggested that the difference in fatal crashes is caused by the difference in size between large trucks and passenger vehicles, putting passenger vehicle occupants at higher risk, when involved in a crash with a large truck [37]. The fact that heavy vehicles are overrepresented in crashes might be explained by their poorer braking performance, compared to passenger vehicles, although it is difficult to prove direct causality [28]. The usage of Anti-lock Braking Systems (ABS), Electronic Braking Systems (EBS) and disc brakes improved significantly the braking behaviour of heavy vehicles. However, the braking distances of heavy vehicles are still higher than the corresponding ones of the passenger vehicles [18], [25]. This problem can be addressed by using faster braking actuators than the ones used in today's heavy vehicle configurations. Using these fast actuators it is possible to confine the slip of the wheels within the vicinity of the optimal point, and therefore, better results can be achieved in terms of braking performance, whether the heavy vehicle is performing straight-line braking or brake-in-turn maneuvers [51]. Furthermore, improved braking performance with fast actuating braking valves (FABV)s leads not only to the increased active safety of heavy vehicles, but also to their reduced air consumption which in turn could lead to reduced tank sizes and easier packaging on the vehicle. Hence, it is important that research will still be going on this particular domain, in order for the development of safer heavy vehicles to be sustainable.

2.1 Physics of Braking

By applying brakes, a torque is applied at the wheel, where the tire creates a friction force with the road. At the contact patch of the tire with the road, a relative speed difference exists, known as slip. The slip λ for braking in longitudinal direction is defined as the ratio of the difference between the longitudinal vehicle speed v_x and the local tire speed ωr at the contact patch, calculated using the rotational velocity ω and the radius of the tire r in longitudinal direction

$$\lambda = \frac{v_x - \omega r}{v_x}. \quad (2.1)$$

Figure 2.1 shows a representation of the different slip-friction curves for different road surfaces [40].

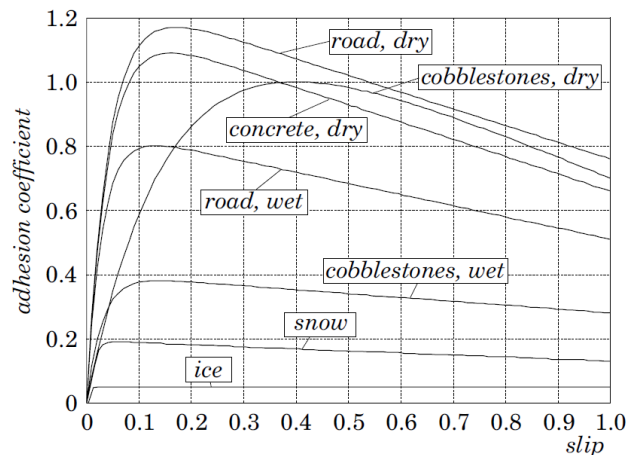


Figure 2.1: Slip-friction curves for different road surfaces for passenger vehicles [40].

According to figure 2.1, the utilized friction coefficient μ is given by

$$\mu_{util} = \frac{F_x}{F_z}, \quad (2.2)$$

where F_x is the longitudinal force and F_z is the normal force. μ which differs for different road surfaces, but more importantly, it differs for different values of slip. For example, the maximum friction coefficient is obtained for slip at an icy road of $\lambda = 0.05$ and on a dry road of $\lambda = 0.15$. For optimal braking performance, it can thus be concluded that the brakes should be actuated such that the wheel slip is as close to its optimum value, as possible. To increase the braking performance of vehicles, Anti-lock Braking Systems (ABS) have been developed over the years. One of the first mentions of this kind of system dates back to 1908, where J.E. Francis introduced a ‘Slip Prevention Regulator for Rail Vehicles’, but the first widely used mechanical ABS came about in the early 1950’s [44]. What ABS tries to achieve is to avoid locking the wheels during hard braking maneuvers.

During the braking process, a truck can be modeled as a point mass, following Newton’s second law of motion

$$\sum F_x = ma_x, \quad (2.3)$$

where F_x are all the forces acting on the vehicle in longitudinal direction, m is the mass of the vehicle and a_x is the acceleration or deceleration of the vehicle. The forces, acting on the vehicle, can be created by braking or accelerating, where the torque on the tire gets transferred to the road through the contact patch. The normal force on each wheel and the friction of each wheel determine the maximum amount of torque that can be transferred. The dynamics of one wheel can be depicted by

$$J_w \dot{\omega} - r_b F_x + T = 0, \quad (2.4)$$

where J_w is the inertia of the wheel, $\dot{\omega}$ is the rotational acceleration of the wheel, r_b is the radius of the wheel, and T is the torque applied on the wheel. Note that other resistances are neglected, but add to the braking force.

2.2 Brake System Configurations for Heavy Vehicles

Heavy Vehicle (HV) braking systems differ significantly from those used on passenger cars and other light vehicles. One important difference between these systems is the working fluid used to provide braking force; HVs typically use compressed air, whereas light vehicles use hydraulic fluid [51].

There are several reasons explaining why the air is preferred as working fluid in heavy vehicle configurations. More specifically, considerably high quantities of hydraulic fluid would be required during braking, as a result of the high number of axles in HVs. Another important reason is that a system, using air as working fluid, presents some fault-tolerant behavior since, in case of a possible leakage, it will still be able to respond to the system’s requirements with a slightly degraded performance, before its complete failure. The aforementioned reason increases significantly the active safety of HVs. In addition, another important reason is that air can be used to operate other auxiliary systems of HVs, like the suspension, but also the trailer which is easily coupled with a pneumatic connection. Furthermore, air is environmentally friendly, since it has unlimited availability and its usage does not cause any kind of environmental pollution [32], [58]. The only drawback of using air, instead of hydraulic fluid, when it comes to the braking systems of HVs, is that the response time of pneumatic systems is significantly higher than that of a hydraulic system.

When it comes to the operation of braking systems on HVs, air is compressed and it remains stored in a tank of the main tractor. When the driver uses the brake pedal, and more specifically, the treadle valve which is directly connected with the brake pedal, air is distributed from the tank to the brake chambers in order for the braking process to be initiated [51]. The simple braking system configuration of a HV can be seen in figure 2.2.

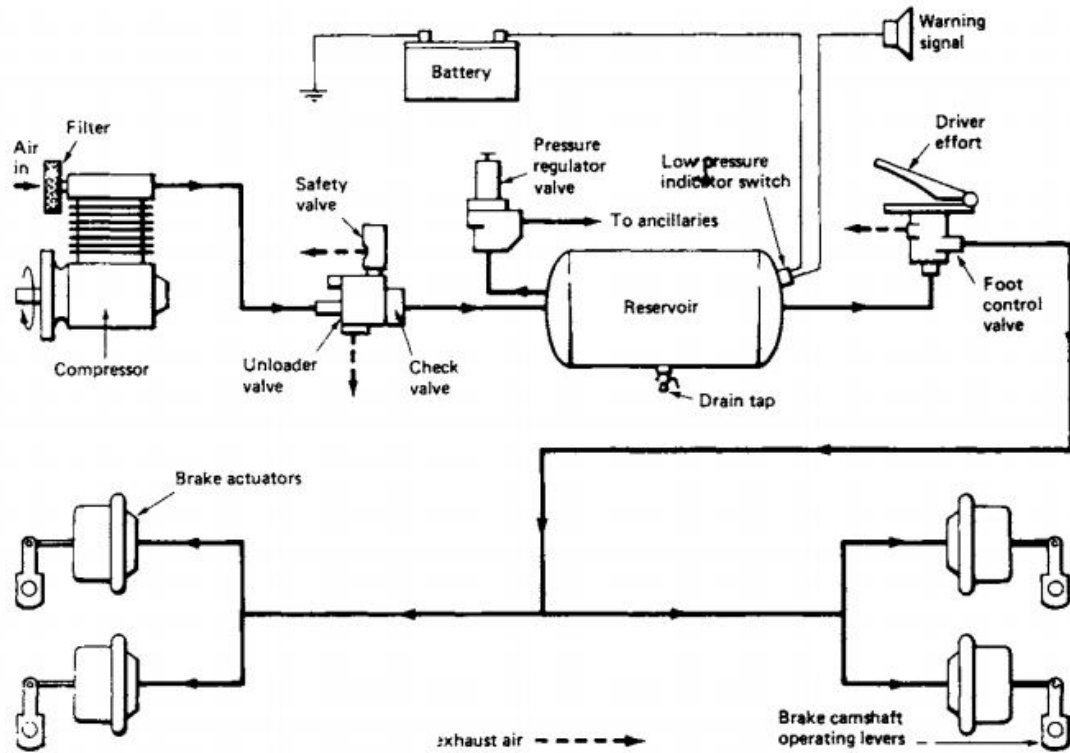


Figure 2.2: Schematic of a basic single-circuit air brake system of an HGV [58]

The brake chambers are equipped with actuators that convert the air pressure, coming from the treadle valve to braking torque, applied on the wheels. More specifically, the high-pressure air, coming from the tank via the treadle valve, pushes a piston and a mechanical advantage is created as a result of the piston's cross sectional area. A bigger mechanical advantage is also created afterwards, as a result of the push rod's motion that is caused by the piston's motion. Then, a lever, which is attached to this specific push rod, presses the friction material against the brake disc or drum. There are two areas inside the brake chamber which are separated by a flexible diaphragm. One area has a very high pressure and the other one has low pressure. When the pressure inside the chamber is low, a return spring resets the brake chamber. Furthermore, brake chambers of HVs are also installed with spring brakes, which apply a braking force, when there is no pressure in the system (for example when the vehicle is parked), or when the pressure in the system is low [51]. A service brake and spring brake assembly of an HV is illustrated in Figure 2.3 with the parking brake and service brake released.

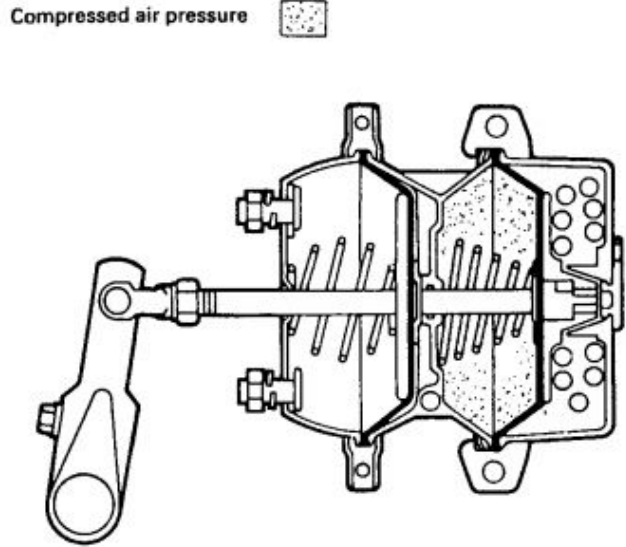


Figure 2.3: *Schematic of a spring brake chamber (Seddon Atkinson) [58]*

Actuators that are mainly used on HVs are either disc brakes or 'S-cam' drum brakes [32]. There are several advantages by using disc brakes on HVs. For example, disc brakes are more resistant to brake fade and have better cooling capabilities, as a result of their superior structural characteristics. They are also more convenient when it comes to their maintenance and their brake torque is proportional to the pedal force. The major disadvantage of disc brakes is that they require large application force, which can be quite high, especially on HVs. On the other hand, drum brakes require low application force, since they can provide large brake factors, due to their self-amplification. However, drum brakes present hysteresis problems [19]. Hence, it is obvious that there are substantial reasons, why disc brakes are mainly preferred over drum brakes, when it comes to the choice of the right actuators on HVs. Figure 2.4 depicts the two different kinds of actuators mainly implemented on HVs.

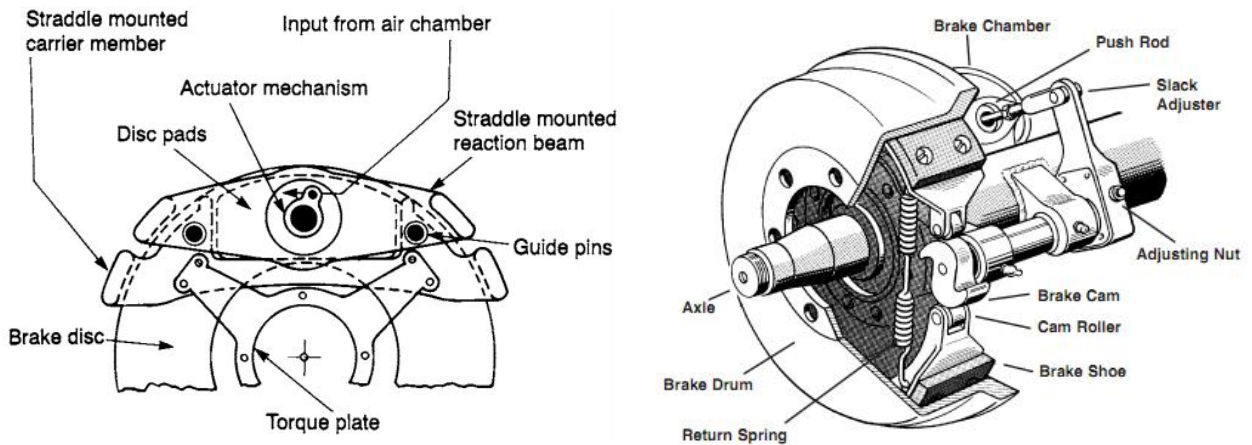


Figure 2.4: *Schematics of (a) air-operated disc brake [58] and (b) S-cam drum brake [32]*

As it has already been said, the main disadvantage of the pneumatic braking system is the longer response time compared to the one of the hydraulic braking system. More specifically, the delays between the initial pressure demand from the driver, and the change of the pressure at the brake chamber of the trailer, in the case of an articulated vehicle, can be up to 300ms [64]. In order to reduce these delays, the air signal, which is sent by the brake pedal to activate the brakes, can be replaced by an electronic signal, which utilizes electronics

for the control side of the vehicle's braking system. The name of this kind of braking system is Electronically controlled Braking System (EBS) and the schematic is shown in figure 2.5. The implementation of EBS on heavy vehicles is beneficial, since it provides more predictable braking control, and therefore it contributes to the reduction of the stopping distances. Moreover, it improves vehicle stability and driver control, as well as it reduces the number of brake system components and airlines [19]. However, since EBS is an electronically controlled system, it is possible that it will not be able to operate in case of an electrical failure. For that reason, it is common practice that an EBS should be installed along with a pneumatically controlled back-up system [32].

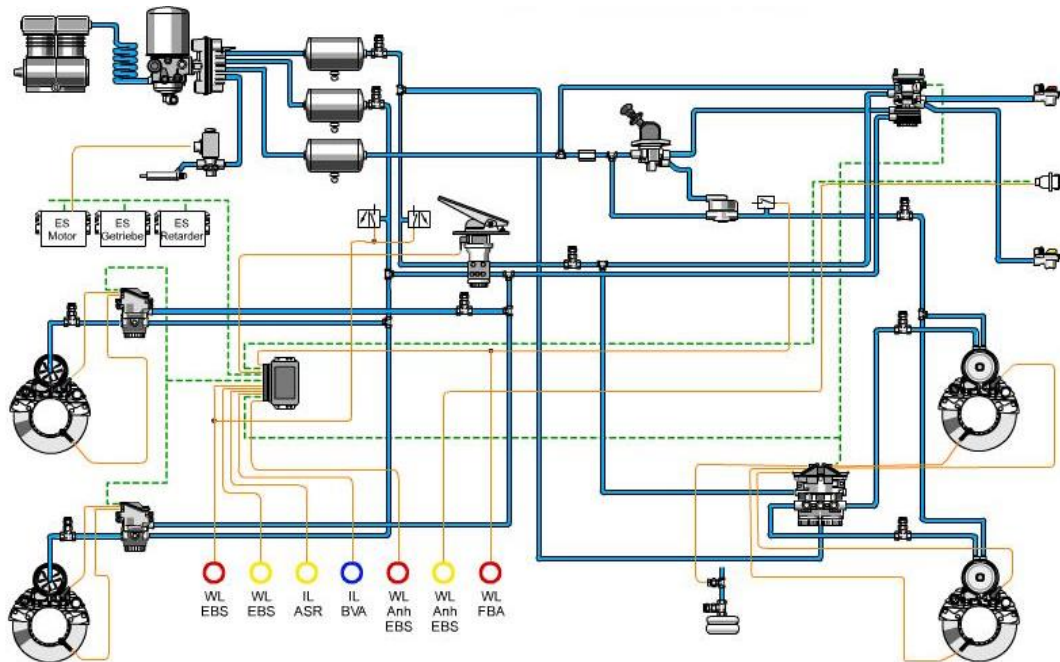


Figure 2.5: Schematic of an electronic braking system circuit of an HGV

2.2.1 Advanced Braking Control Systems

Both passenger and heavy vehicles are equipped with control systems for controlling the motion of the vehicle, especially during extreme braking maneuvers. More specifically, anti-lock braking systems (ABS) have been developed to control the relative slip velocity of the wheels, and to prevent their lock-up (i.e. slip is 100 percent), during emergency braking situations. There are many reasons why it is necessary to avoid the wheels' lock-up during braking. When the wheels of a vehicle are locked-up during braking, they are less able to generate longitudinal and lateral forces. Therefore, the vehicle presents high levels of driving instability, which can be further translated to increased stopping distances and loss of its steer-ability. Especially in heavy and articulated vehicles, the effects of wheel lock-up could be more devastating, since locking-up the wheels may also lead to jackknifing and rollover incidents [33].

The main function of ABS is to regulate brake pressure by holding, releasing or restoring brake pressure, when the wheels are about to lock. Furthermore, it is a prerequisite that the ABS allows the brakes to operate in their normal non-wheel-lock-up mode again, as soon as the possibility of locking up the wheels has been diminished [65], [58]. ABS works in a similar way for heavy vehicles as it does in passenger vehicles. Nevertheless, there is one important difference; the working fluid is air, instead of some kind of hydraulic fluid. This difference is the reason why ABS in heavy vehicles shows pressure cycles in frequencies of 1-2Hz, while in passenger cars ABS shows pressure cycles in frequencies of 6-8Hz [32], [58] [50] [21].

According to the control logic behind ABS, two main categories of ABS can be distinguished: "Individual Control" and "Axle Control". Individual control means that the stopping distance is determined by an individual control system of each wheel. The main limitation, using individual control on each wheel, is that it is

difficult to determine the reference velocity of each wheel. Furthermore, individual control requires more control channels to be able to control each wheel independently. In case of split- μ braking, the vehicle's motion is influenced by large values of yaw moments caused by differences in pressure per wheel, especially towards areas with higher friction. In heavy vehicles, such event could be translated to jackknifing [19], [23], [41]. On the other hand, axle control means that the control system controls each axle individually. Therefore, using wheel speed sensors at each wheel, the reference velocity signal is transferred to the correspondent wheel speed signal of each axle, but this signal is not transferred to the other axles of the vehicle. The axle control is separated into two main subcategories, depending on the velocity, which is fed to each axle's pressure regulator. The names of these two subcategories are "Select-Low Axle Control" and "Select-High Axle Control". Select-Low axle control means that the lowest wheel's speed of an axle is being fed to the axle's pressure regulator, and determines the brake pressure, coming out from the regulator of this specific axle. Using this kind of strategy, the optimal braking distance is sacrificed in order for the steer-ability and overall stability of the vehicle to be enhanced. Select-High axle control means that the highest wheel's speed of an axle is being fed up to the axle's pressure regulator and determines the brake pressure, coming out of the regulator of this axle. Using this strategy, the overall stability of the vehicle can still be reassured, and the braking distance can be decreased significantly. However, the steer-ability of the vehicle is decreased [19]. Since there are these differences when it comes to the control logics behind ABS operation, most common vehicles use a combination of individual control on each wheel, along with select-low control on each axle. In that way, not only the brake torques are controlled separately, but also the differences, when it comes to the braking forces between the left and right wheels of the vehicle, are restrained to a specific level [8], [32].

2.2.2 Alternative Advanced Braking Control Systems

As it has already been mentioned in the previous subsection, the purpose of ABS is to control the relative slip velocity of the wheels, during braking by regulating braking pressure in order to prevent wheels' lock-up. However, there are substantial reasons to control the slip of the wheels during braking around its optimal point. This can be explained thoroughly by taking a look at Figure 2.6, where the range of operation of an ABS can be seen.

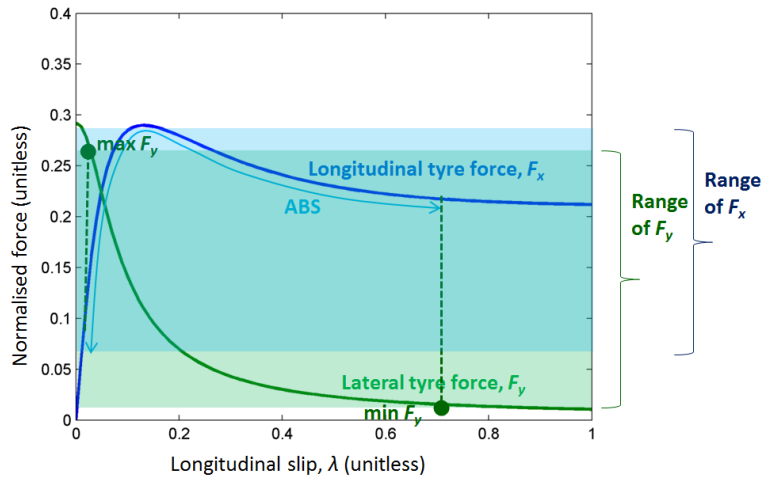


Figure 2.6: Longitudinal and lateral tyre curve for a wet road - ABS [42]

In Figure 2.6, the range of operation of ABS can be seen during braking for different slip values between two conditions, i.e. free rolling of the wheel ($\lambda = 0$) and lock-up of the wheel ($\lambda = 1$). Some field tests have shown that the longitudinal slip during braking, using an ABS algorithm, varies between 0.05 and 1 [42]. The most interesting feature of Figure 2.6 is the range of either longitudinal (F_x), or lateral (F_y) tyre forces. Both longitudinal and lateral tyre forces appear to have a large range when an ABS control algorithm is used for braking. Furthermore, the frequent locking and unlocking of the wheels, during the operation of the ABS can cause increased braking distances, as well as large consumption of compressed air. The high demands, when it comes to air consumption, are caused by the operation of the ABS, since it tries to release brake pressure, when the wheel is about to lock-up, and reapplies brake pressure when the wheel's lock-up has been avoided [42]. Nowadays, the waste of air and increased braking distance make ABS not such an efficient control system,

when it comes to braking.

Braking using wheel slip control offers some great advantages, in comparison with the method using ABS control, since the slip can be controlled around the optimum braking point. Some of the advantages are depicted in the Figure 2.7, where the longitudinal and lateral tire curves for a wet road, during braking using wheel slip control are illustrated.

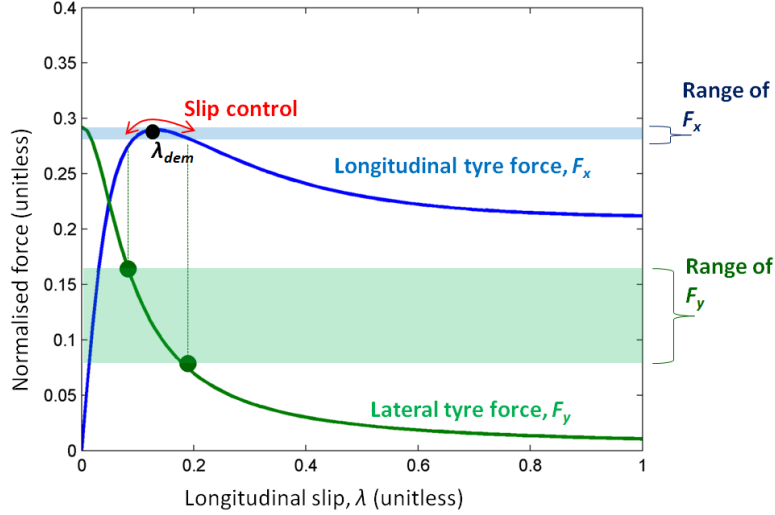


Figure 2.7: Longitudinal and lateral tyre curve for a wet road - Wheel Slip Control [42]

As it can be seen in Figure 2.7, using a wheel slip control method during braking offers great advantages in terms of the amounts of longitudinal and lateral tire forces. More specifically, the range of both tire forces is significantly lower than the correspondent one using the ABS control method, during braking. Besides, using wheel slip control during braking provides decreased braking distances, as well as lower levels of air consumption [42]. The controller, used for wheel slip control braking, should be able to track the optimum slip point. Hence, the longitudinal and lateral tire force characteristics should be either known to the controller, or at least estimated (for instance using a force observer). Limited slip controllers often use a default optimum slip point around $\lambda = 0.2$ for computational reasons [31], [38]. However, the ideal approach would be that the controller will be able to calculate the optimum slip point, independently on the kind of surfaces, by fitting adhesion-slip curves in real-time [52], [51].

The main limitation of using a wheel slip control system to track the slip around its optimal point is the delay of the brake system, next to the difficulty of accurately calculating the reference speed when the wheels are in deep slip. This delay can be defined as the time between the driver's push of the brake pedal (production of the brake signal), and the actual change in brake torque at the wheel, due to this signal [34]. More specifically, in order for the controller to be able to track the optimum slip point, the brake system delay should be around 5ms. The time delays that occur during braking on a HV are caused for many reasons, such as the long pipe lengths of the braking system, the compressibility of air and the slow pneumatic control valves [51]. One way to reduce the brake system delay is to replace the pneumatic actuators that are used in the system. Common ABS control systems utilizing pneumatic valves with an orifice size of 8mm present delays between 20 and 40ms [32], [34]. The aforementioned amounts of braking delay are much bigger than the ideal 5ms brake system delay, needed in order for the controller to track the slip around its optimal point. However, after carrying out some Hardware-in-the-loop (HiL) braking tests, Miller showed that there is a potential of achieving significant lower brake system delay, comparable to the ideal one (5ms). In order for this improvement to be achieved, fast-acting braking modulators with 3ms switch time and 8mm orifice can be used, along with the implementation of the wheel slip control system [51], [53], [32].

2.2.3 Advanced Brake Actuators on Heavy Vehicles

The need for developing fast-acting actuators has encouraged companies to replace the common pneumatic and hydraulic actuators with electrical ones [32]. More specifically, Siemens has developed electric brake actuator prototypes called wedge brakes. The main difference between the wedge brake and the conventional brake disc system is that electric motors are responsible for the pad's turning and pushing onto the brake disc. This behavior occurs due to the fact that the electric motors are used for pressing the connected-to-a-wedge brake pad to the disc and the rod. Figure 2.8 illustrates the so-called electric wedge brake, proposed by Siemens [26], [35].

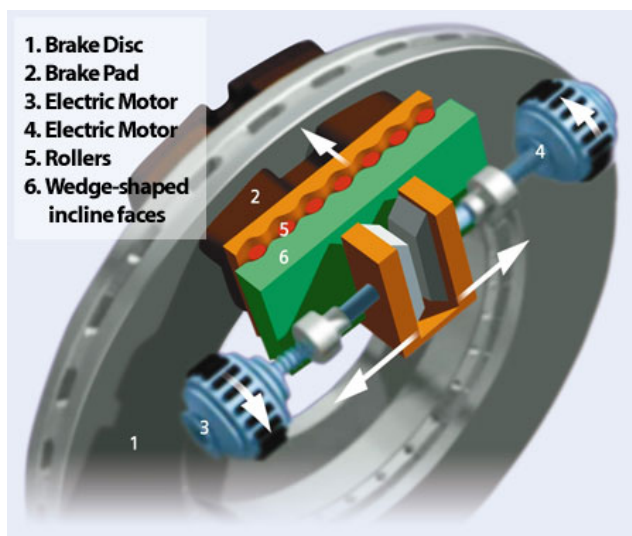


Figure 2.8: *Electronic Wedge Brake actuator (Siemens) [35]*

The reason for using a wedge is that power is multiplied with minimal energy expenditure. The concept of self-energizing brakes offers one tenth of the energy expenditure of the common hydraulic brakes, according to Siemens. Hence, the braking force will be always increasing, as long as the vehicle is driven faster. The Electronic Wedge Brake (EWB) can be characterized as a brake-by-wire system, since there is no mechanical connection between the brake pedal and the brakes. More specifically, there are wheel-speed sensors, which can measure wheel-speed one hundred times per second, and therefore the brake forces and the wedge position can be determined with paramount accuracy [26], [35]. It should also be mentioned that in a brake-by-wire system a fault-tolerant approach is necessary in order to guarantee the operation of the braking system, in case of possible failures. Therefore, EWB is connected to not only one, but two power supplies (main and backup) to reassure the vehicle's safety [26], [35].

Apart from Siemens, Haldex Brake Products Ltd. proposed their own electromechanical brake actuator which has been implemented on a Heavy Goods Vehicle (HGV). Using their own solution, when it comes to the braking actuators, and after carrying out straight-line braking tests using a tractor-semitrailer HGV, they achieved reductions of up to 24% in braking distance on low friction conditions. However, it should be mentioned that the aforementioned electric braking actuators were using the slip control braking approach, instead of the common ABS control strategies, in order to achieve these great results in terms of braking performance [32].

Another approach similar to the electric brake actuator designs, in terms of braking performance, has been proposed and developed by the Cambridge Vehicle Dynamics Consortium (CVDC) [51], [54]. More specifically, using bi-stable high-speed pneumatic valves in a brake actuator results in a braking system, which is an order of magnitude faster than the ABS control system with its conventional pneumatic valves [32]. Using these high speed modulators, the brake system delay could be reduced to up to 6-7 ms [34]. Schematics of these high speed modulators can be seen in Figure 2.9.

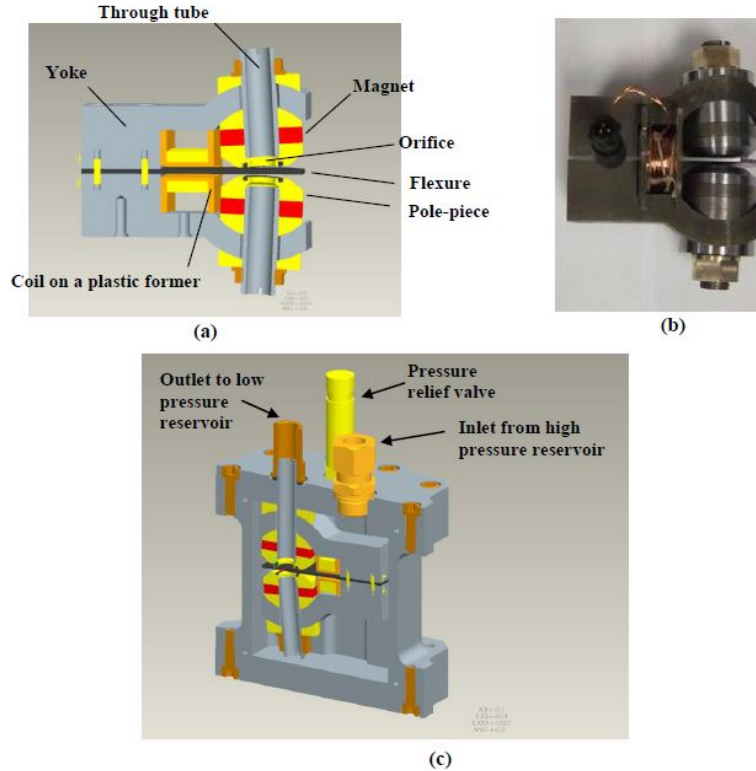


Figure 2.9: CVDC bi-stable valve, (a) Cross-section of the valve, (b) Picture of the prototype, (c) Cross-section of the valve in its enclosure [32]

As it can be seen in Figure 2.9, the valve's cantilevered flexure is located between two permanent magnets. Switching of the valve between two states (inlet/exhaust) is triggered by electrical pulses, sent to the wire coil. The valve switches in almost 3ms as a result of the motion of the low mass of the flexure, as well as the flexure's high stiffness. The diameter of the valve's orifice is 8mm and it can therefore directly be used in-line [32].

2.3 Tire modeling

As a result of the development of high performance braking systems, like electronically controlled braking systems and wheel-slip control braking systems, new ways of estimating friction forces, transferred by the road via tires have been proposed. More specifically, the research around tire-road friction modeling has been started almost 40 years ago. Since then, it has become more and more popular to determine the correct vehicle dynamics characteristics. To reach this goal an adequate tire friction model should be established [46].

The connection between slip ratios and friction forces is determined by the tire-road friction modeling. However, this relationship is very vague, in terms of vehicle dynamics, since it is influenced by many factors. For example, these factors could be tire pressure, normal loads, road surface conditions and so on. These factors can have multiple causes like the condition of the tires (wear), the deformation of the tires and the adhesion limits of each road surface [55], [27], [24], [75]. Since some of these factors vary stochastically, the precise connection between slip ratios and friction forces becomes very difficult as well.

A proper tire model can help to incorporate nonlinear tire characteristics, like hysteresis, which can not be described easily, using mathematical formulas. Therefore, it becomes necessary that data from measurements are recorded and converted to tire properties. Tire models are also of paramount importance in high performance braking control systems, since tire properties can be derived as a result of the tire characteristics parameters, coming from the tire models [46].

From a theoretical point of view, tire models can be separated into two main categories: empirical tire models

and analytical tire models. One important advantage of the empirical tire models is that they are able to capture the steady-state characteristics of tire-road friction [5], [7], [62]. On the other hand, empirical tire models have difficulties in capturing dynamic characteristics of the tires, like hysteresis, as well as it is not possible to incorporate the influence of specific factors, like tire pressure, or the wetness of the road. For that reason, analytical tire models have been developed to capture the dynamic characteristics of the tires. In order for the tire-road friction properties to be described, analytical tire models use differential equations [46].

Next, several tire models are described. As the work in this thesis focuses mainly on longitudinal dynamics and braking, the main focus will be on longitudinal tire dynamics.

2.3.1 Pacejka Tire Model (Magic Formula)

In 1980, Pacejka developed the empirical Magic Formula in collaboration with Volvo [5], [7], [62]. The Magic Formula is given by

$$\mu = C_1 \sin(C_2 \tan^{-1}(C_3 s_x - C_4(C_3 s_x - \tan^{-1}(C_3 s_x))))), \quad (2.5)$$

where $C_i, i = 1, \dots, 4$, are determined by fitting experimental data and the longitudinal slip s_x , during acceleration, is defined as

$$s_x = \frac{r\omega - v_x}{v_x} \quad (2.6)$$

The Pacejka tire model has been altered a lot in the last three decades, and it is the most popular tire model today, since it is used for many tire-road friction simulations and for advanced control system design [7], [62]. Nevertheless, as a result of the high number of parameters describing this tire model, it is difficult for this tire model to be analyzed.

2.3.2 Brush Tire Model

In this tire model, the tread rubber in the contact area is modeled as flexible bristles. Using this tire model, the force is generated by the deflection of the aforementioned bristles, due to slip. The tire will start sliding, when the force between the road and the bristle tip becomes too large [19]. In some literature, the brush tire model is regarded as a dynamic tire model, since it can be used to represent dynamic tire-road friction phenomena [46].

During straight-line acceleration or braking, the longitudinal force increases, as long as the wheel's angular velocity is not the same as the wheel's angular velocity of free rolling. Using the brush tire model under longitudinal slip during traction, the bristles in touch with the road at the contact area front edge (a,0), will be displaced more and more, since the velocity difference forces them to move through the contact area (figure: 2.10) [19], [63].

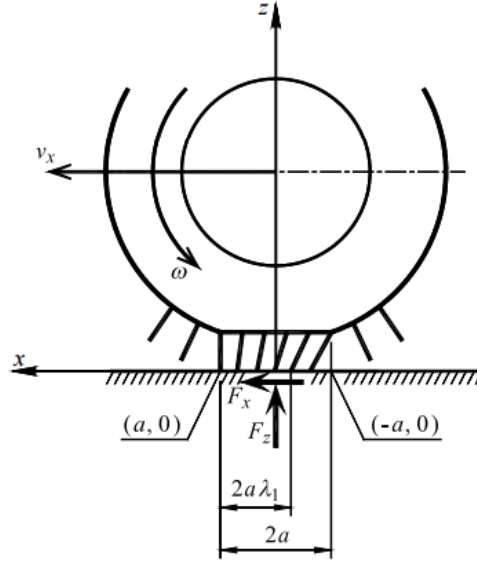


Figure 2.10: *Bristle deformations during traction [19]*

According to Figure 2.10, if the velocity at the center of the wheel is v_x , then after time Δt , the coordinate for a bristle tip at the contact area front edge $(a,0)$ will be:

$$x_t = \alpha - v_x \Delta t. \quad (2.7)$$

The upper end of the bristle, which moves with velocity $r\omega$, will have the coordinate:

$$x_u = \alpha - r\omega \Delta t. \quad (2.8)$$

The bristle longitudinal displacement u thus becomes

$$u = x_1 - x_u = r\omega \Delta t - v_x \Delta t = \frac{r\omega - v_x}{v_x} (v_x \Delta t) \quad (2.9)$$

$$= \frac{r\omega - v_x}{v_x} (\alpha - x) = s_x (\alpha - x) = -s_x (x - \alpha), \quad (2.10)$$

During braking, the slip varies between 0 (free rolling) and -1 (locked wheel). Hence, it is now possible to derive the longitudinal force:

$$F_x = C_s s_x f(\lambda_1) \quad (2.11)$$

where:

$$f(\lambda_1) = \begin{cases} \lambda_1(2 - \lambda_1), & \lambda_1 \leq 1 \\ 1, & \lambda_1 > 1 \end{cases} \quad (2.12)$$

and

$$\lambda_1 = \frac{F_z \mu}{2C_s |s_x|}. \quad (2.13)$$

The longitudinal slip stiffness is defined as:

$$C_s = \left[\frac{\partial F_x}{\partial s_x} \right]_{s=0} = 2\alpha^2 c_{pl}, \quad (2.14)$$

where 2α is the contact area length and c_{pl} is the longitudinal bristle stiffness per unit length.

2.3.3 Fancher Tire Model

The Fancher tire model is based on different assumptions of the brush tire model regarding the vertical pressure distribution and sliding properties of the rubber [70]. The primary assumptions are [22]:

- The contact patch can be divided into a sliding region and an adhesion region.
- The shear force generated in the adhesion region depends upon elastic properties of the tire.
- The shear force in the sliding region depends upon the frictional properties of the tire-road interface.

The longitudinal force is given by

$$F_x = \frac{(\mu F_z)^2(1 - \lambda)}{4C_0\lambda} + \mu F_z(1 - L_x) \quad (2.15)$$

where F_z is the tire normal force, C_0 is the longitudinal tire stiffness at zero slip and L_x is the fraction of the contact patch that is not sliding. μ is calculated by

$$\mu = \mu_f + (\mu_0 - \mu_f)e^{\frac{v_x - \omega R_r}{V_f}} \quad (2.16)$$

where μ_0 is the coefficient of static friction, μ_f is the coefficient of sliding friction and V_f is a shaping factor. L_x is given by

$$L_x = \frac{\mu F_z(1 - \lambda)}{2C_0\lambda} \leq 1 \quad (2.17)$$

2.3.4 Dahl Tire Model

The analytical Dahl tire-road friction model was developed by Dahl in the 1970s, and in general terms is a generalization of Coulomb friction. A big advantage of using this tire model is that it can provide a smooth transition around zero velocity. The hysteresis that it is presented during the period before sliding can be described by a first order equation of the position, which depends only on the sign of the velocity [14], [15].

The equation that Dahl proposed is given by:

$$\frac{dF}{dt} = \sigma_0(1 - \text{sgn}(u_r) * \frac{F}{F_s})^{\delta_d} u_r, \quad (2.18)$$

where σ_0 represents the initial stiffness of the contact at velocity reversal, δ_d illustrates a model parameter, determining the shape of the hysteresis, and u_r depicts the relative moving velocity [46].

In general, the Dahl model is able to capture many dynamic phenomena, like hysteresis and displacement, when the slip is zero. On the other hand, it cannot represent the relationship between the friction and the velocity. Hence, Dahl's proposal about dynamic modeling triggered the development of other tire models, like the LuGre tire model and so on [46].

2.3.5 LuGre Tire Model

This analytical tire model was developed by Canudas de Wit and it took its name by the universities, where it was developed, i.e. University of Lund and University of Grenoble. The LuGre tire model was inspired by the Dahl tire model, however, the LuGre tire model incorporates other steady-state characteristics [16], [17]. When a tangential force is applied, the friction force rises, since the bristles will deflect like springs (Figure: 2.11a). In Figure 2.11b the average deflection of the asperities is represented by the variable z [46].

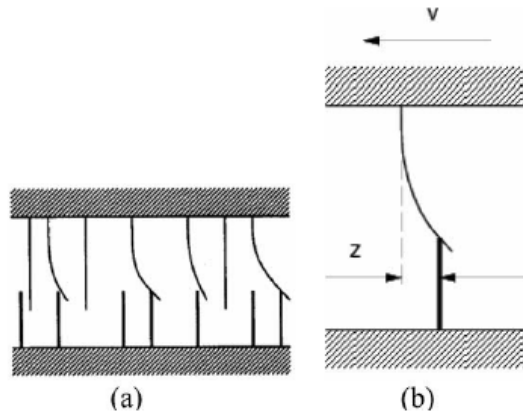


Figure 2.11: *Bristle model. (a) Friction interface between two surfaces is thought of as a contact between bristles (b) Average deflection of the asperities [16]*

The LuGre tire model for the tire-road friction can be formulated as:

$$\frac{dz}{dt} = v_x - \sigma_0 \frac{|u_r|}{g(u_r)} z \quad (2.19)$$

$$u_r = u_x - r\omega \quad (2.20)$$

$$F_x = (\sigma_0 z) + \sigma_1 \frac{dz}{dt} + \sigma_2 u_r \quad (2.21)$$

where σ_0 is the stiffness, σ_1 is the damping coefficient, and σ_2 is a coefficient proportional to the relative velocity to account for viscous friction [46].

2.4 Friction Estimation

As it has already been mentioned, optimal braking can be achieved when the wheel slip is close to the maximum friction coefficient in the slip-friction curve. To obtain this optimal value beforehand, information about the tire-road friction coefficient need to be known. This information can be obtained by means of friction estimation.

Friction estimation has received a great deal of interest from the academic world. Gustafsson was one of the first to successfully estimate the tire-road friction coefficient in 1997 by means of wheel slip [29]. Using the non driven rear wheels as zero slip reference, the slip of the front wheels could be estimated. By means of a Kalman filter and the magic formula [67], the tire-road friction coefficient was estimated. Around the same time, Ray used a different approach for friction estimation. Using knowledge about vehicle dynamics and more importantly about load transfer, he used a Kalman-Bucy filter and Bayesian hypothesis selection to estimate the friction coefficient. This way, no tire force model is required and tire-modeling can be done off-line. In 1999, Canudas de Wit proposed a dynamical tire/road friction model, together with a non-linear observer, to estimate the tire/road characteristics and the slip ratio, using only the rotational wheel velocity and the LuGre tire model [10].

In 2003 Yi stated that using only wheel angular velocity is insufficient to accurately and rapidly estimate the velocity and relative velocity, and proposed to use observers to estimate several states [76]. Using these states, an adaptive emergency braking controller was designed, which was able to determine the tire/road friction conditions under normal traction events. Muller showed in 2004 that it is possible to estimate the friction curve using low slip levels during braking [71]. In the same year, Lee used observers for the effective wheel radius and the tire normal force in order to compute the slip ratio from wheel speed and vehicle speed measurements. Using a tractive force estimator and a brake gain estimator, the friction coefficient could be estimated, as well [45]. Based on the work, done by Gustafsson [29], Wang proposed a slip-slope based friction estimation method in 2004, utilizing a nonlinear longitudinal tire model. More specifically, the innovation of his system in comparison with the research that it had already been done in literature, was that it was able to estimate the friction coefficient for a variety of vehicle configurations, slip ratios and driving events (acceleration or

braking) [73]. In 2005, Alvarez proposed an adaptive control scheme for emergency braking, based on the LuGre tire model, using the wheel angular speed and longitudinal vehicle acceleration [4]. His results looked very promising, and no information about the tire parameters was needed. Li showed an extensive review of the state of the art in 2006, expressing the importance of friction estimation, focusing on both longitudinal and lateral friction modeling [46]. In 2009, Ahn showed a dynamic and algebraic approach to friction estimation, focusing on the gains of the observers in the dynamical approach, and a linear least squares method in the algebraic approach [1, 2].

The models for friction estimation are becoming more and more extensive, and in 2010, Cho proposed to estimate friction using vertical tire force estimation, shaft torque estimation, longitudinal tire-force estimation, based on simplified wheel dynamics, and lateral tire-force estimation and using a random-walk Kalman filter [13]. Using friction ellipses, in 2011, Hsiao proposed a robust tire force estimator, which was able to estimate the longitudinal and lateral tire forces for each wheel separately [36]. In 2012, Rajamani proposed three different observers to estimate the friction coefficients of the individual wheels, using different sensor data. This method required knowledge of both slip ratio and tire forces in order to give an estimate about the friction coefficient, using a recursive least-squares parameter identification formulation [66].

With the rise of electric motors, new ways of exciting the vehicle become available, and Albinsson tried to exploit electric motor torques to estimate the friction in an electric vehicle [3]. In 2015, Long Chen proposed the use of an Unscented Kalman Filter (UKF) and mean-square-error-weighted fusion in order to achieve real-time estimation of tire-road friction coefficient [12]. Using load sensing bearings, Madhusudhanan proposed new methods to estimate the friction, which do not rely on a tire model. Individual tire estimation has become possible with inexpensive algorithms, provided that the wheel forces are directly known [49, 48].

The aforementioned papers stress the importance of friction estimation for vehicle dynamics and traffic safety. Proper knowledge about the tire-road friction coefficient leads to improved vehicle handling characteristics, and braking performance. This in turn leads to the development of safer vehicles, since vehicles will be able to stop faster and with more precision. Resemblance in the proposed methods can be found, when it comes to the use of different tire models, in combination with different types of observers and filters. Most papers recognize the Pacejka tire model [6], otherwise known as the magic formula, as a model with very good properties. The downside of the Pacejka tire model is its complexity and this makes it difficult for on-line friction estimation. One of the tire models that has gotten a lot of attention is the LuGre tire model. The simplicity of this model makes it easy to incorporate in different types of estimation algorithms.

In general, most of the abovementioned models make use of either Kalman filters, or observers to estimate the friction coefficient and tire parameters. The reason for this is that the required physical properties are often unknown. For example, vehicle longitudinal velocity is mostly derived from wheel angular velocity. The angular wheel velocity needs to be filtered first to give a correct estimation about the vehicle longitudinal velocity, and a Kalman filter provides this function. Observers are sometimes called virtual sensors, as they use sensor data from certain physical quantities to estimate other physical quantities. For instance, the normal loads on the wheels can be estimated from the acceleration of the vehicle, using an appropriate vehicle dynamics model.

2.5 Optimization Techniques

Optimization plays an important role in many fields of design. In control engineering, optimization can be used to design multi-criteria controllers, to estimate system parameters and much more [72].

The first step of optimization is defining the cost function or objective function, and/or the constraints. The second step is the selection of the most efficient optimization algorithm. Finally, the stopping criterion has to be established. There is a large number of optimization algorithms available, which can roughly be divided in the following:

- Linear optimization
- Convex optimization

- Global optimization

Examples of linear optimization algorithms are the simplex method and the interior point method. They are used for linear optimization problems. For convex optimization problems, which are slightly more complex, the modified simplex method, cutting plane algorithm and interior point algorithm can be used, among others, depending on the type of constraints. When there exist multiple local minima, other kinds of optimization algorithms should be used, such as multi-start local optimization, simulated annealing, Monte Carlo optimization, or genetic algorithm. With these algorithms, it is not possible to guarantee finding the global minimum, but given the correct starting parameters, they should give a good approximation [72].

Identification of the required algorithm is often not trivial and it requires some engineering experience. A grid-search could help in finding the nature of the optimization problem, regarding complexity and the need for a local, or global algorithm [72].

2.6 Validation

Simulation models are used to evaluate the functions developed in this thesis. The utilization of models is favorable in many industries because of the possibility to rapidly test new functions and methods without expensive real life tests. In case of vehicle dynamics, accurate vehicle models can save a lot of time and money.

The development of vehicle models is not trivial and the validation of vehicle models is often difficult. Kutluay gives a good overview of validation methods in vehicle dynamics [43]. The most forthcoming conclusion is that there is no such thing, as absolute validation. Furthermore, what might be sufficient for one model, could be insufficient for another model. It is therefore needed to determine a priori what modes of operation need to be modeled, and to what extent these modes need to mimic real experimental data.

3 Volvo Transportation Model Integration and Validation

The Volvo Transportation Model (VTM) is a MATLAB Simulink based toolbox used throughout Group Trucks Technology (GTT) for vehicle dynamics modeling and function development. For this thesis project, a quarter car model, based on the work of Miller [51] is incorporated in the VTM to simulate full vehicle behavior during braking. The quarter car model uses a slip control architecture with a Fancher tire model. This chapter covers the quarter car model and VTM integration, as well as the validation using test results obtained during winter testing by Volvo Trucks in 2017.

3.1 Quarter Car Model

The quarter car model used for slip control braking, and used in this report was created by Henderson, based on the work of Kienhofer, Miller and Henderson [42, 51, 53, 32]. The quarter car model is a simplified single wheel setup with suspension, as can be seen in Figure 3.1. The longitudinal motion of the vehicle is given by

$$F_x = (m_s + m_u)\dot{v}_x = 0, \tag{3.1}$$

and the tire dynamics during braking are given by equation 2.4, where the torque T is replaced by the braking torque T_B resulting in

$$J_w\dot{\omega} - r_b F_x + T_B = 0. \tag{3.2}$$

To calculate the forces on the road, the simple tire model based on the brush tire model, called the Fancher tire model, which has already has been described in subsection: 2.3.3, is used. This tire model has been validated against HGV tire test data ([22]).

This chapter gives an overview of the systems, used in the quarter car model, and the governing equations created by the above mentioned authors.

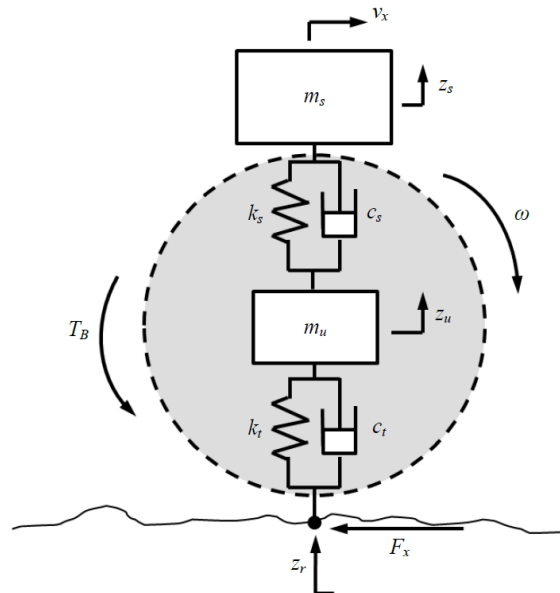


Figure 3.1: Quarter car model using sprung and unsprung mass, connected by spring damper systems representing the tire and suspension dynamics [32].

The forces and torques on the quarter car model are determined using using a series of controllers, observers and other models. In this section, these will be discussed briefly, as they play an important role, when it comes to their integration with the VTM.

3.1.1 Slip and Slip Error Calculation

First, slip is calculated using data from the quarter car model. The wheel speed ω is conditioned to represent wheel speed sensor data. Using equation 2.1, wheel slip is calculated. A lookup table is used to create the reference slip signal λ_{ref} using information about the vehicle speed v_x , as the optimum slip level is dependent on vehicle speed according to the Fancher tire model. Finally the slip error $\lambda_{ref} - \lambda$ is created.

3.1.2 Force Observer

For the calculation of the required pressure demand, the contact patch force F_x is used. As it is difficult to measure this force at the contact patch directly, a force observer is used mentioned by [51]. A discrete time Luenberger Observer with pole placement is used to estimate the unknown variable \hat{F}_x , according to equation 3.2. The state-space equation of the tire dynamics is given by equation 3.4, and the Luenberger observer equation is given by 3.5. Note that it is assumed that \dot{F}_x is constant.

$$\underbrace{\begin{bmatrix} \dot{\omega} \\ \dot{\hat{F}}_x \\ \dot{\hat{F}}_x \end{bmatrix}}_{\hat{x}} = \underbrace{\begin{bmatrix} 0 & -r_b/J_w & 0 \\ 0 & 0 & 1 \\ 0 & 0 & 0 \end{bmatrix}}_{\mathbf{A}} \underbrace{\begin{bmatrix} \omega \\ F_x \\ \dot{F}_x \end{bmatrix}}_x + \underbrace{\begin{bmatrix} -K_{BR}/J_w \\ 0 \\ 0 \end{bmatrix}}_{\mathbf{B}} \underbrace{P_c}_u \quad (3.3)$$

$$y(k) = \underbrace{\begin{bmatrix} 1 & 0 & 0 \end{bmatrix}}_{\mathbf{C}} \underbrace{\begin{bmatrix} F_x \\ \omega \\ \dot{\omega} \end{bmatrix}}_x \quad (3.4)$$

$$\hat{x}(k+1) = \mathbf{A}\hat{x}(k) + \mathbf{L}[\omega(k) - \mathbf{C}\hat{x}(k)] + \mathbf{B}u(k) \quad (3.5)$$

3.1.3 Sliding Mode Controller

The 'heart' of slip control braking is the sliding mode controller [69]. A first order sliding surface is defined by

$$s_s = \lambda - \lambda_{ref}, \quad (3.6)$$

resulting in the expression for the pressure demand

$$P_{SMC} = \frac{R_r r_b \hat{F}_x - (1 - \lambda) a_x J_w}{K_{BG} R_r} - k_s \left(\frac{s_s}{|s_s| + \delta_s} \right) - \Phi_s s_s, \quad (3.7)$$

where R_r is the wheel rolling radius, K_{BG} is the brake gain, which will be mentioned later on, and k_s, δ_s and Φ_s are tunable controller gains. Figure 3.2— shows a graphical representation of the sliding mode controller with its inputs and its outputs.

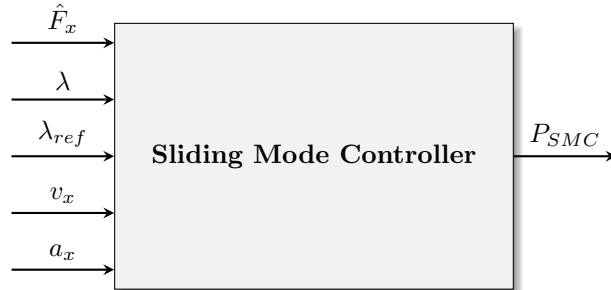


Figure 3.2: *Sliding mode controller block representation*

3.1.4 Pressure Controller

The required pressure P_{SMC} from the sliding mode controller is passed to the pressure controller. The pressure controller is a simple proportional controller, producing a pulse-width-modulation (PWM) mark-space ratio

demand R_{MS} for the inlet and outlet valves connected to the brake chamber given by

$$R_{MS} = k_{press}(P_{dem} - P_c), \quad (3.8)$$

where the R_{MS} is converted to a PWM signal where one and zero correspond to fully opened and fully closed valves states respectively. P_c is the pressure in the brake chamber [51]. This pressure is either measured directly, or it is first fed through a pressure observer. The demand pressure P_{dem} is either the sliding mode pressure P_{SMC} , or the pressure demanded by the driver, depending on which pressure is minimum.

3.1.5 Valve and Brake Chamber Plant

The valve plant converts the mark-space ratio to a brake torque [51]. A delay is introduced to simulate the switching time of the valves, with a value of 3 ms for the bi-stable brake valves, creating the valve state S_v from R_{MS} . The air mass flow through the orifices is represented by the first order equations

$$\dot{m}_v = S_v C_f A_v C_1 \frac{P_u}{\sqrt{T_{cham}}} \quad \text{if } \frac{P_d}{P_u} \leq p_{cr} \quad (\text{chocked}) \quad (3.9)$$

$$\dot{m}_v = S_v C_f A_v C_2 \frac{P_u}{\sqrt{T_{cham}}} \left(\frac{P_d}{P_u}\right)^{\frac{1}{\gamma}} \sqrt{1 - \left(\frac{P_d}{P_u}\right)^{\frac{\gamma-1}{\gamma}}} \quad \text{if } \frac{P_d}{P_u} > p_{cr} \quad (\text{non-chocked}) \quad (3.10)$$

where C_f is the valve discharge coefficient, A_v is the valve orifice cross-sectional area, P_u is the upstream pressure, P_d is the downstream pressure, and γ is the heat capacity ratio. C_1 and C_2 are defined by

$$C_1 = \sqrt{\frac{\gamma}{R} \left(\frac{2}{\gamma+1}\right)^{\frac{\gamma+1}{\gamma-1}}} \quad (3.11)$$

and

$$C_2 = \sqrt{\frac{2\gamma}{R(\gamma-1)}} \quad (3.12)$$

where R is the specific gas constant. p_{cr} is the critical pressure ratio, defined by

$$p_{cr} = \left(\frac{2}{\gamma+1}\right)^{\frac{\gamma}{\gamma-1}} \approx 0.5 \quad (\text{for air}) \quad (3.13)$$

The air mass flow is directly fed to the brake chamber, where the brake chamber pressure is described by

$$\alpha_{in} \dot{m}_{in} - \alpha_{out} \dot{m}_{out} = \frac{V_c \dot{P}_c}{RT_c} + \frac{\alpha_c \dot{V}_c P_c}{RT_c}. \quad (3.14)$$

The air within the brake chamber is modeled as a polytropic gas with $PV^\alpha = \text{constant}$. P_c is the absolute chamber pressure, V_c is the absolute chamber volume, T_c is the the brake chamber temperature and α is a value between 1 and γ , depending whether the process is behaving isothermally or adiabatically.

The brake torque is calculated using a brake gain K_{BG} given by

$$T_B = K_{BG} P_c. \quad (3.15)$$

3.2 Volvo Transporation Models

The VTM used in this thesis is based on an 8x4 (eight wheels, four driven) truck with a tag axle (axle that can be lifted) to simulate the braking performance using the fast actuating braking valves. For the simulations in this thesis the tag axle is lifted. Figure 3.3 shows a graphical representation of the vehicle.

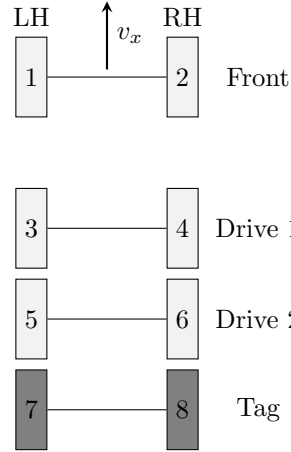


Figure 3.3: Graphical representation of the truck used in this thesis. The gray wheels show the tag axle. v_x shows the normal driving direction.

The architecture of the whole VTM can be represented by Figure 3.4.

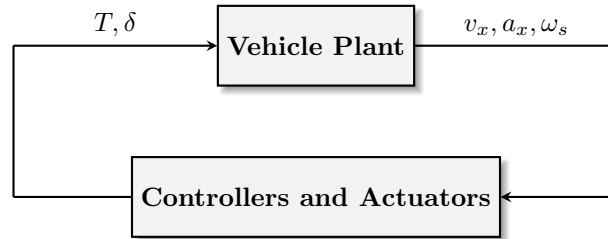


Figure 3.4: VTM architecture, showing the vehicle plant, controllers and actuators and inputs and outputs used in this thesis.

3.2.1 Vehicle Plant

The VTM based vehicle plant has the following inputs: steering angles (front axle and tag axle), torques on each wheel and road roughness. As outputs, various vehicle dynamics data are available of which longitudinal acceleration and velocity (a_x, v_x), as well as tire rotational velocity (ω_s) are the most interesting signals for longitudinal braking. For more demanding dynamic situations, pitch, yaw and roll information is available, along with slip angles and tire forces.

The dynamics of the VTM are modeled by two masses representing the chassis (one front and one rear), and by a Pacejka tire model including 28 parameters.

3.2.2 Controllers and Actuators

The controllers and actuators determine the behavior of the vehicle. In this thesis project, the reference speed is created to simulate a braking driving cycle. Figure 3.5 shows the control architecture that is used to either increase, or decrease the speed of the truck in the simulation.

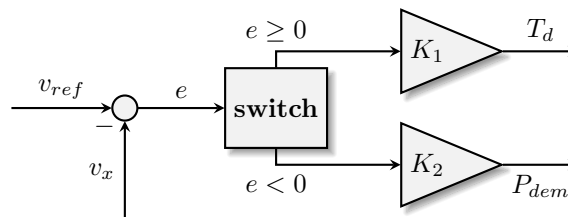


Figure 3.5: Control architecture of vehicle speed. K_1 and K_2 are proportional gains.

The torque demand T_d is converted into a drive torque going to the vehicle plant using a first order transfer function

$$T(s) = \frac{1}{0.4s + 1} T_d(s). \quad (3.16)$$

The same pressure demand is sent to all wheels and is converted by a brake plant to a braking torque for each wheel. This brake plant consists of ABS control logic using wheel slip and brake fade in the original VTM.

3.3 Integration

Integrating Miller’s combined slip controller and brake actuator model with the VTM enables function development on vehicle wide scale. To do this, the wheel slip control architecture of the quarter car model presented in section 3.1 is detached from the quarter car vehicle plant. The wheel slip control part then replaces the ABS control architecture, but it uses the same pressure demand P_{dem} to create the braking torque T_b . This control part will be henceforward known as the local brake controller.

3.3.1 Local Brake Controller

The local brake controller takes over the function of the ABS in the VTM. Figure 3.6 shows the block architecture of the local brake controller.

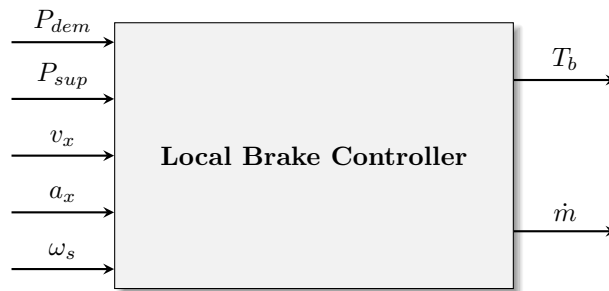


Figure 3.6: *Local brake controller overview, to the left are the inputs, the outputs are the braking torque T_b and the air mass flow rate \dot{m} .*

Figure 3.7 shows a block diagram of the local brake control system. Now, inside the local brake controller, slip is calculated similar to the way that it was calculated in the quarter car model. Using information about the velocity, the reference slip signal is created. The local brake controller also runs the force observer as mentioned in 3.1.2. Now, all the inputs for the sliding mode controller are available, and the sliding mode pressure can be created. This pressure, when it is fed through the pressure controller, using information from the pressure chamber observer, it is able to create the mark-space ratio R_{MS} . The mark-space ratio is fed through the valve and brake chamber plant, and the local brake controller block outputs the braking torque.

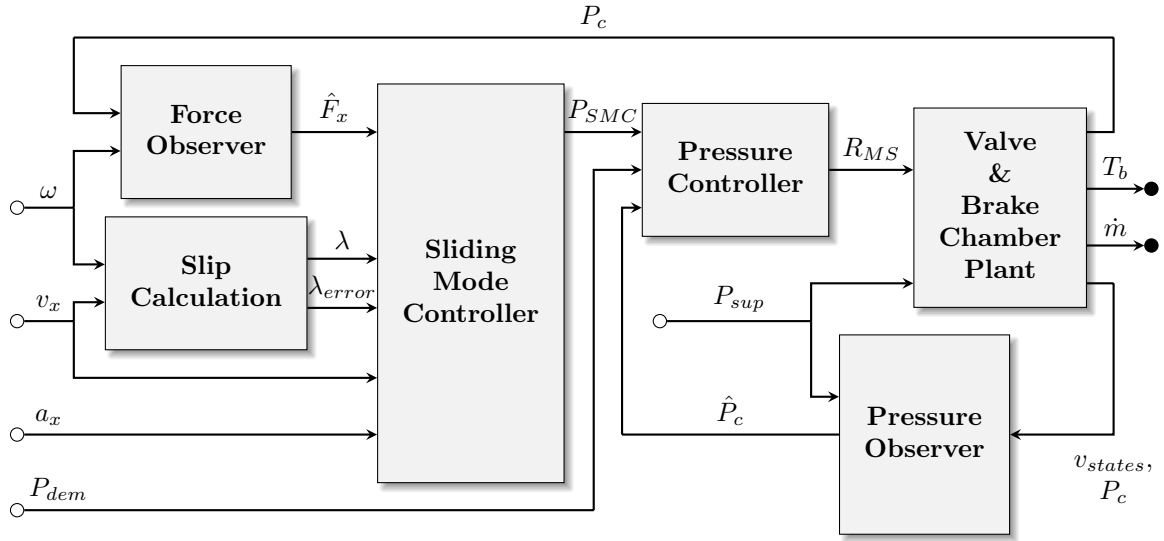


Figure 3.7: Schematic overview of the individual local brake controller components. The white circles represent system inputs, where the black circles represent the outputs.

3.3.2 Parameter Changes

As the VTM and the quarter car model were independently developed, most of the parameters did not match, or parameters with the same name had different values. This resulted in a discrepancy that was challenging to solve.

The parameters of the VTM differed from both the experimental truck and the quarter car model. For the quarter car model, some parameters had different names or different values. The physical properties of the truck used in the experiment were also not matching with those used in VTM. Using logged data and measurements from the experiment, the parameters of the VTM were adapted to match as close as possible to those of the real truck.

The experiments were carried out on ice, snow and dry asphalt. On snow, both straight-line braking and brake-in-turn maneuvers were tested. Table 3.1 shows the different gains used in the experiment. Consequently, these gains will be used in the sliding mode controller during simulation.

Another part of the model that had a major influence on the results are the tire models. As mentioned in 3.2.1, VTM uses a Pacejka tire model with 28 adaptable parameters. Of these, the scale factors for maximum friction coefficient in both lateral and longitudinal directions had to be changed from surface to surface. As the truck used in the experiment was not as heavy as the tire model was designed for, also the scale factor for the nominal rated load has been altered to match more closely to the characteristics of the tire in the experiment. Please note that it is very difficult, if not impossible, to get the tire parameters of the Pacejka model matched to the tires, used in the experiment. However, with these parameter changes, the behavior of the model should be at least similar to the truck of the experiment.

Table 3.1: Controller gains for the four different braking scenarios. Note that Rear captures both the Drive 1 and Drive 2 axle.

Parameter	Dry Asphalt Straight-Line 60km/h	Packed Snow Straight-Line 80km/h	Polished Ice Straight-Line 60km/h	Packed Snow Brake-In-Turn 60km/h
Delta gain SMC δ_s	0.02	0.02	0.02	0.02
Phi gain SMC Φ_s	100000	100000	100000	100000
K gain SMC k_s	70000 [Front] 75000 [Rear]	60000 [Front] 50000 [Rear]	50000 [Front] 50000 [Rear]	60000 [Front] 60000 [Rear]
Slip Reference Off- set λ_{ref}	0.14 [Front] 0.16 [Rear]	0.08 [Front] 0.12 [Rear]	0.05 [Front] 0.10 [Rear]	0.06 [Front] 0.12 [Rear]

3.4 Validation

With the local brake controller implemented in the VTM and the incorporation of the modified parameters, the behavior of the model can now be compared to the truck using the wheel slip controller. Data of the vehicle were collected during winter tests in 2017. These tests included straight line braking and brake-in-turn maneuvers. Validation means that the model should match the experimental data reasonably well. The validation consists of two parts: partial validation of the local brake controller and validation of the complete vehicle model. Key features of the validation entail deceleration, brake pressure and wheel slip. For the brake-in-turn maneuvers, yaw angle, longitudinal and lateral acceleration and side-slip angle will be compared.

For deceleration, both average deceleration from the start of braking to full stop and Mean Fully Developed Deceleration (MFDD) are used [20]. The MFDD is given by

$$d_m = \frac{v_b^2 - v_e^2}{25.92(s_e - s_b)}, \quad (3.17)$$

where d_m is the MFDD, v_b is the initial speed in km/h, v_0 is the vehicle speed at $0.8v_0$, v_e is the vehicle speed at $0.1v_0$, s_b is the distance traveled between v_0 and v_b in meters, and s_e is the distance traveled between v_0 and v_e in meters.

Furthermore, the distance from the beginning of the braking maneuver to the full stop of the braking maneuver is used, next to the corrected braking distance to account for small discrepancies in initial vehicle speed [57], given by

$$s_c = \left(\frac{v_{0,t}^2}{v_0^2} \right) s, \quad (3.18)$$

where s_c is the corrected stopping distance, $v_{0,t}$ is the target initial speed, v_0 is the initial test speed and s is the actual stopping distance.

Wheel slip will be evaluated as the error between the actual wheel slip and the reference wheel slip. The absolute mean error will be used for both the experimental and VTM results. These results will be compared per axle and per experiment.

The figures and plots will show the performance of the VTM with slip control, in comparison with the experiment. For straight-line braking, the Fancher tire model is also implemented in the VTM replacing the Pacejka tire model, in order to compare the performance of the Pacejka tire model and the Fancher tire model (Brush) with respect to the experimental data.

3.4.1 Partial Validation

In order for the complete VTM-integrated local brake controller model to be verified, some kind of partial validation was done beforehand. Two different kinds of partial validation were done, according to the availability of the models and available experimental data. The first partial validation is validation of the local brake controller model using the quarter car model and the second one validation of each of the sub-models of the local brake controller using the experimental data gathered from winter testing .

Quarter Car Model

The main purpose of this validation was to investigate if the local brake controller block without the VTM integration works properly, even when it is configured along with a different vehicle plant. More specifically, using the simplified quarter car model (MIRA 2013 Model) evaluated at the MIRA test track in 2013 [33], it was necessary to investigate the output signals of the local brake controller block. It should be also mentioned that the timestep of the simulation, the kind of the solver, as well as the tasking and sample time options were changed to the values that they were used in the MIRA 2013 model, in order for the comparison of the signals to be more fair.

The wheel slip controller (SMC) is the 'core' of the local brake controller block, since using the error slip signal, it produces the pressure demand signal (P_{dem}), which is fed to the proportional pressure controller. Provided

that the slip signal (input to the SMC) and the pressure demand signal (output of the SMC) are the same for both the local brake controller integrated with the quarter car model and the complete MIRA 2013 model, it can be concluded that the local brake controller block works properly.

The plots of wheel slip (input to the SMC) and pressure demand (output of the SMC) for both the local brake controller with the integrated quarter car model and the MIRA 2013 model are illustrated in Figure 3.8.

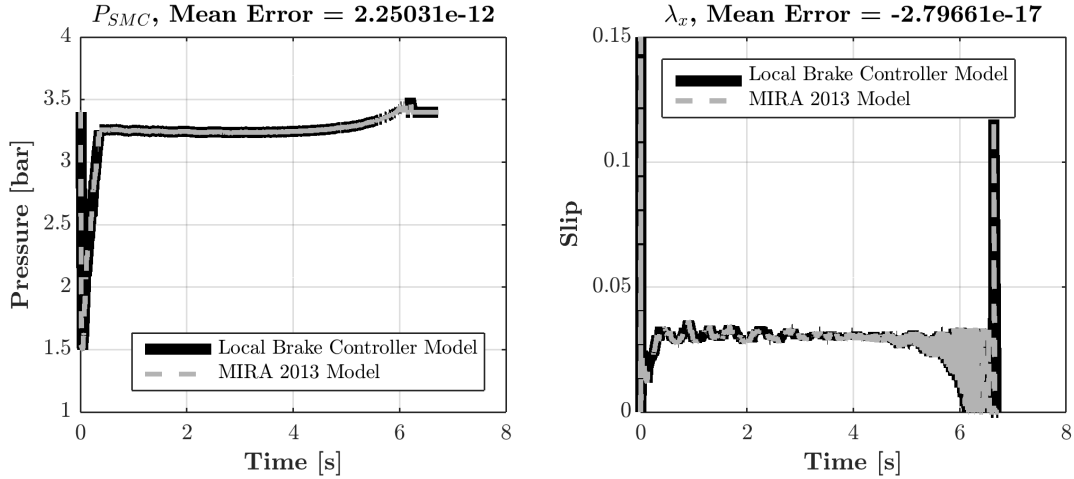


Figure 3.8: Comparison of (a) longitudinal slip and (b) pressure demand between the local brake controller and MIRA 2013 model

In figure 3.8a it can be seen that the longitudinal slip being fed to the sliding mode controller is similar for both the local brake controller model and the MIRA 2013 model. This could be confirmed also by the fact that the mean error value for these two signals is only $2.25031e-12$. When it comes to figure 3.8b, it can be seen that the output pressure of the sliding mode controller is similar for both models with a very low mean error value, i.e. $-2.7966e-17$.

The conclusion of this kind of partial validation is that the local brake controller block works properly, regardless of the vehicle plant that it is being used each time, given that the simulation properties of the model have been determined correctly.

Experimental Data

In the partial validation using experimental data, a different approach was used in order to validate the performance of the local brake controller block. The local brake controller block is comprised of different sub-blocks, like the force observer block, the sliding mode controller block, the pressure controller block, the valve plant block, the reference slip block and so on. Each of these blocks has its own inputs and outputs, but all of them are necessary in order to formulate a complete local brake controller block. The logic behind this kind of partial validation is to feed the right signals of the experimental data (gathered by the supervisor of the thesis during winter testing of the same truck) to each of the aforementioned sub-blocks, and to try to compare their output signals to the correspondent signals of the experimental data. Obviously, this kind of partial validation requires signals of both the inputs and outputs of each local brake controller sub-block, hence, due to the nonavailability of some of the signals it was not possible for all the sub-blocks of the local brake controller to be checked for individual validation. More specifically, the sub-blocks of the local brake controller which were individually validated are the sliding mode controller sub-block, the force observer sub-block, the valve plant sub-block and the pressure controller sub-block. When it comes to the kind of test and data that was used for partial validation, it should be mentioned that winter test data from straight-line braking tests from 80 - 0 km/h on packed snow surface were used.

As it can be seen in Figure 3.7, the inputs of the sliding mode controller are F_x , λ , λ_{error} , v_x , and α_x , while the output is P_{SMC} . By isolating the sliding mode controller block from the rest of figure (3.7) and by feeding to it the correspondent input signals, taken by the data of the abovementioned experiment, the following plot

of the output of the sliding mode controller sub-block can be derived.

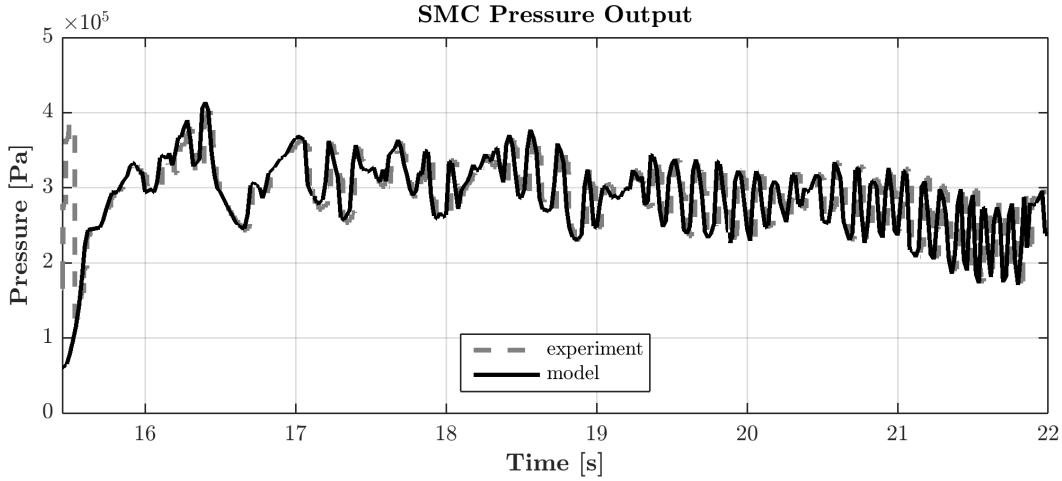


Figure 3.9: Comparison of the SMC pressure output between the experiment and the model

Figure 3.9 depicts that by looking at the SMC output during the braking event, the behavior of the SMC pressure output of the model, using the experimental data as inputs, matches the behavior of the SMC pressure output signal, taken directly by the experiment. For that reason it can be concluded that the sliding mode controller sub-block works properly and is individually validated against winter test data.

A similar procedure like the one that it had been followed during the partial validation of the sliding mode controller block is going to be followed again, when it comes to the partial validation of the longitudinal force (F_x) observer sub-block. The wheel angular speed and the relative chamber pressure (inputs of the F_x observer sub-block according to figure 3.7) have been taken directly by the winter test data and they are being fed to the force observer sub-block. At this point it should be mentioned that an offset pressure ($P_{crack} = 9000Pa$) has been added to the relative chamber pressure signal before its input to the force observer. That happened because P_{crack} appeared in the C-code implemented on the real truck, and hence it was an essential addition to the partial validation of the force observer sub-block, since it is necessary to have a fair comparison between the force observer output of the sub-block and the estimated longitudinal force signal, taken directly by the experimental data. This comparison is illustrated in the figure below.

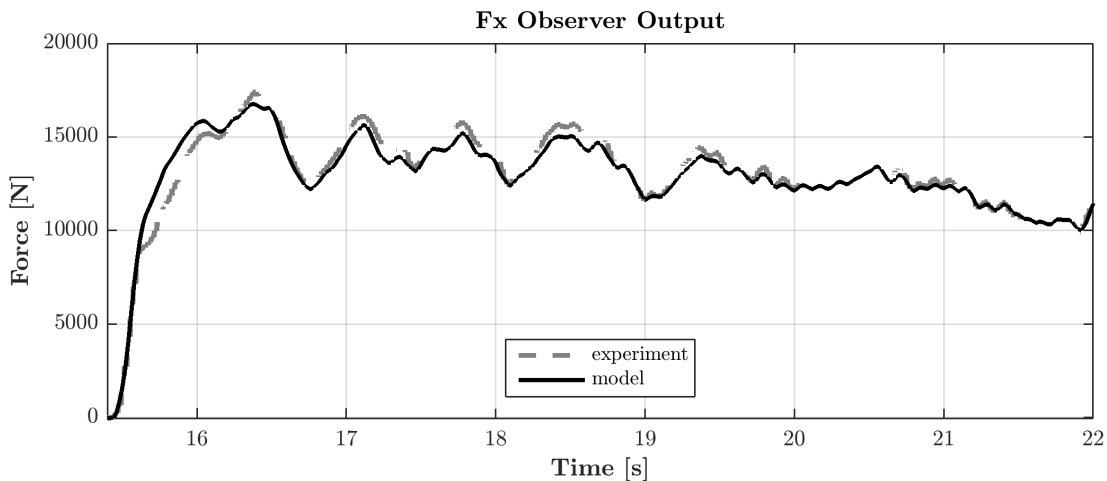


Figure 3.10: Comparison of the F_x observer output between the experiment and the model

Figure 3.10 illustrates that the trend of the estimated longitudinal force (\hat{F}_x) during the braking procedure, coming out of the force observer sub-block, is comparable to the behavior of the estimated longitudinal force, taken directly by the experimental data. Therefore, the force observer sub-block is individually validated

against winter test data.

The next sub-block of the local brake controller which is going to be validated against winter test data is the valve plant. According to figure 3.7 the inputs of the valve plant are two, i.e. the supply pressure coming out from the tank (P_{sup}) and the mark-space ratio (R_{MS}) coming out from the pressure controller sub-block. It should be mentioned that since the tank supply pressure (P_{sup}) signal was not available from the experimental data, a constant tank supply pressure signal ($P_{sup} = 8.6bar$) was fed into the valve plant, in order to mimic the behavior of this signal. When it comes to the mark-space ratio signal taken by the experimental data, it should be mentioned that it was divided with 14.7692 because of bit shift operations which were used to translate the internal valve control states on the vehicle into integer based diagnostic signals for logging. The next figure illustrates the output of the valve plant, i.e. relative chamber pressure, and it compares it to the direct relative chamber pressure signal, taken by the experimental data. However, again, like in the case of the partial validation of the force observer, a pressure offset ($P_{crack} = 9000Pa$) has been added to the output relative chamber pressure signal, coming out from the valve plant sub-block, in order to be able to be compared to the relative chamber pressure signal, taken by the experiment.

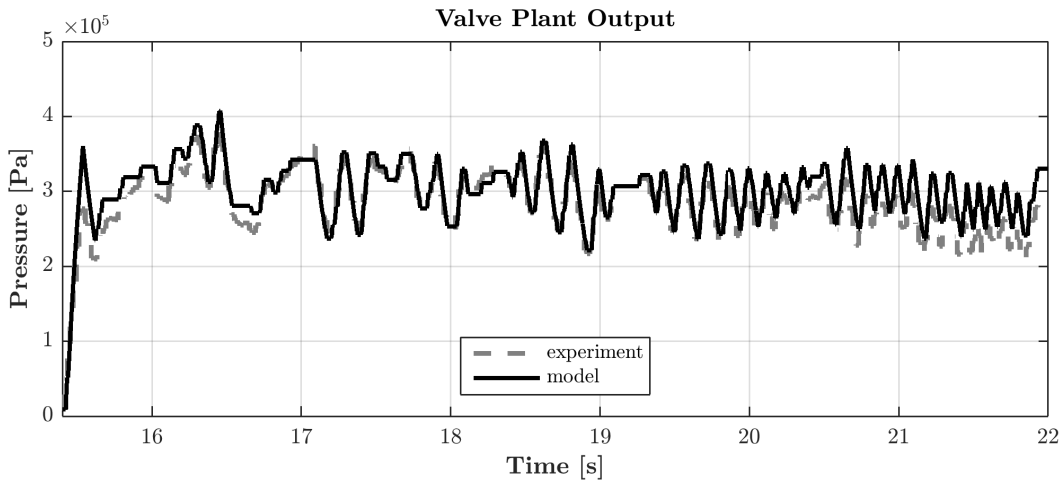


Figure 3.11: Comparison of the valve plant output between the experiment and the model

As can be seen in Figure 3.11 the behavior of the relative chamber pressure coming out from the valve is similar to the relative chamber pressure signal, taken by the experiment. However, it is obvious that on average there is an overestimation of the relative chamber pressure coming out from the valve plant sub-block in comparison with the one taken directly by the real data. The reason is that on the real truck, the tank pressure is depleting during the braking maneuvers, and this is something which can not be represented precisely on the partial validation of the valve plant sub-block. And, since during the partial validation of the valve plant, the tank supply pressure is constant at 8.6 bars and it is not depleting together with the braking maneuver, it is reasonable that the relative chamber pressure output of the valve plant sub-block is going to be a bit overestimated. Nevertheless, as it has already been mentioned, the overall trend of the relative chamber pressure signal is similar, either for the output of the valve plant or for the correspondent signal, taken directly by the experiment. Hence it can be concluded that the valve plant is individually validated against winter test data.

The last sub-block of the local brake controller that can be validated against winter test data is the pressure controller sub-block. As it can be seen in figure 3.7, the pressure controller sub-block has three inputs, i.e. the pressure demand signal, given by the driver (P_{dem}), the pressure output signal of the sliding mode controller (P_{SMC}) and the absolute chamber pressure signal (P_c), coming either from the valve plant, or from the pressure observer. In this case, it is considered that the pressure controller uses the absolute chamber pressure signal, taken by the valve plant, instead of the estimated absolute chamber pressure signal, taken by the pressure observer, since there is no signal from the experiment that can give direct information about the observed absolute chamber pressure. The output of the pressure controller sub-block is the mark-space ratio (R_{MS}), according to figure 3.7, and this output is going to be compared with the mark-space ratio signal, taken by the experimental data, as it can be seen in the following figure. At this point, it should be also mentioned that

during the determination of either the inlet state, or the outlet state of the valves, inside the pressure controller block, an additional pressure offset of $1/16$ is added every time that each of the valves is open. This action has been made after comparing the Simulink architecture of the pressure controller sub-block with the C-code script of the real truck, which was used for winter testing. Furthermore, as it has already been mentioned earlier during the valve plant partial validation, the experimental mark-space ratio signal has been divided with 14.7692 in order to be compared with the correspondent mark-space ratio signal of the model's pressure controller sub-block, since it is scaled differently in comparison with the mark-space ratio coming out from the pressure controller output.

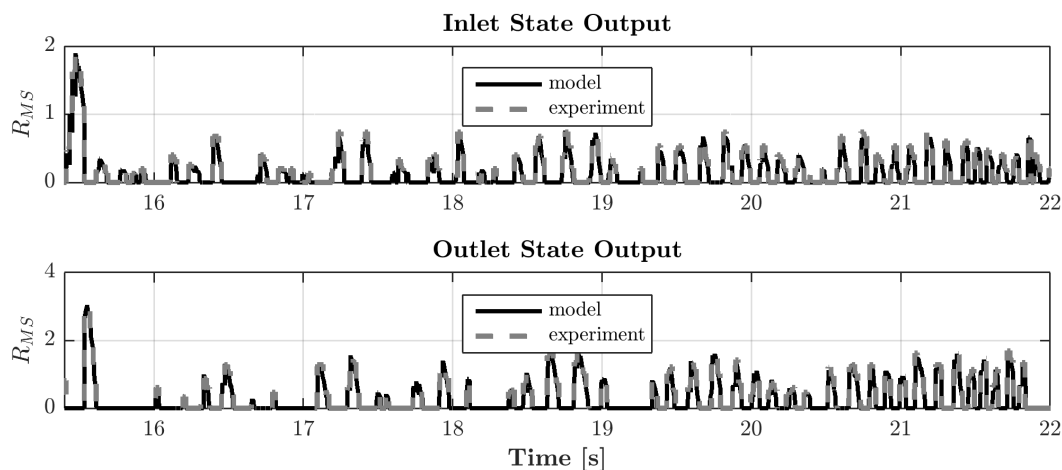


Figure 3.12: Comparison of the pressure controller output between the experiment and the model

Figure 3.12 shows that the behavior of the mark-space ratio signal of the model at the output of the pressure controller matches the behavior of the correspondent mark-space ratio signal, taken directly by the experiment, either for the inlet, or for the outlet state of the valves. Hence, it can be concluded that the pressure controller block is individually validated against winter test data.

3.4.2 Complete Model Validation Results

The complete model validation includes both straight-line braking and brake-in-turn maneuvers. First, the results on polished ice, packed snow and dry asphalt are shown consequently. After that, the brake-in-turn maneuver is shown. Finally, the metrics for distance and deceleration conclude the results of the validation. For straight-line braking, results of only the left-hand (LH) side of the vehicle will be shown, as the behavior of the vehicle is symmetric.

Straight-Line Braking, Polished Ice

Figure 3.13 shows the speed profile of experimental data and simulation data for both models using the Pacejka and Fancher (brush) tire model. It can be seen that the start of braking is equal for all, and the profile is fairly similar. Both models and experiment stop around roughly the same point.

Figures 3.14, 3.15 and 3.16 show the wheel slip and brake pressure for all simulations. Note that for braking at higher speeds, both the wheel slip and brake pressure are very similar. For both brush tire model and Pacejka tire model, the wheel slip starts having a higher amplitude at the end of the braking procedure compared to the experiment. The Pacejka tire model has an even higher amplitude than the brush model at these lower speeds.

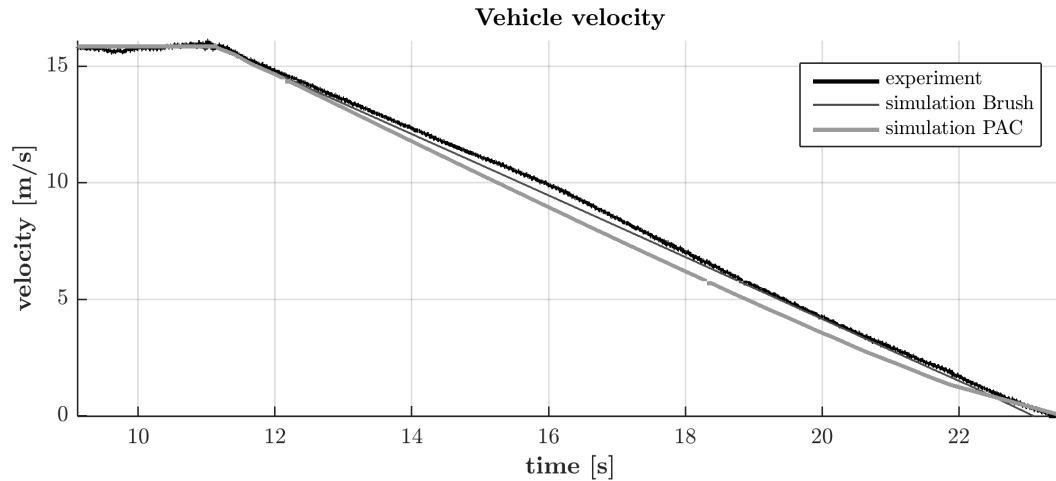


Figure 3.13: *Vehicle velocity under slip control braking on ice.*

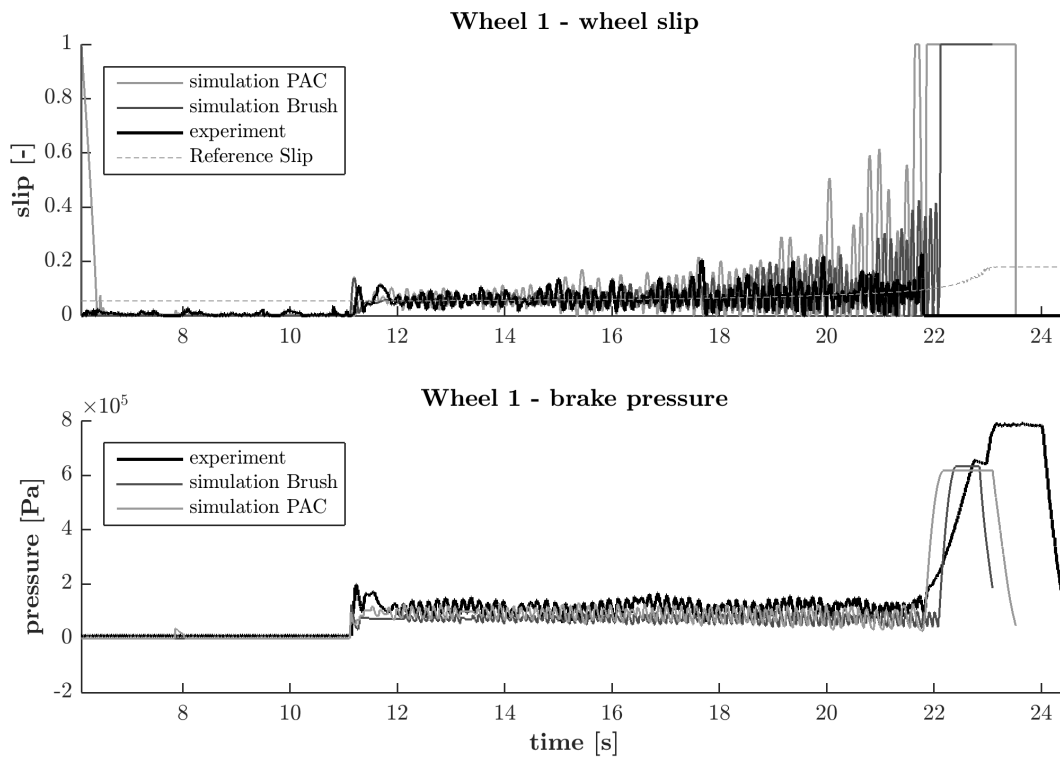


Figure 3.14: *(top) Wheel slip for the Pacejka and Fancher tire model simulation compared to experimental wheel slip. (bottom) Brake pressure for Pacejka and Fancher tire model simulation compared to the actual experimental braking pressure. Wheel 1 is the front axle left hand wheel.*

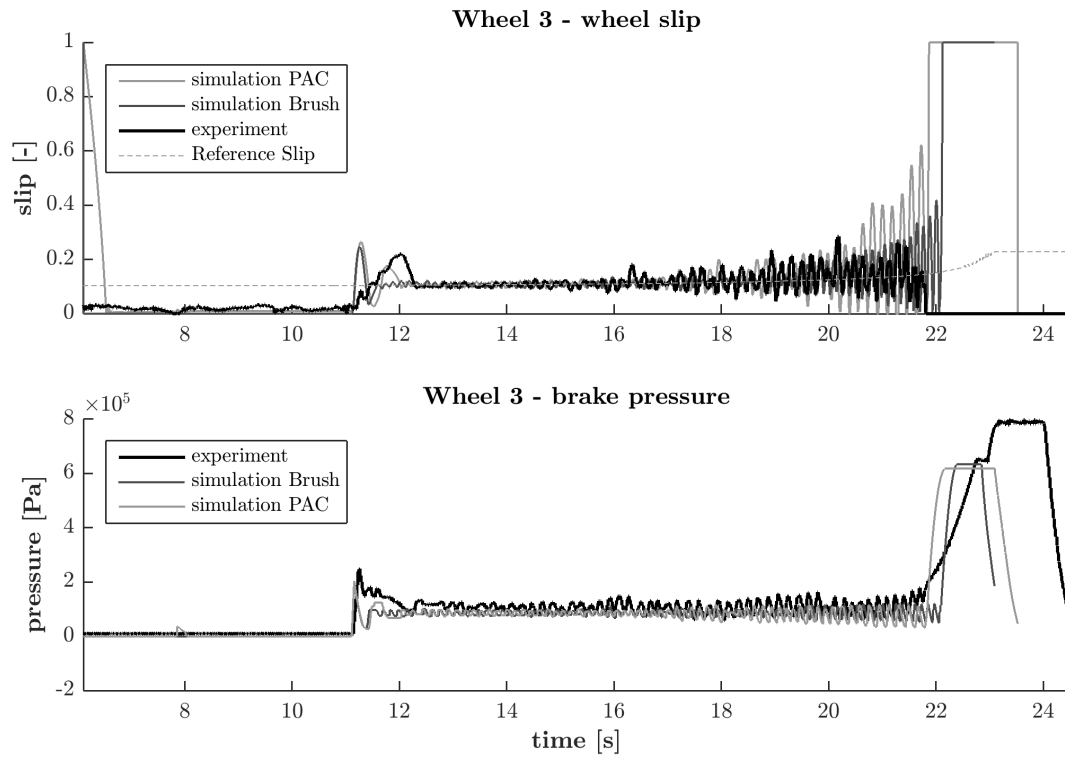


Figure 3.15: *(top)* Wheel slip for the Pacejka and Fancher tire model simulation compared to experimental wheel slip. *(bottom)* Brake pressure for Pacejka and Fancher tire model simulation compared to the actual experimental braking pressure. Wheel 3 is the drive 1 axle left hand wheel.

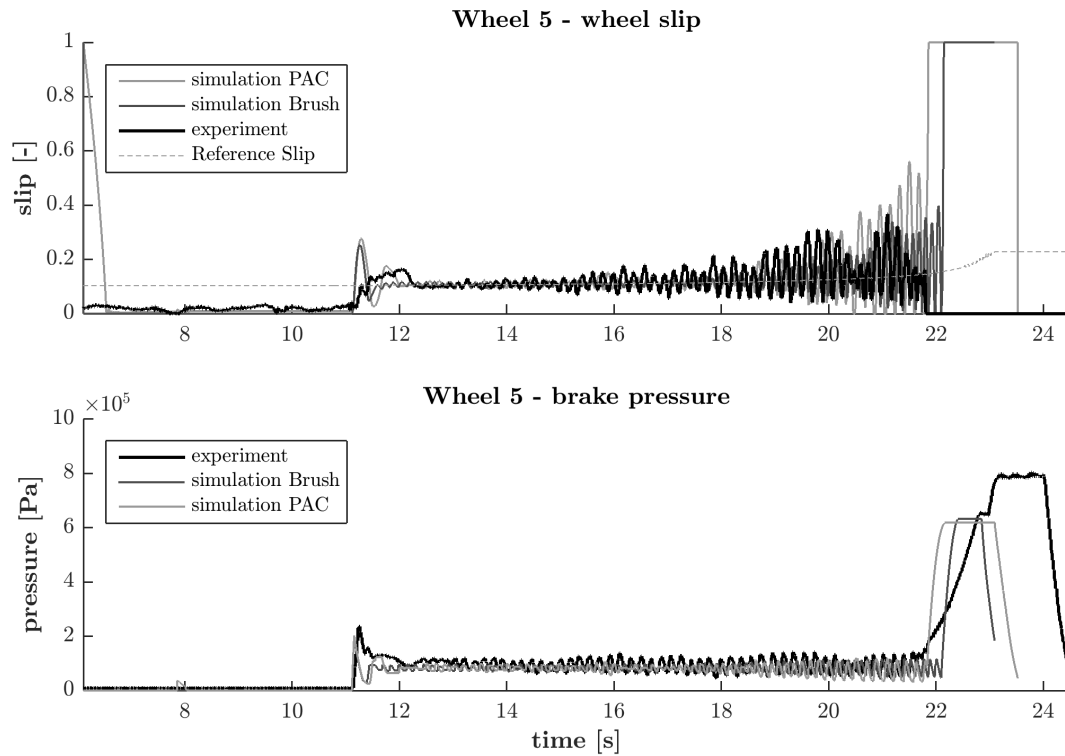


Figure 3.16: *(top)* Wheel slip for the Pacejka and Fancher tire model simulation compared to experimental wheel slip. *(bottom)* Brake pressure for Pacejka and Fancher tire model simulation compared to the actual experimental braking pressure. Wheel 5 is the drive 2 axle left hand wheel.

Straight-Line Braking, Packed Snow

Figure 3.17 shows the speed profiles during braking on packed snow. The observed performance seems similar to that of polished ice, where the speed profile of both simulation brush tire model, as well as simulation Pacejka tire model are similar to that of the experimental data. Note that at lower speeds, a small discrepancy starts to occur.

Figures 3.18, 3.19 and 3.20 show the wheel slip and braking pressure for the simulations on snow. Similar to polished ice situation, at high speeds both models match the experimental data well. At the beginning of the braking cycle, there is however a difference for the Pacejka model simulation, as a peak can be observed in the slip for both drive 1 and drive 2 axles. Again, at the end of the braking cycle, the amplitude of the wheel slip of both models increases more than that of the experimental data, where again the increase of the Pacejka model is even greater.

The brake pressure from both models seems to be slightly lower than that of the experimental data for all wheels.

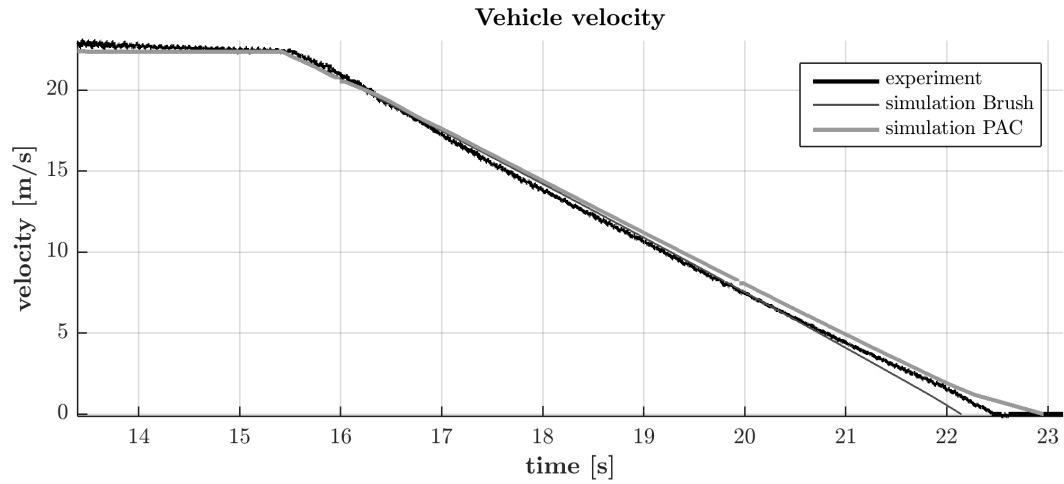


Figure 3.17: *Vehicle velocity under slip control braking on snow.*

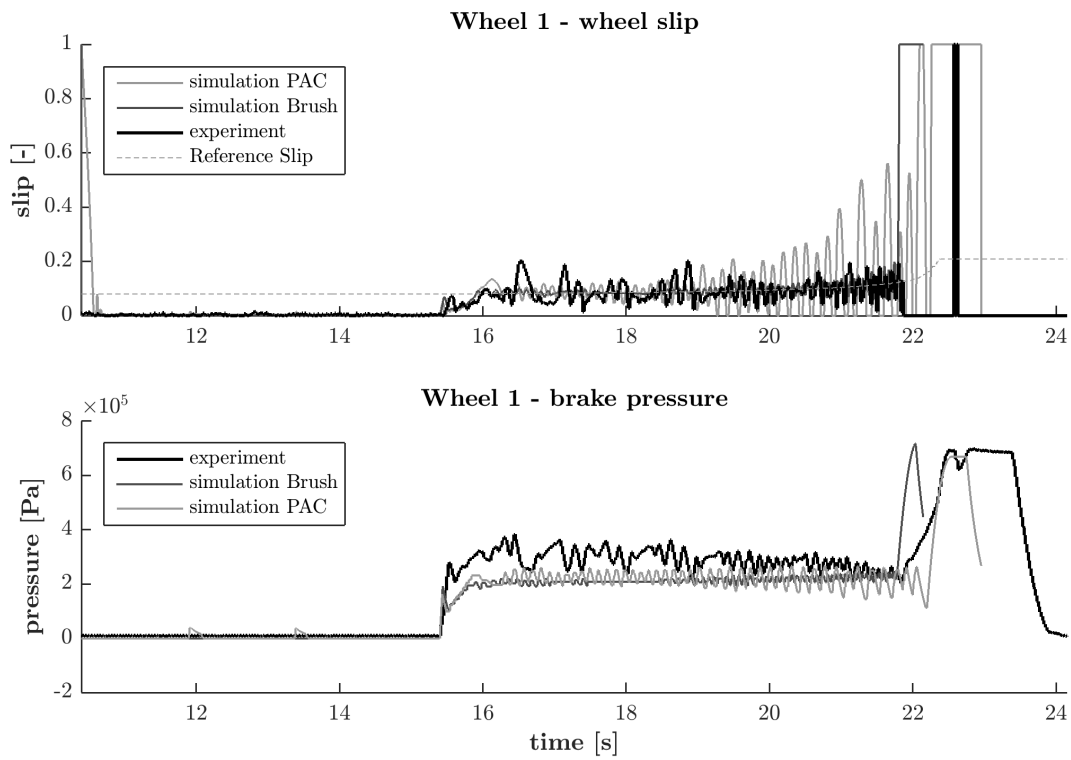


Figure 3.18: *(top) Wheel slip for the Pacejka and Fancher tire model simulation compared to experimental wheel slip. (bottom) Brake pressure for Pacejka and Fancher tire model simulation compared to the actual experimental braking pressure. Wheel 1 is the front axle left hand wheel.*

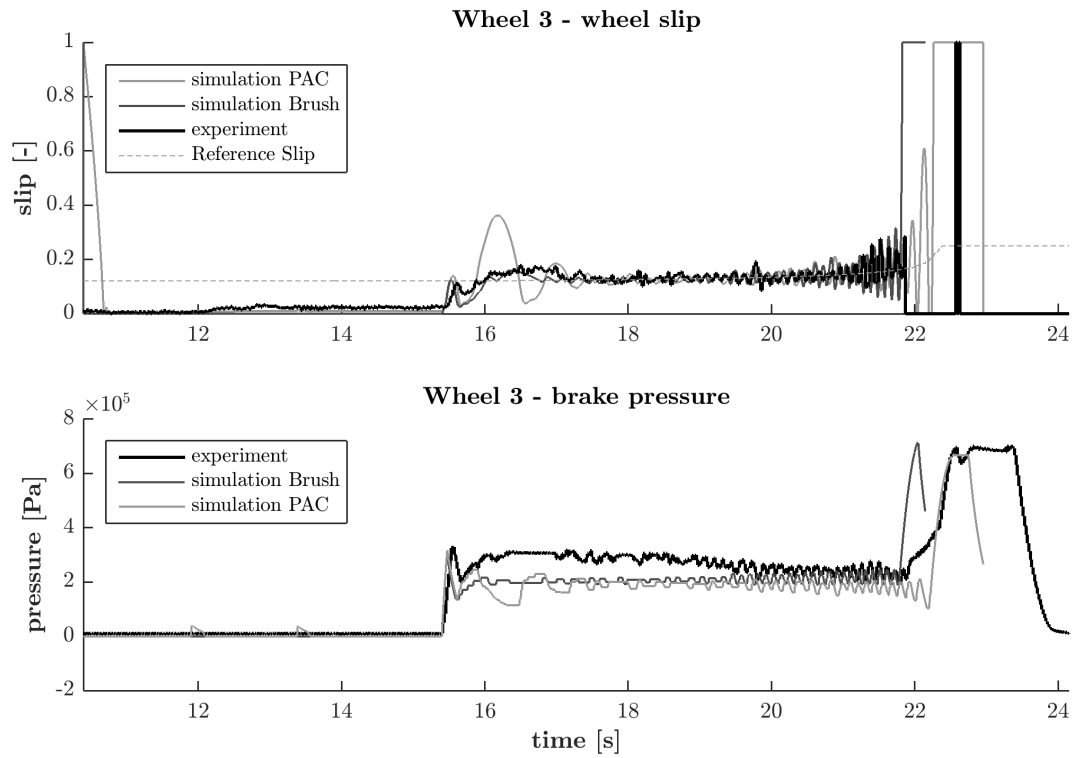


Figure 3.19: *(top)* Wheel slip for the Pacejka and Fancher tire model simulation compared to experimental wheel slip. *(bottom)* Brake pressure for Pacejka and Fancher tire model simulation compared to the actual experimental braking pressure. Wheel 3 is the drive 1 axle left hand wheel.

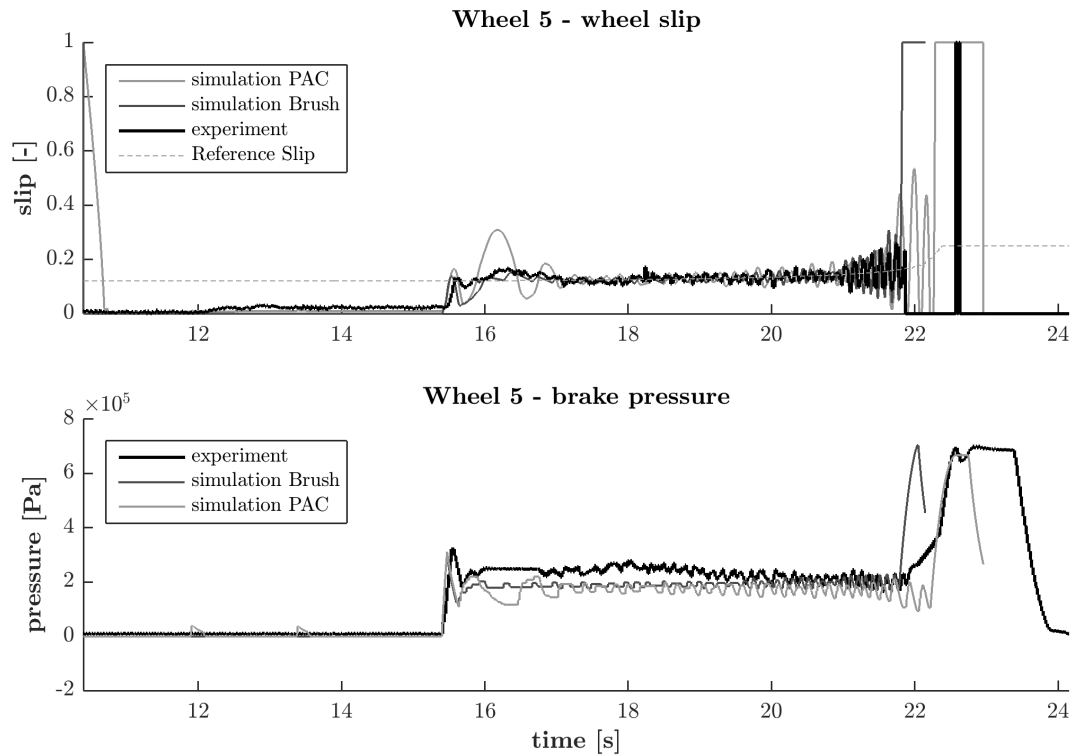


Figure 3.20: *(top)* Wheel slip for the Pacejka and Fancher tire model simulation compared to experimental wheel slip. *(bottom)* Brake pressure for Pacejka and Fancher tire model simulation compared to the actual experimental braking pressure. Wheel 5 is the drive 2 axle left hand wheel.

Straight-Line Braking, Dry Asphalt

Here, Figure 3.21 shows the speed profiles during braking on packed snow. The observed performance seems to differ a little from that of ice, showing that the deceleration of both brush and Pacejka tire model simulations are slightly higher during the first part of the braking maneuver with respect to the experimental data. At some point however, the speed of the Pacejka model simulation starts to match with the experimental data again, where that of the brush model does not.

Again, 3.22, 3.23 and 3.24 show the wheel slip and braking pressure for the simulations, but this time on dry asphalt. However, there is a large discrepancy now between the experimental data and the simulation results. For example, when looking at wheel 1, it can be seen that the slip of the experiment is not able to track the reference signal properly. When looking at the models for wheel 1, the brush model seems to track the reference slip very nicely, but the Pacejka model has a peak in the beginning, and has a rather large amplitude, not tracking the reference slip properly either. This peak at the beginning of the braking maneuver can be seen even more clearly for wheel 3 and wheel 5. For both drive axles however, the tracking of the slip after this peak is better for the Pacejka model.

As a result of the difference in slip, also a difference in brake pressure is present. Since the slip of the experiment is mostly far off for wheel 1, the pressure is increased, whereas this does not happen for the simulations, as they are better able to track the slip. For wheel 3 and wheel 5 the brake pressure is still fairly similar, and even the frequency and the amplitude of the brake pressure signal seem to be comparable.

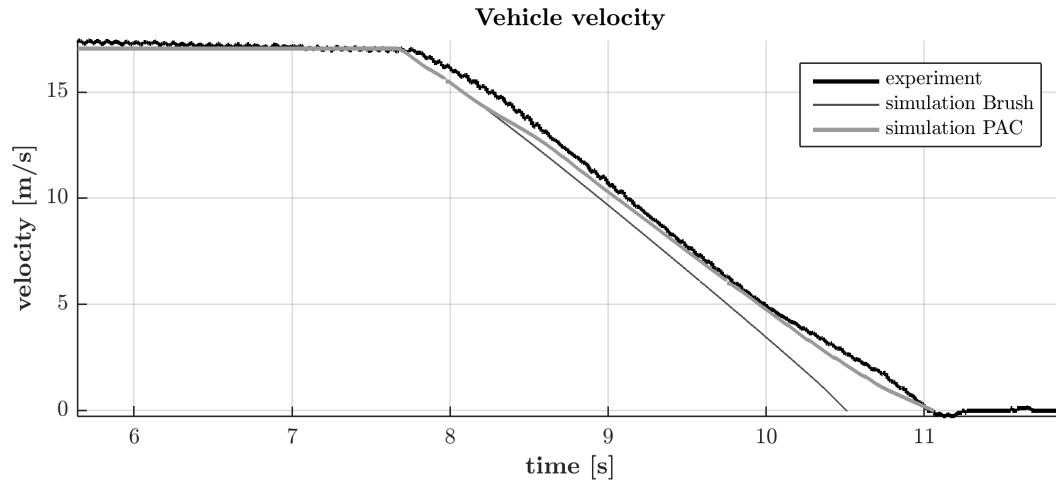


Figure 3.21: *Vehicle velocity under slip control braking on dry asphalt.*

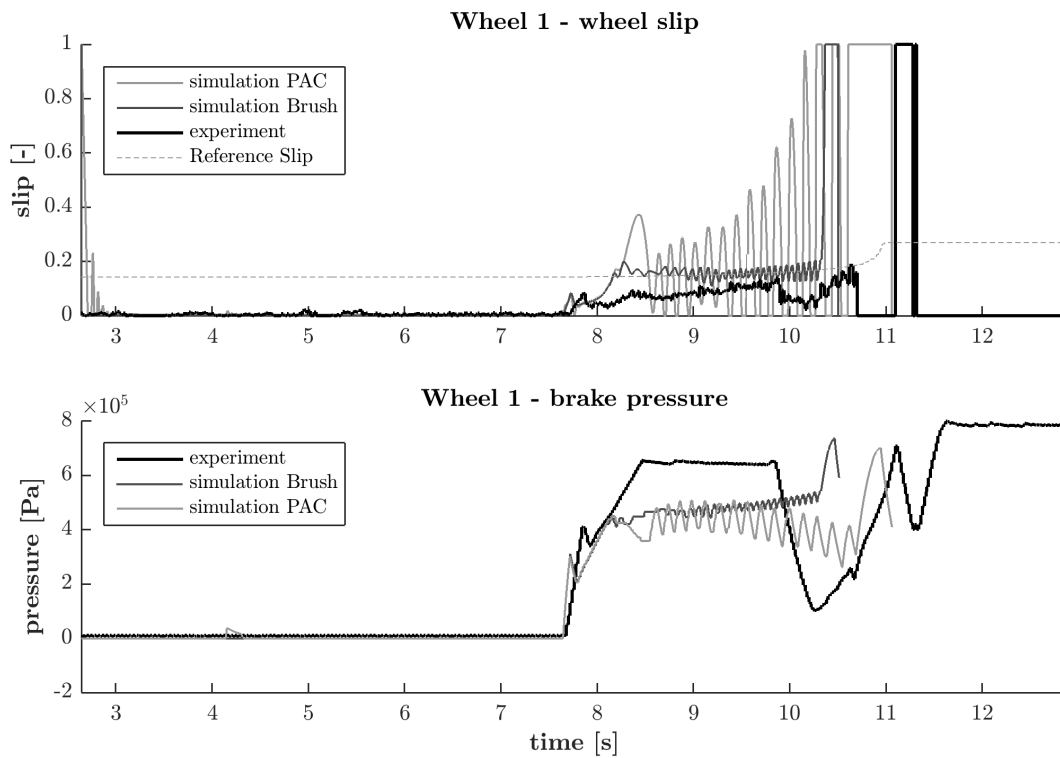


Figure 3.22: *(top) Wheel slip for the Pacejka and Fancher tire model simulation compared to experimental wheel slip. (bottom) Brake pressure for Pacejka and Fancher tire model simulation compared to the actual experimental braking pressure. Wheel 1 is the front axle left hand wheel.*

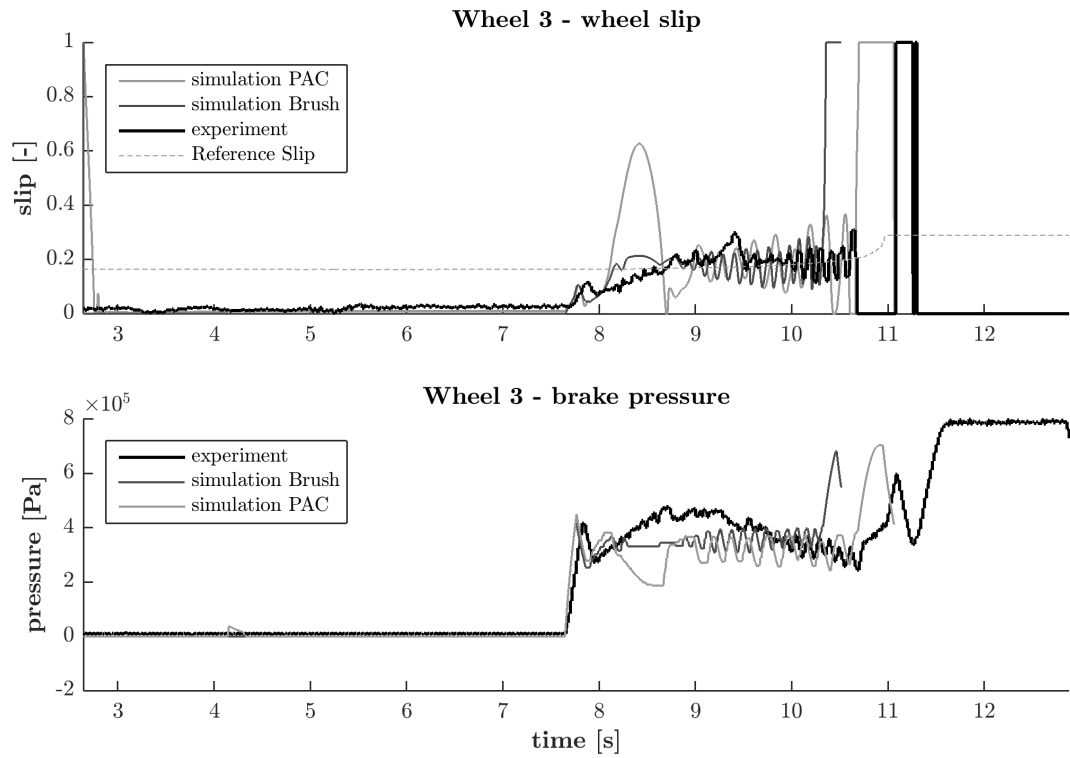


Figure 3.23: *(top)* Wheel slip for the Pacejka and Fancher tire model simulation compared to experimental wheel slip. *(bottom)* Brake pressure for Pacejka and Fancher tire model simulation compared to the actual experimental braking pressure. Wheel 3 is the drive 1 axle left hand wheel.

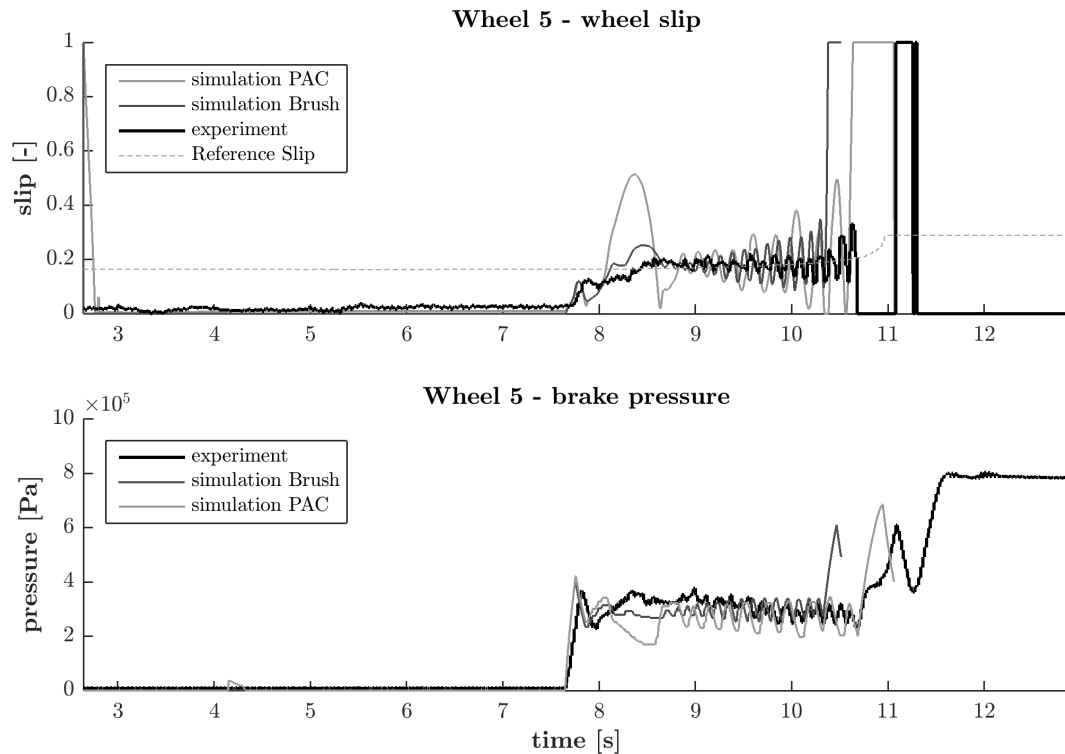


Figure 3.24: *(top)* Wheel slip for the Pacejka and Fancher tire model simulation compared to experimental wheel slip. *(bottom)* Brake pressure for Pacejka and Fancher tire model simulation compared to the actual experimental braking pressure. Wheel 5 is the drive 2 axle left hand wheel.

Brake-In-Turn, Packed Snow

Now, the results are shown for the brake in turn maneuver. The lateral dynamics are introduced by inputting the logged steering signal from the experimental data directly into the VTM. Figure 3.25 shows the velocity profile of the vehicles during the brake-in-turn maneuver. For the first part of braking, it appears that the simulation model has slightly higher deceleration compared to the vehicle of the experimental data. On the other hand, when looking more closely, it seems that the model of the experimental data starts to brake a little later. The overall trend however shows that the simulation model and the vehicle of the experimental data match well enough.

For the brake-in-turn maneuver, all wheels are shown regarding wheel slip and brake pressure in Figures 3.26, 3.27, 3.28, 3.29, 3.30 and 3.31, as it cannot be assumed anymore that the behavior is symmetric. However, it seems that, for every axle, the results of the simulation with the Pacejka tire model matches the experimental data very well. Again, the simulation results of the model show higher amplitude for the slip signal than the one that it can be seen from the vehicle of the experimental data. The brake pressure however is very similar. Both drive 1 and drive 2 axles show excellent resemblance regarding brake pressure and wheel slip. Even a peak in wheel slip, which is observed at the beginning of braking for the experimental data, can be observed in the simulation data, as well. Again, at low speed, the amplitude of the slip signal increases. However, this can also be seen happening especially for the left hand side wheels in the experimental data.

Figure 3.32 shows the lateral acceleration of the simulation and the experiment, where the experimental data are filtered with a low-pass Butterworth filter at one/tenth of the sampling frequency. Apart from the harmonics, it can be seen that the signal is fairly similar regarding the trend, but also in magnitude, e.g. the maximum deceleration. The figure also shows the mean error and the standard deviation between the signals.

Figure 3.33 shows the yaw rate of the experiment and the model. It can be seen that they are fairly similar, apart from the behavior of the model between 11 and 13 seconds. Figure 3.34 shows the sideslip of

both the model and the experiment. Here, it can be observed that for both simulation model and vehicle of the experiment, first positive sideslip occurs, followed by negative sideslip. The difference however, is that positive sideslip is bigger for the model, and negative sideslip is bigger for the experimental truck. The maxima and minima between the simulation model and experimental truck are close however with respect to time.

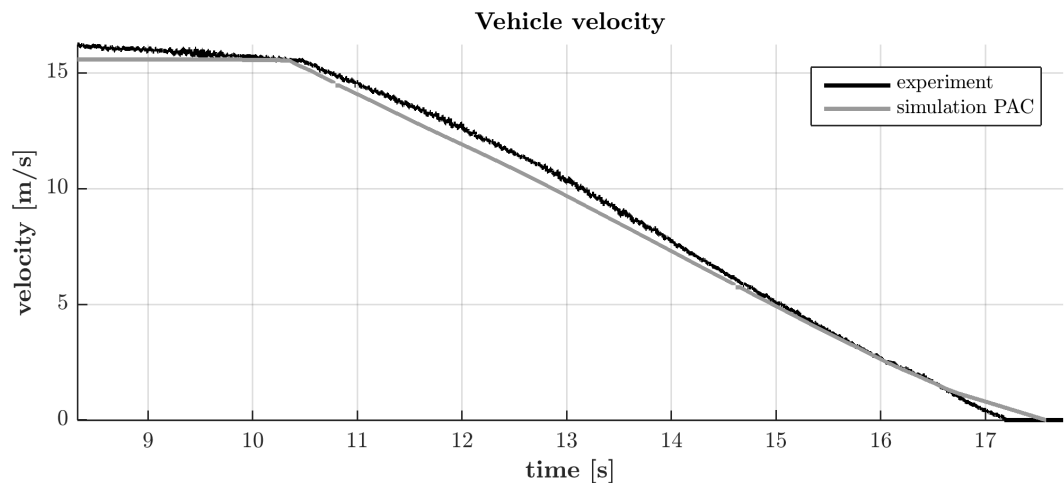


Figure 3.25: *Vehicle velocity during the brake-in-turn maneuver on packed snow.*

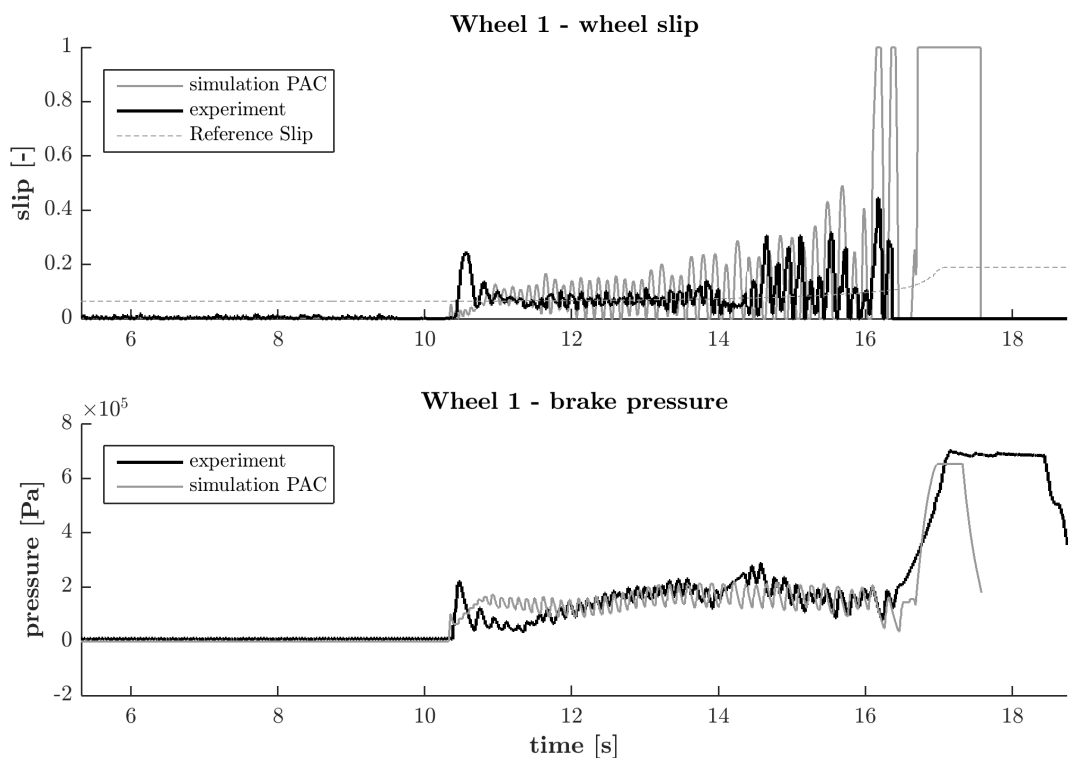


Figure 3.26: **(top)** *Wheel slip for the Pacejka tire model simulation compared to experimental wheel slip.* **(bottom)** *Brake pressure for the Pacejka tire model simulation compared to the actual experimental braking pressure. Wheel 1 is the front axle left hand wheel.*

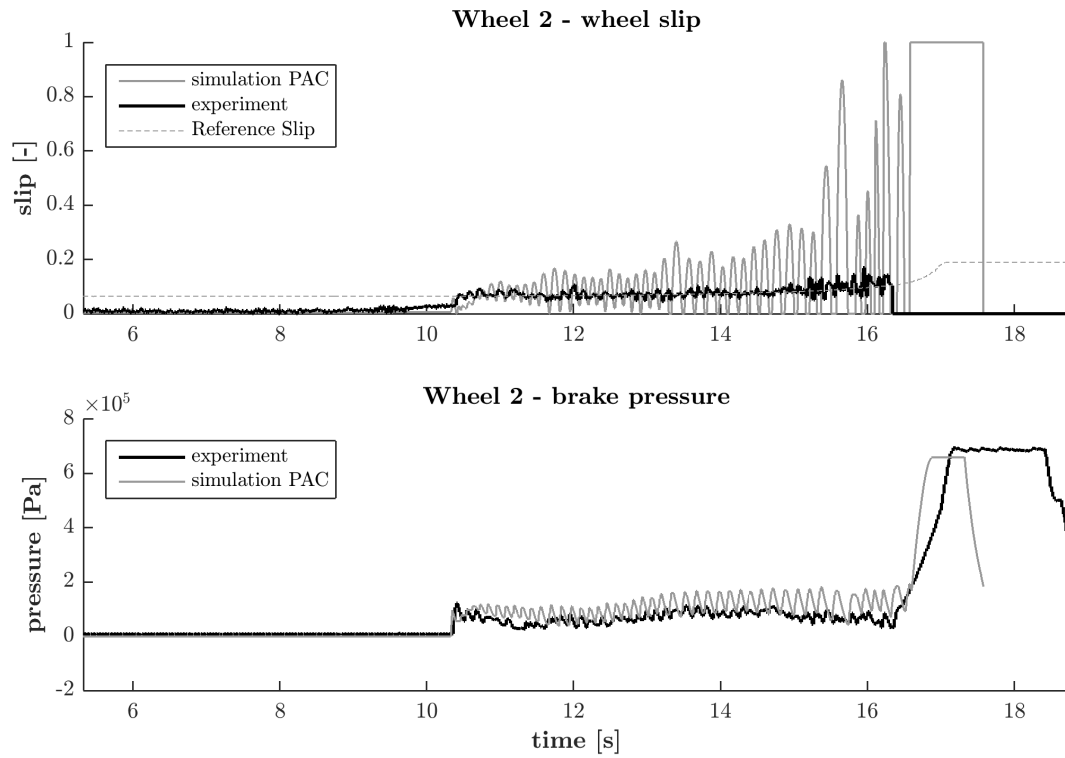


Figure 3.27: *(top)* Wheel slip for the Pacejka tire model simulation compared to experimental wheel slip. *(bottom)* Brake pressure for the Pacejka tire model simulation compared to the actual experimental braking pressure. Wheel 2 is the front axle right hand wheel.

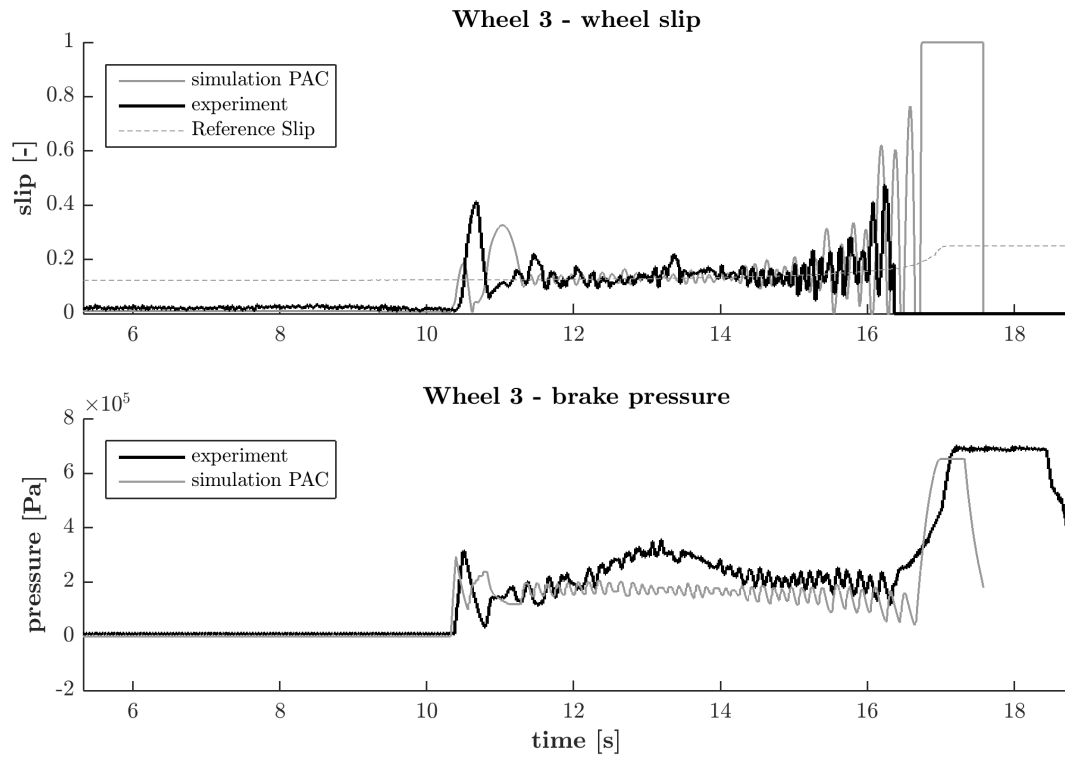


Figure 3.28: *(top)* Wheel slip for the Pacejka tire model simulation compared to experimental wheel slip. *(bottom)* Brake pressure for the Pacejka tire model simulation compared to the actual experimental braking pressure. Wheel 3 is the drive 1 axle left hand wheel.

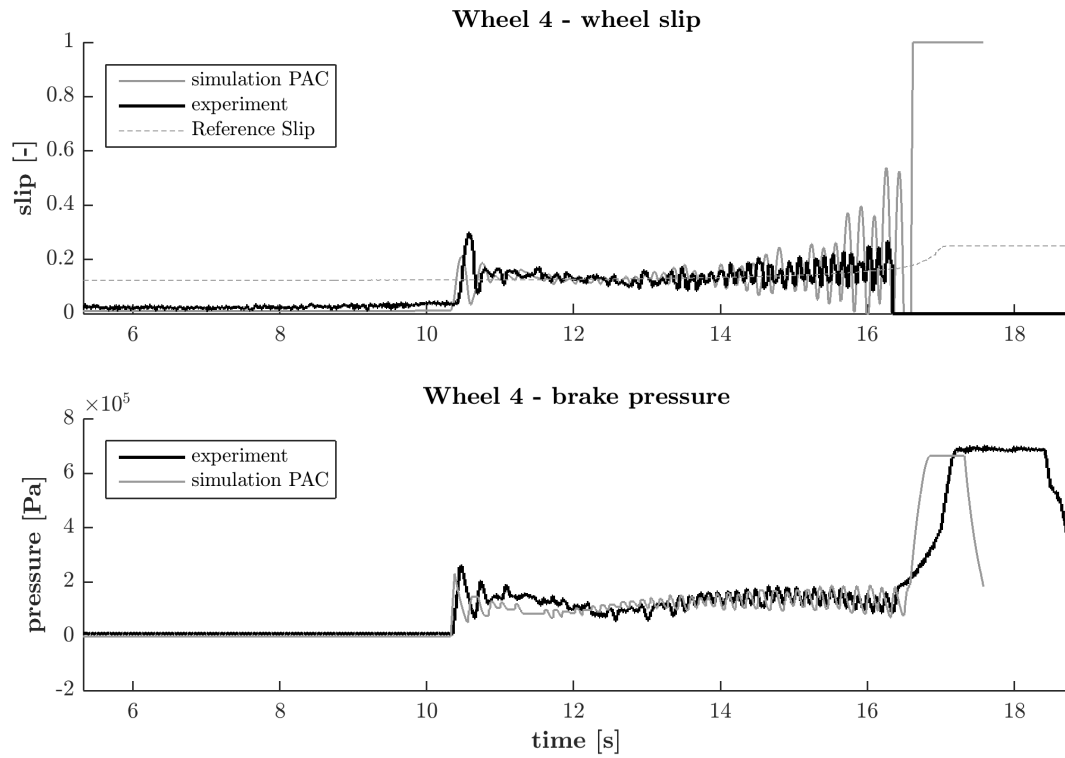


Figure 3.29: *(top)* Wheel slip for the Pacejka tire model simulation compared to experimental wheel slip. *(bottom)* Brake pressure for the Pacejka tire model simulation compared to the actual experimental braking pressure. Wheel 4 is the drive 1 axle right hand wheel.

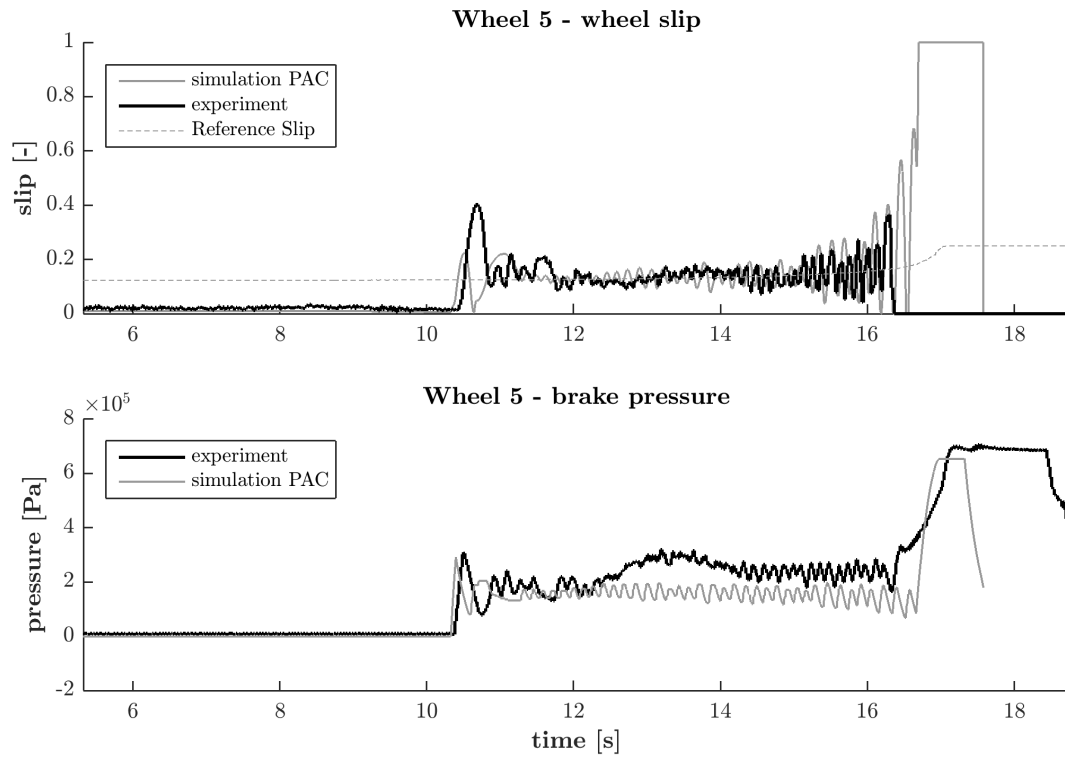


Figure 3.30: *(top)* Wheel slip for the Pacejka tire model simulation compared to experimental wheel slip. *(bottom)* Brake pressure for the Pacejka tire model simulation compared to the actual experimental braking pressure. Wheel 5 is the drive 2 axle left hand wheel.

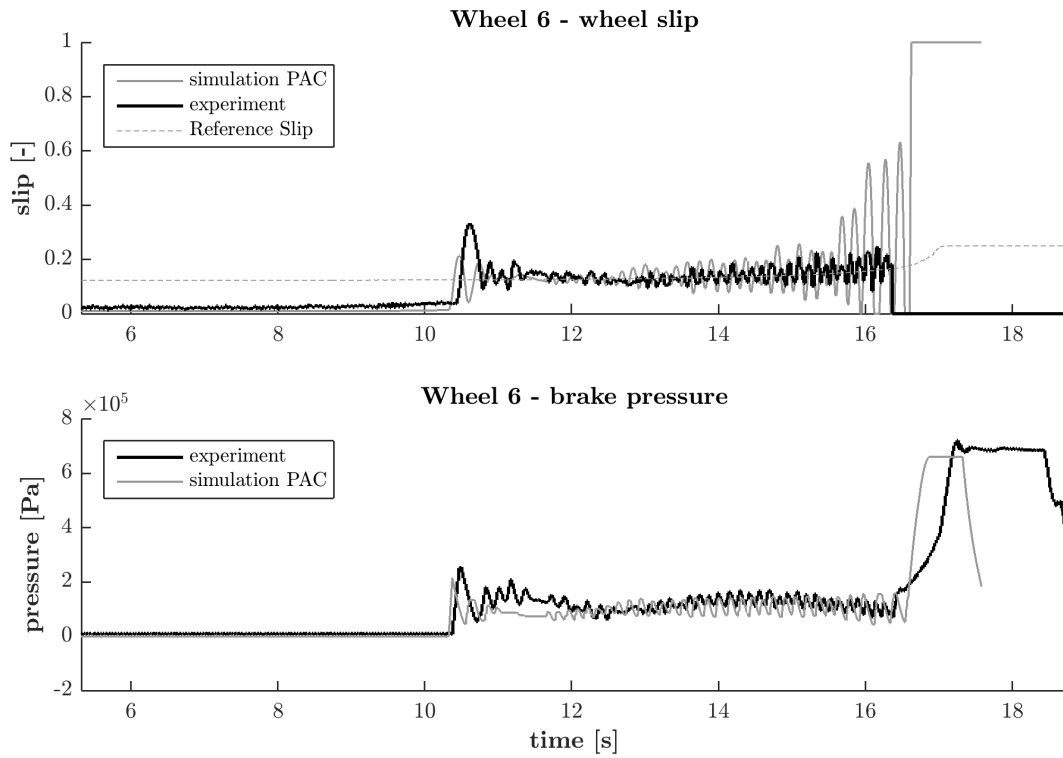


Figure 3.31: *(top)* Wheel slip for the Pacejka tire model simulation compared to experimental wheel slip. *(bottom)* Brake pressure for the Pacejka tire model simulation compared to the actual experimental braking pressure. Wheel 6 is the drive 2 axle right hand wheel.

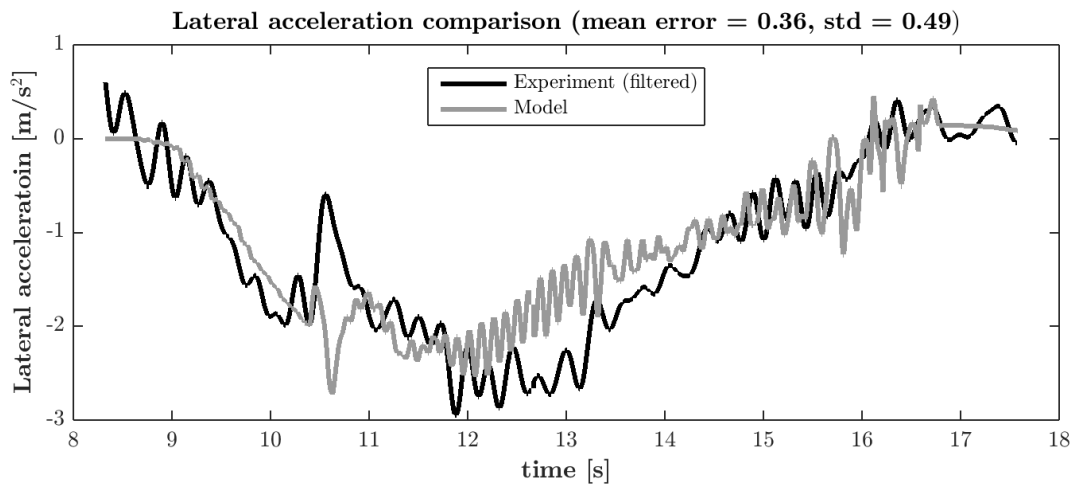


Figure 3.32: Lateral acceleration in the Center of Gravity (CoG) of the model and the experiment (filtered).

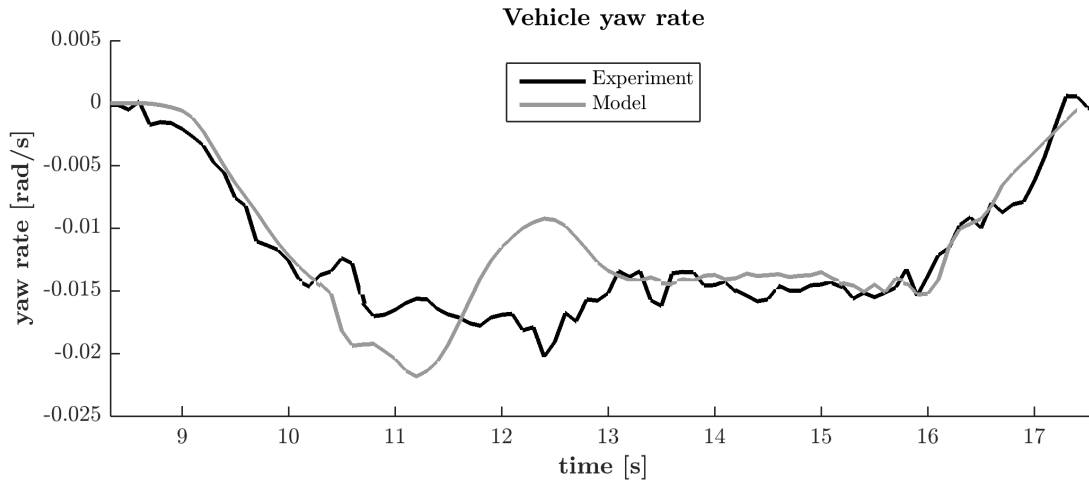


Figure 3.33: Yaw rate of the experiment and the model. Note that the yaw rate model suddenly rises between 11 and 12 seconds.

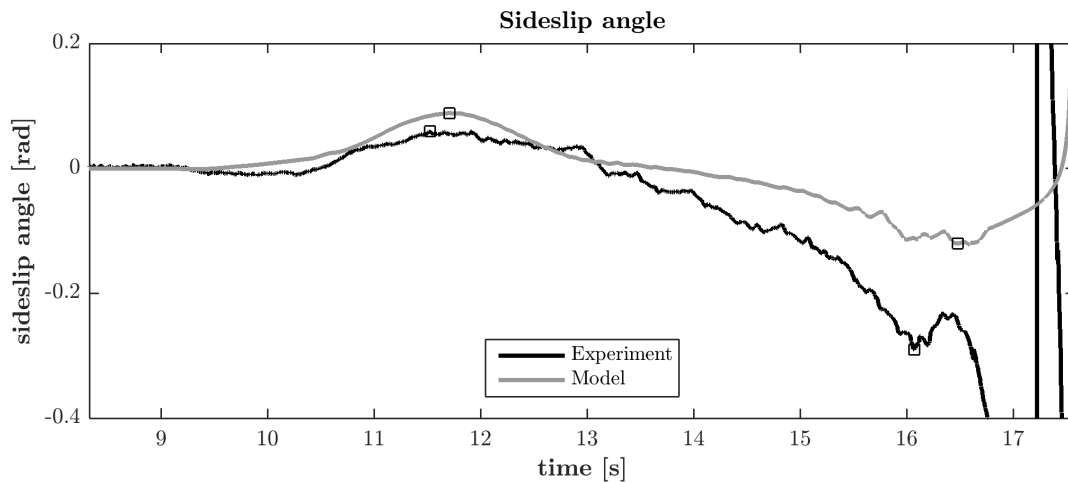


Figure 3.34: Comparison of the sideslip angles. The squares mark the points where sideslip is maximum. Note that the maximum sideslip for the model is bigger than that of the experiment, but the minimum sideslip for the experiment is bigger than that of the model. Here, positive sideslip is associated with oversteer, while negative sideslip is associated with understeer.

Stopping Distance and Deceleration Results

Tables 3.2 and 3.3 show the performance of the VTM compared to the vehicle of the experimental data with respect to stopping distance and deceleration for all four driving cycles. The table data were created by combining the three runs per cycle for all four driving cycles. It can be seen that, except for the deceleration with the brake-in-turn maneuver, all metrics are within 10 % error. Table 3.4 shows the slip averaged over the three runs per experiment per axle, compared to the results from the VTM. It can be seen that, except for the packed snow case, the front axle has a higher error with respect to the experiments.

Table 3.2: Errors in stopping distance between the experiments and the results of the VTM

Braking Test	Condition	Results	Braking Distance [m]	Corrected Braking Distance [m]
Straight-Line 60km/h	Dry Asphalt	Model	28.1718	27.9846
		Experiment	29.5619	29.3588
		Error [%]	-4.7	-4.68
Straight-Line 80km/h	Packed Snow	Model	79.4983	80.6301
		Experiment	75.3055	76.3691
		Error [%]	5.57	5.58
Straight-Line 60km/h	Polished Ice	Model	92.4545	101.3139
		Experiment	100.3358	109.7058
		Error [%]	-7.85	-7.65
Brake-In-Turn 60km/h	Packed Snow	Model	56.5234	63.6136
		Experiment	58.3204	65.6752
		Error [%]	-3.08	-3.14

Table 3.3: Errors in mean deceleration between the experiments and the results of the VTM

Braking Test	Condition	Results	Deceleration [m/s ²]	MFDD [m/s ²]
Straight-Line 60km/h	Dry Asphalt	Model	4.9622	5.2261
		Experiment	5.0396	5.7515
		Error [%]	-1.48	-9.14
Straight-Line 80km/h	Packed Snow	Model	2.9506	3.1656
		Experiment	3.2037	3.3418
		Error [%]	-7.90	-5.27
Straight-Line 60km/h	Polished Ice	Model	1.2758	1.3796
		Experiment	1.2780	1.2964
		Error [%]	-0.17	6.42
Brake-In-Turn 60km/h	Packed Snow	Model	2.1048	2.209
		Experiment	2.3939	2.3628
		Error [%]	-12.08	-6.51

Table 3.4: Errors in slip between the experiments and the results of the VTM for the three different axles.

Braking Test	Condition	Results	Front	Drive 1	Drive 2
Straight-Line 60km/h	Dry Asphalt	Model	0.05	0.05	0.05
		Experiment	0.22	0.13	0.12
		Error	0.17	0.08	0.07
Straight-Line 80km/h	Packed Snow	Model	0.06	0.08	0.08
		Experiment	0.07	0.02	0.2
		Error	0.01	-0.06	-0.06
Straight-Line 60km/h	Polished Ice	Model	0.04	0.03	0.05
		Experiment	0.09	0.04	0.04
		Error	0.05	0.01	-0.01
Brake-In-Turn 60km/h	Packed Snow	Model	0.4	0.04	0.03
		Experiment	0.12	0.05	0.05
		Error	0.08	0.01	0.02

3.4.3 Discussion

The first kind of partial validation showed that the local brake controller block can be configured with a different vehicle plant, and it can produce reasonable outputs. The second kind of partial validation illustrated that the sub-blocks that formulate the local brake controller block are individually validated against winter test data. By taking into account the results of these two kinds of partial validation, it can be said that the local brake controller block has been constructed correctly.

Knowing that the local brake controller block is correct, the next step is complete vehicle validation. The results showed overall good similarity of the experimental results to that of the simulation model. There are however some points that need extra analysis.

In all figures with wheel slip, it could be observed that the wheel slip calculated by the Pacejka tire model and the Fancher tire model had greater magnitude than the wheel slip from the experimental data, especially at lower speeds. There are several reasons for this to happen. One of the most obvious reasons is that the tire models used in the simulation were not set up close enough to the tires used on the real truck. The effects could have been caused by different relaxation length, cornering stiffness and other less prominent tire characteristics. Another possibility is that the slip signal from the experimental data is filtered, as it comes from a wheel speed sensor and it is compared to the vehicle's actual velocity. On the other hand, the trend that the magnitude of the slip goes up at lower speeds is observed for both the models and the experimental data, which suggests that this behavior is at least partly modeled correctly.

For both the polished ice and the packed snow scenario, the wheel slip and brake pressure are very similar for the models and the experimental data. Unfortunately, the same cannot be said for the straight-line braking maneuver on dry asphalt. As a matter of fact, even the experimental data shows that the truck is not able to follow the reference slip correctly for the front axle. That does not explain however the peak observed in the brake pressure for the drive 1 and drive 2 axle in the beginning of the braking cycle (Figures 3.23, 3.24). Even though the Pacejka tire model is probably partly responsible for this behavior, the peak could also be caused by a combination of the tire model and load transfer. Unfortunately, there is no reliable load transfer data available from the experiments, so this presumption cannot be tested. For the front axle, both models have show lower brake pressure than the experimental data. One of the most obvious reasons for this is that the experimental data shows the slip to be quite far off from the reference slip, hence increasing the brake pressure.

For the brake-in-turn maneuver, an interesting contrast can be seen between the left hand side and right hand side slip. For wheel 1, the wheel slip of the experimental data increases toward lower speeds, whereas this almost does not happen for wheel 2. For the Pacejka model, this distinction is not that clear, and the wheel slip increases for both wheels at the end. For the drive 1 axle however, this effect can also be seen for the Pacejka model, showing that the effects of lateral load transfer are captured in the VTM. As the wheel slip of all wheels from experimental data correspond closely to that of the VTM, also the brake pressure is very similar.

Regarding the lateral behavior, the results show good resemblance. The lateral acceleration as shown in Figure 3.32 shows that both the magnitude and the trend of lateral acceleration are very similar. However, looking only at acceleration does not give good insights, when it comes to the lateral performance. For this reason, also the yaw rate and sideslip angle are shown. The yaw rate shows the same magnitude for both the simulation model and the experiment. There is however a slight discrepancy in the trend when looking between 11 and 13 seconds. Here, the behavior of the model shows a rapid increase in yaw rate after which it reverts to behavior similar to that of the experiment again. It is hard to point out what is causing this, but it seems that this is caused by the transition from oversteer to understeer. In this transitional part, the vehicle's dynamic stability is easily influenced, perhaps causing this behavior. The sideslip angle appears to be quite different between the model and the experiment, but the most important trend is captured, as both vehicles go through positive sideslip first, followed by negative sideslip, where the peaks of both appear at roughly the same time. The sideslip angle however is very much dependent on the vehicle parameters, especially again the tire parameters. It is thus probable that the model parameters allow for similar yaw rate, while the sideslip angle is slightly different, due to different lateral friction, cornering stiffness and other variables.

The deceleration and stopping distance performance of the model with the Pacejka tire model compared

to the real vehicle is very good, as most of the metrics are within 10% of error margin. Only the deceleration of the brake-in turn maneuver on packed snow is slightly different, but that is partly because the three sets of experimental data vary more from each other than any of the other tests. The Mean Fully Developed Deceleration shows nonetheless that even the deceleration of the brake-in-turn maneuver is not bad at all compared to the data. Regarding braking distance, all tests are within 8% of error margin, whereas the majority of them actually underestimates the braking distance except for the packed snow test. If more information would have been known about the exact friction coefficient of the surface, this error might have been reduced even further.

The slip error, one of the most important metrics, shows very good results. For polished ice and packed snow, the slip error is very close to that of the experimental data. This holds especially for the drive 1 and drive 2 axles. Even more, for packed snow straight-line braking, the slip error of the VTM is even smaller than that of the experiment for the drive 1 and drive 2 axles. This shows that the VTM is able to approximate the slip with a good enough accuracy.

3.5 Conclusions

In this chapter, the integration of the quarter car model and the VTM has been discussed. Various aspects of the validation have been explained and the results of integration were shown with respect to the experimental data. First, it was shown that the local brake controller block works exactly as it is supposed to do, and that its performance is very similar to the system running on the real truck. Looking at the complete vehicle, when it comes to wheel slip and brake pressure, the model has proven to be sufficiently similar to the real truck. The same holds for the results of its braking performance regarding deceleration and braking distance. The lateral dynamics were also captured reasonably well. However, for development of lateral dynamics functions, the lateral dynamics need to be evaluated further. Altogether, it can be concluded that the performance of the vehicle model with the Pacejka tire model is sufficient for further function development and that the longitudinal dynamics are captured satisfactory.

4 Function Development

With the validated vehicle model and local brake controller, the possibility arises to create new functions to improve the performance of the slip controller. This chapter proposes two methods working together to achieve this goal. First, a method to estimate friction in real-time is described. Using this information, the controller can be optimized, which is described in the second part of this chapter.

4.1 Online Friction Estimation

After the extended literature review about different friction estimation approaches presented in section 2.4, it was decided that the slip-slope based friction estimation method is going to be implemented on the Volvo's transportation model. This method is described extensively in a book and a paper by Rajamani ([65] and [66] respectively), but it was firstly proposed by Gustafsson in 1997 [29] and extended by Wang in 2004 [73] in order to incorporate estimation of the friction coefficient during low-slip and high-slip events.

The main feature of this method is that for the estimation of the tire-road friction coefficient, only longitudinal vehicle dynamics, such as a non-linear longitudinal tire force model and longitudinal motion measurements, are utilized. This friction estimation approach can be used for either accelerating or braking events, provided that the correspondent longitudinal tire force signals, needed for the estimation, are available. In addition, this method can be used for different kinds of vehicle configurations, such as front-wheel drive, rear-wheel drive and all-wheel drive vehicles. The main advantage of this method is that it can provide remarkable friction estimation results for a wide range of slip ratios, and it can be used along with advanced active safety systems, like electronically brake control systems, collision avoidance systems and wheel-slip control systems. Therefore, this method is expected to yield promising results in combination with the Volvo's transportation model, using wheel-slip control braking.

4.1.1 Method

The forces that are generated by the tires during the vehicle's motion have a significant function, since they constitute the only way for the vehicle to obtain information about the ground. Depending on their orientation towards the tire they are acting on, they are characterized as longitudinal (F_x), lateral (F_y) and normal or vertical (F_z) forces. In general the normalized tire force is given by the following formula [65]:

$$\rho = \frac{\sqrt{F_x^2 + F_y^2}}{F_z} \quad (4.1)$$

Since, the friction estimation approach that is implemented on this thesis project utilizes only longitudinal vehicle dynamics, the correspondent normalized tire force becomes:

$$\rho = \frac{F_x}{F_z} \quad (4.2)$$

According to equation 4.1 for a specific F_z acting on a tire, the maximum value of the friction coefficient determines the maximum forces that can be produced by the tire. So, the main purpose of the friction estimation method is to estimate the maximum value of the friction coefficient that the tires can provide.

Figure 4.1 illustrates the relationship between the normalized longitudinal force and longitudinal slip [73].

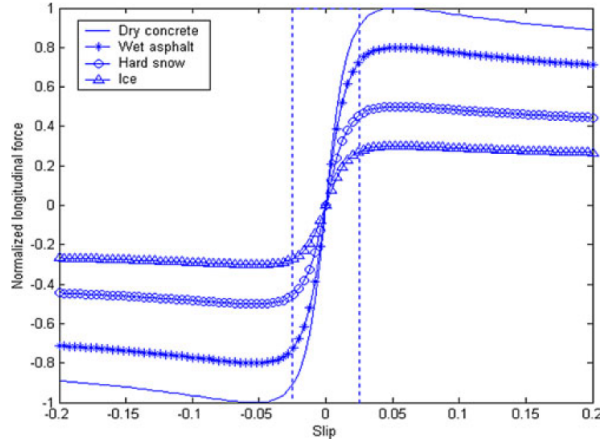


Figure 4.1: *Normalized longitudinal force with respect to longitudinal slip [73]*

Considering equation 4.2 and figure 4.1, it can be said that as long as the slip increases, the longitudinal tire force (F_x) is also increasing, for a specific value of normal load (F_z). At the point that the slip value is optimal for each case, the longitudinal tire force $F_x = \rho F_z$. Obviously when the maximum normalized force $\rho = 1$, then maximum values of both longitudinal and vertical forces can be generated, and this is happening when the slip value is optimal for each case independently. However, when the maximum friction coefficient is less than one, then the maximum longitudinal force that can be generated is considered as a fraction of the normal force [73], [65], [66].

The slip-slope can be defined as the relationship between normalized force (ρ) and slip (λ) at low values of slip [65]. The main concept of the slip-slope based friction estimation approach is to collect the data about the normalized tractive/braking force on the linear part of the slip curve (figure 4.1), and use them in order to discover the linear connection between slip and tire forces (i.e. slip-slope) at low-slip regions. Afterwards, using the slip-slope, the maximum value of the friction coefficient can be found for each surface [73]. However, in literature there is some discrepancy, concerning the opinions of different authors, about the linear relationship between friction coefficient and slip at very low slip values ($\lambda < 0.005$). More specifically, the peak friction coefficient of the analytical brush tire model which is presented in [56] does not vary with respect to the slip-slope, and hence, the slip-slope based friction estimation method cannot predict the friction coefficient at very low-slip regions.

As it has already been explained, independently on the kind of surface and the normal force acting on an individual tire, at low-slip levels, the normalized longitudinal force of each tire is proportional to its slip. This linear relationship is illustrated by the following formula:

$$\rho = \frac{F_x}{F_z} = K\lambda \quad (4.3)$$

where K is the slip-slope. The K -values can be used for estimating the tire-road friction coefficient, according to the road surface conditions.

The slip-slope based friction estimation method has a different implementation on high levels of slip. More specifically, at high values of slip, the normalized longitudinal force becomes constant and is independent on the slip. The constant value of the normalized longitudinal force is a function of the friction coefficient. Therefore, when the tire is modeled at high slip levels, the constant value of the normalized longitudinal force is independent on the tire-road friction coefficient [65].

The equation 4.3 can be rewritten in a standard parameter identification format as:

$$y(t) = \phi^T(t)\theta(t) \quad (4.4)$$

where

$$y(t) = \frac{F_x}{F_z} \quad (\text{system output}) \quad (4.5)$$

$$\theta(t) = K \quad (\text{unknown parameter}) \quad (4.6)$$

$$\phi(t) = \lambda \quad (\text{system input}) \quad (4.7)$$

As it can be seen by equations 4.5 and 4.7, the system's input is the longitudinal slip, while the system's output is the normalized longitudinal force. The unknown parameter K (equation 4.6) can be estimated using parameter identification techniques in real time, and afterwards it can be used for the real time estimation of the friction coefficient. However, this parameter identification format presented by equations 4.4, 4.5, 4.6 and 4.7 is valid only at low-slip regions, where the normalized longitudinal tire force is proportional to the slip of the tire. On high slip levels of the tire, the slip-slope based friction estimation method cannot provide reasonable results, concerning the prediction of the friction coefficient. However, during hard braking events, where the slip levels of the tire are quite high, the normalized longitudinal braking force (ρ) can be used directly to provide information about the friction coefficient. This can be done by using the standard parameter identification format, introduced by the equation 4.4, with different variables, when it comes to system inputs, system outputs and unknown parameters. The new variables to the system are presented below:

$$y(t) = F_x \quad (\text{system output}) \quad (4.8)$$

$$\theta(t) = \mu \quad (\text{unknown parameter}) \quad (4.9)$$

$$\phi^T(t) = F_z^T = F_z \quad (\text{system input}) \quad (4.10)$$

As it can be seen by equations 4.8, 4.9 and 4.10, at high levels of slip, the system's input is the measured longitudinal tire force, the system's output is the normal force, while the unknown parameter will be the estimated friction coefficient.

4.1.2 Recursive Least-Squares (RLS) Identification

The standard parameter identification format introduced by equation 4.4 can be altered to the following slightly different parameter identification form in order to be used by the RLS algorithm [66]:

$$y(t) = \phi^T(t)\theta(t) + e(t) \quad (4.11)$$

where, $\theta(t)$ is the vector of the estimated parameters, $\phi(t)$ is the input regression vector, and $e(t)$ is the identification error between the measured $y(t)$ and estimated value $\phi^T(t)\theta(t)$.

Using the RLS algorithm presented in [39], [30] and [68] on equation 4.11, it is possible to iteratively update the unknown parameter vector $\theta(t)$, at each sampling time, using the past input and output data contained within the regression vector $\phi(t)$. The RLS algorithm updates unknown parameters (K or μ) in order to minimize the sum of the squares of the modeling errors [66].

Two ways of implementing the RLS method using the System Identification Toolbox software of MatLab were investigated on this thesis project. One method used the forgetting factor λ adaptation algorithm and the other the Kalman filter adaptation algorithm.

The steps of the RLS method using the forgetting factor λ adaptation algorithm are illustrated below:

Step 1: Measure the system output $y(t)$ and calculate the regression vector $\phi(t)$.

Step 2: Calculate the identification error $e(t)$, which is the difference between system's actual output at this sample and the predicted model output obtained from the estimated parameters in previous sample $\theta(t-1)$, i.e.

$$e(t) = y(t) - \phi^T(t)\theta(t-1) \quad (4.12)$$

Step 3: Calculate the update gain vector $K(t)$, i.e.

$$K(t) = \frac{P(t-1)\phi(t)}{\lambda + \phi^T(t)P(t-1)\phi(t)} \quad (4.13)$$

and calculate the covariance matrix $P(t)$, i.e.

$$P(t) = \frac{1}{\lambda} \left[P(t-1) - \frac{P(t-1)\phi(t)\phi^T(t)P(t-1)}{\lambda + \phi^T(t)P(t-1)\phi(t)} \right] \quad (4.14)$$

Step 4: Update the parameter estimate vector $\theta(t)$, i.e.

$$\theta(t) = \theta(t-1) + K(t)e(t) \quad (4.15)$$

The λ parameter of equations 4.13 and 4.14 is called the forgetting factor and it is mainly used in order to determine the influence of the previewed data to the current estimation (avoid covariance wind-up problem). The value of λ varies between 0.9 and 1 and it uses a batch of $N = \frac{2}{1-\lambda}$ data to update the current estimation [30]. There is trade-off between the immunity to noise of the RLS algorithm and its ability to detect changes in parameter values quickly. More specifically, when λ value is close to 0.9 the sensitivity of the estimation procedure to noise will increase, (the parameters will turn to be more oscillatory), but the convergence will be fast. On the other hand, when the forgetting factor is close to 1, the convergence will be slow, since the algorithm will use all the previews data from the initialization of the simulation to update the estimate [65].

The implementation of the RLS method using the Kalman filter adaptation algorithm is slightly different in comparison with the correspondent method of the forgetting factor, when it comes to the step 3 (i.e. update of the gain vector $K(t)$ and calculation of the covariance matrix $P(t)$), mentioned earlier about using RLS method with the forgetting factor, as well as to its tuning parameter. Nevertheless, the rest of the procedure when it comes to implementation of the Kalman filter adaptation algorithm is similar to the one using the forgetting factor algorithm, i.e. same enabling condition, same equations, written in standard parameter identification format, and same switching condition, when it comes to which method should be chosen by the algorithm, according to the slip level.

The steps of the RLS method using the Kalman filter adaptation algorithm are illustrated below:

Step 1: Measure the system output $y(t)$ and calculate the regression vector $\phi(t)$.

Step 2: Calculate the identification error $e(t)$, which is the difference between system's actual output at this sample and the predicted model output obtained from the estimated parameters in previous sample $\theta(t-1)$, i.e.

$$e(t) = y(t) - \phi^T(t)\theta(t-1) \quad (4.16)$$

Step 3: Calculate the update gain vector $K(t)$, i.e.

$$K(t) = \frac{P(t-1)\phi(t)}{R_2 + \phi^T(t)P(t-1)\phi(t)} \quad (4.17)$$

and calculate the covariance matrix $P(t)$, i.e.

$$P(t) = P(t-1) + R_1 - \frac{P(t-1)\phi(t)\phi^T(t)P(t-1)}{R_2 + \phi^T(t)P(t-1)\phi(t)} \quad (4.18)$$

Step 4: Update the parameter estimate vector $\theta(t)$, i.e.

$$\theta(t) = \theta(t-1) + K(t)e(t) \quad (4.19)$$

The Kalman filter adaptation algorithm considers that the true parameters $\theta(t)$ are described by a random walk [11]:

$$\theta(t) = \theta(t-1) + w(t) \quad (4.20)$$

where $w(t)$ is the Gaussian white noise with the following covariance matrix:

$$R_1 = E[w(t)w^T(t)] \quad (4.21)$$

R_2 is the variance of innovations $e(t)$ in the equation 4.11.

4.1.3 Parameter Initialization and Conditions for the RLS algorithms

As it has already been explained in subsection 4.1.1 and according to [73] the RLS algorithm cannot provide an accurate friction coefficient estimate if the measured longitudinal acceleration is less than 0.3 m/s^2 and measured slip is less than 0.005. Therefore, the aforementioned conditions have been incorporated to the friction estimation model architecture of VTM along with two more conditions in order for the enabling of the friction estimation algorithm to be determined. More specifically, the friction estimation algorithm works only when the requested pressure demand signal P_{dem} is higher than 1 bar and the longitudinal force has positive value (positive values of the longitudinal force mean braking longitudinal forces). The last two enabling conditions of the RLS algorithm have been set in order to avoid some initial strange behavior of the longitudinal braking force, coming from the tire model of the VTM.

One important addition that has been made to the RLS algorithm is that when the excitation of the tire forces are not high enough for the algorithm to give a proper friction coefficient estimate (i.e. some of the enabling conditions of the RLS algorithm are not satisfied), then the algorithm will keep the previous value of the estimate in order to avoid abnormalities of its behavior.

As it has already been explained in subsection 4.1.2 the influence of the forgetting factor plays an important role when it comes to the estimation of the friction coefficient. Hence, according to the needs for precision on the friction coefficient estimate, when it comes to the Simulink model, along with the suggestions made by [73] and [66], the forgetting factor was set to be 0.995.

Using the Kalman filter adaptation algorithm, it is assumed that R_2P is the covariance matrix of the estimated parameters, and $\frac{R_1}{R_2}$ is the covariance matrix of the parameter changes. R_1 is the noise covariance matrix specified by the user. In this simulation model the noise covariance matrix was chosen to have a very small value, i.e. $1e-03$, but not zero. Zero value in the noise covariance matrix can be translated to estimation of constant coefficients, while values larger than zero correspond to time-varying parameters. Large values of the noise covariance matrix correspond to rapidly changing parameters [47]. It is important to note that during the implementation of this algorithm the R_1 and $P(t=0)$ matrices are scaled such that $R_2 = 1$, however, this scaling does not affect the parameter estimates. The forgetting factor algorithm for $\lambda = 1$ is equivalent to the Kalman filter algorithm with $R_1 = 0$ and $R_2 = 1$.

As it has been already explained in subsection 4.1.1, at low-slip region the friction coefficient varies proportionally with the slip-slope. According to Rajamani [65], [66], this linear relationship was found experimentally and it can be expressed as:

$$\mu = AK + C \quad (4.22)$$

where K is the slip-slope, A is the proportionality constant and C is a bias constant. The proportionality constant A of the equation 4.22 is the same for all different kinds of surfaces, but it is different, when it comes to the chosen tire model, according to [66]. In the case of the model that it was used for simulation, the proportionality constant A were found to be 0.025 through trial and error, while there were no bias constant, hence, C constant was set to be 0.

At this point it should be also mentioned that the switching condition for determining when the algorithm will estimate the friction coefficient using the method, described for low levels of slip (subsection 4.1.1), or the method, described for high levels of slip (subsection 4.1.1), has been created according to the measured slip signal. More specifically, when the longitudinal measured slip is less than 0.025, the algorithm assumes that there is a linear relationship between the friction coefficient and the longitudinal slip, hence, it uses the slip-slope based friction estimation method for the estimation of the friction coefficient. On the other hand, when the slip is higher than 0.025, there is no linear relationship between the longitudinal slip and the friction

coefficient, and the normalized longitudinal force can be used directly to provide the correct estimate about the friction coefficient, using the correspondent method.

4.1.4 Input and Output Signals of the Friction Estimator

In order for the friction estimator block to be able to work properly and give reasonable estimates about the friction coefficient, it has to use proper input signals. The signals that are needed from the friction estimator are depicted in the figure below:

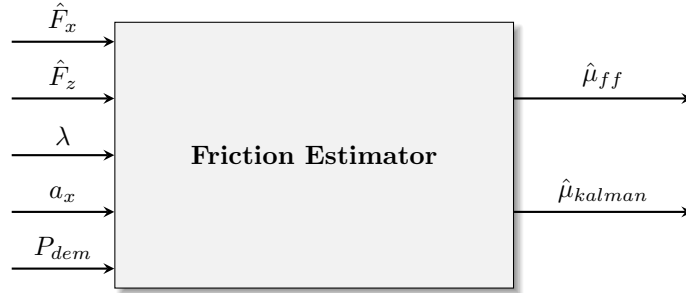


Figure 4.2: *Friction Estimator block diagram*

The signal of the estimated longitudinal tire force (\hat{F}_x) is coming from the longitudinal force observer, which has been described in subsection 3.1.2. As it has already been said, the longitudinal tire force has been used for the enabling condition of both forgetting factor and Kalman filter adaptation algorithms, and positive longitudinal force is perceived as braking force in the Simulink model.

The signal of the estimated normal force (\hat{F}_z) is coming from the normal force observer, which uses sensor signals of longitudinal and lateral acceleration, as well as a vector of axle mass distribution in order to estimate the normal force on each wheel. The estimated normal force is calculated using the static normal force distribution and the dynamic change on normal force due to longitudinal acceleration, dependent on wheelbase and vehicle configuration. And that is the reason why the dynamic change of the normal force has been tuned due to its dependence on the vehicle's wheelbase and configuration. The tuning of the normal force estimator has been done in order for the behavior of the normal forces per wheel, coming from the normal force estimator block, to match the behavior of the normal forces per wheel, estimated by VTM. Three different kinds of surface were tested, i.e. dry asphalt, packed snow and polished ice, during the tuning of the normal force estimator.

The signals of driver demand pressure (P_{dem}) and longitudinal acceleration (a_x) are derived by controllers/users and the correspondent sensors respectively. Both of them are used for setting the enabling conditions inside the friction estimator block.

The slip signal is used for many reasons inside the friction estimator block, as it has already been explained in subsections 4.1.1 - 4.1.3. Therefore, its quality should be paramount in order to be able to give a good estimate about the friction coefficient when it is used. Unfortunately, the calculated slip signal used during friction estimation presented some harmonics with a specific frequency, and during hard braking events, the longitudinal tire slip was too often equal to zero. That phenomenon caused problems during the operation of the RLS algorithm, since the longitudinal slip is used not only for the enabling condition of the algorithm, but also as a switching condition, in order to distinguish effectively which friction estimation method is going to be used according to the slip level, as well as a regression vector for estimating the friction coefficient using the slip-slope based method. Therefore, in order to improve the signal of the longitudinal tire slip a first-order filter has been designed, with the goal of removing the harmonics behavior of the signal, given by:

$$\frac{1}{\tau s + 1}. \quad (4.23)$$

When it comes to the outputs of the friction estimator, i.e. the estimated friction coefficient using the forgetting factor adaptation algorithm ($\hat{\mu}_{ff}$) and the estimated friction coefficient using the Kalman filter adaptation

algorithm ($\hat{\mu}_{kalman}$), it can be said that both of them can be used for further function development like slip controller optimization and so on.

4.2 Slip Controller Optimization

With the ability to get information about the tire-road friction coefficient, control systems throughout the vehicle could be improved, resulting in better vehicle performance. When it comes to the sliding mode controller, using information about the road-tire friction coefficient can lead to improved braking performance regarding both braking distance and air usage.

During the winter testing experiments, both the reference slip signal λ_{ref} and the sliding mode controller switching gain k_s were varied per surface condition as mentioned in table 3.1. This difference per road surface leads to the assumption that per road condition, different controller parameters are needed for optimal performance.

4.2.1 Reference Slip

The reference slip is used as control signal by the sliding mode controller. As mentioned in 2.2.2, controlling around the peak reference slip ensures best braking performance regarding maximum friction utilization. Using the Pacejka tire model from the VTM, Figure 4.3 shows the friction curves for the front axle of the 8x4 truck model used in this thesis project.

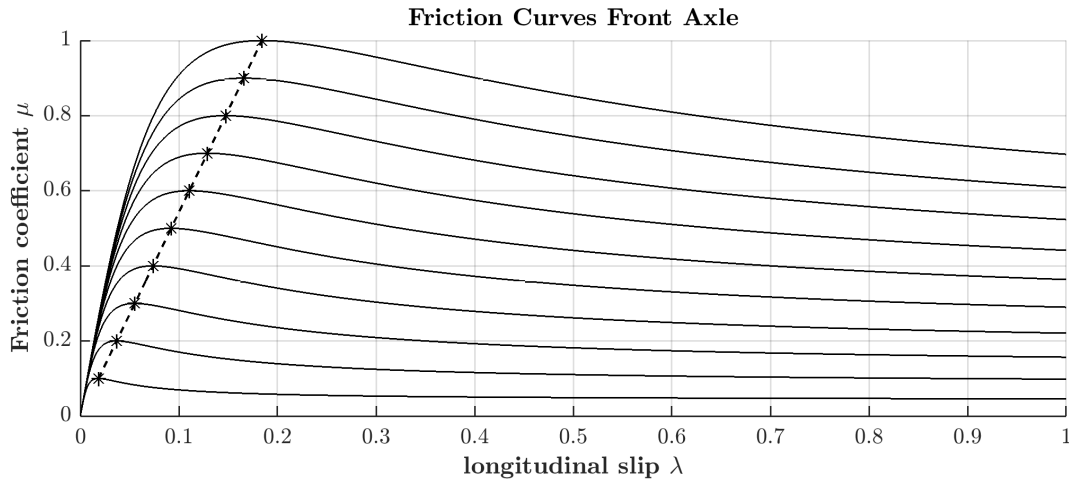


Figure 4.3: *Friction curves for different road surfaces using the Pacejka tire model. The dotted line represents the slip for the maximum friction coefficients.*

The function

$$\lambda_{ref} = f(\hat{\mu}) \quad (4.24)$$

is proposed to solve this optimization. As the tire data is known in advance for the Pacejka tire model in the VTM, its peak slip values can be used to create a lookup table. This lookup table can also be created using measured data from the tire on the real truck. If such data is not available, the Pacejka tire model is expected to represent the real tire sufficiently to give better results using the combination of the above mentioned lookup table and online friction estimation.

4.2.2 Switching Gain

The switching gain k_s plays a major role on the performance of the sliding mode controller. As can be seen in table 3.1, the value of this parameter varies around 60,000 for different surfaces. The influence of k_s on a specific surface can be seen in Figure 4.4. This figure shows the air usage and braking distance, which both constitute important braking performance metrics. There appears to be a conflict between braking distance and air usage. For low values of the switching gain, the controller allows for little extra air usage, increasing the

braking distance. But for increasing switching gain, more air is used. For the highest region of switching gain, the control uses a lot of air to minimize the error between slip and reference slip, but the pressure is increased so much each time that slip just increases more with respect to the reference slip. This last effect is also known as chatter. A subjective optimal point can be found where both braking distance and air usage are relatively good. It is however very difficult to define a cost function using these two variables.

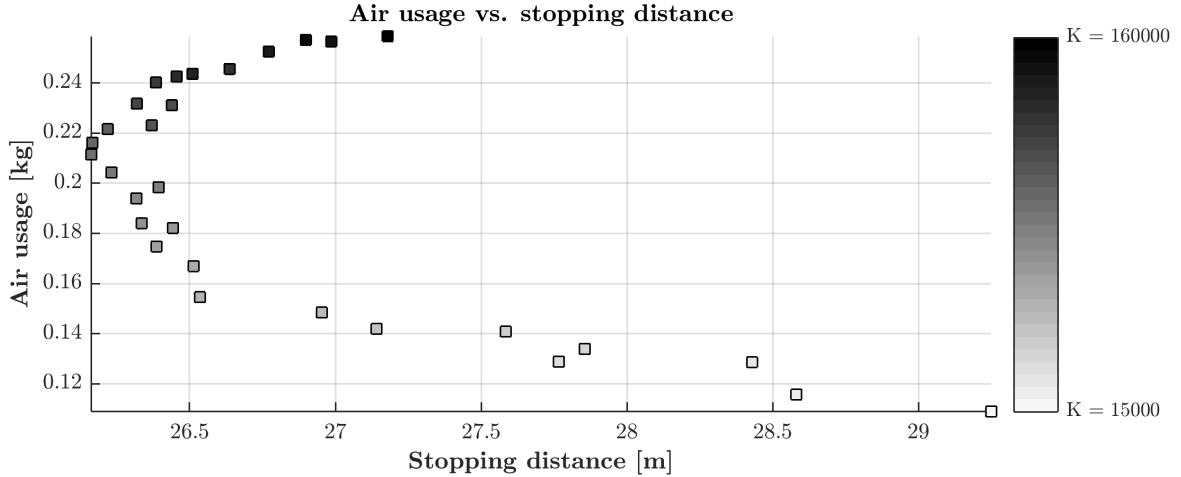


Figure 4.4: Conflict plot showing the influence of the controller parameter k_s on the braking performance on dry road regarding stopping distance and air usage.

On the other hand, it is evident that finding an optimal value for k_s will result in improved performance of the slip control braking system. Another way to define the performance of the controller is to find the values which minimize the control error, defined as $\lambda - \lambda_{ref}$. Figure 4.5 shows the mean absolute slip error for different values of k_s for the three separate axles. It can be seen that the rear axles achieve the smallest error around $k_s = 80,000$. The front axle seems to have the smallest error for lower switching gains.

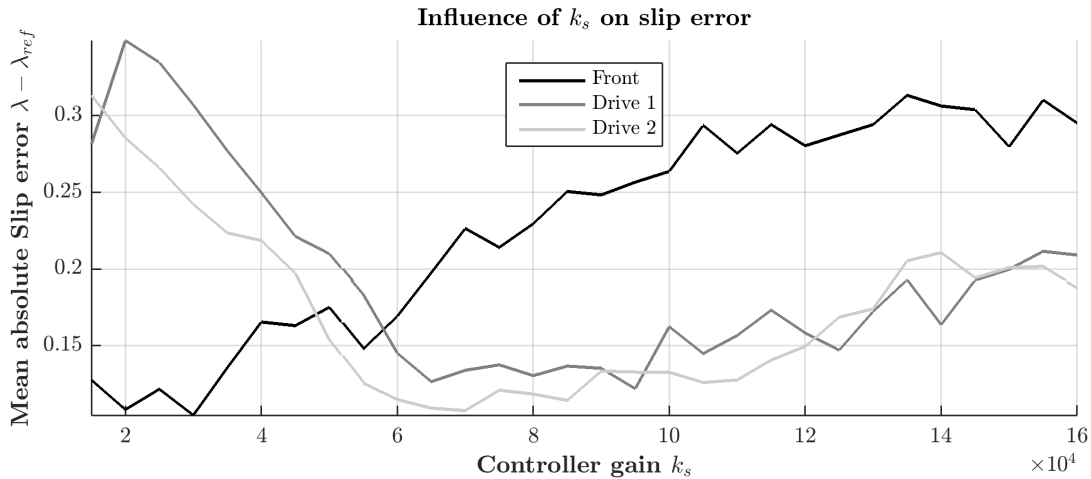


Figure 4.5: Mean absolute slip error for the three different axles for dry road.

Nonetheless, it is difficult to draw direct conclusions from this figure as the performance of one single axle influences that of the others. Therefore, a single wheel parameter optimization approach is proposed, applicable to online gain optimization.

The objective of the gain optimization is minimizing the slip error, defined as

$$\min_{\lambda - \lambda_{ref}} f(k_s). \quad (4.25)$$

Since each surface will have different optimal controller gains, a distinction has to be made during optimization. This is done by running a separate optimization for each friction bin, defined by table 4.1.

Table 4.1: Friction coefficient bins for controller gain optimization.

Bin	1	2	3	4	5	6
μ	0-0.1	0.1-0.3	0.3-0.5	0.5-0.7	0.7-0.9	0.9-1

The number of bins is chosen to be small enough to represent a reasonable difference of friction coefficient, but at the same time to be big enough to have some tolerance for incorrect estimation of the friction coefficient.

It has to be possible to obtain a large number of data samples during braking for fast optimization of the controller gain. Unfortunately, the slip signal shows harmonics caused by the controller with a frequency of around 0.1-0.15 Hz when it comes to the braking on dry surface. Therefore, a sampling frequency is chosen of 2 Hz to give a good representation of the slip error over one sample for a given controller gain k_s .

As can be seen in figures 4.4 and 4.5, the optimization problem is neither convex nor linear. This requires the use of a global optimization algorithm. Adding to the complexity, the function value $f(k_s)$ is usually not equal for same values of k_s , making it difficult to implement standard global optimization algorithms like simulated annealing or genetic algorithm directly. Therefore, a new global optimization method is proposed using methods found in Monte Carlo optimization and simulated annealing.

Figure 4.6 shows the results for the algorithm for a simple convex optimization problem given by

$$\min_x \frac{1}{2}(x - 4)^2 - 2. \quad (4.26)$$

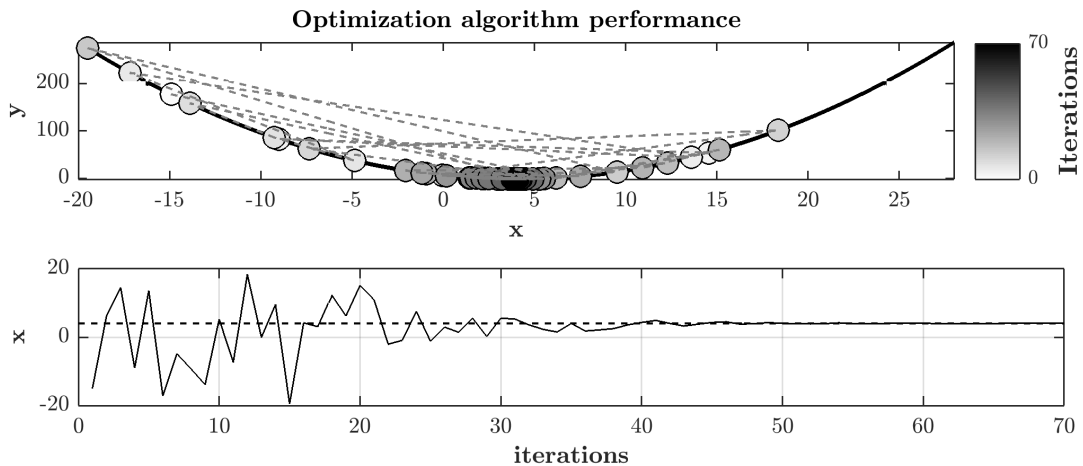


Figure 4.6: The optimum function value of $y = 0$ is reached for $x = 4$. It can be seen that this function value is approached within a finite number of steps.

Here, the optimization parameters are given by

N_{min}	$k_{s,min,1}$	$k_{s,max,1}$	$k_{s,min,2}$	$k_{s,max,2}$
20	-20	20	-10	-10

4.3 Updated Local Brake Controller

Figure 4.7 shows the updated local brake controller with the friction estimation and gain optimization in place. The only new input to the local brake controller block has become the estimated normal load \hat{F}_z , coming from the normal load estimator. For optimization, only the estimated friction coefficient using the recursive least

squares identification with forgetting factor is used, as this method is slightly faster, and it is expected that its results do not differ that much.

Since fast estimation about the normal force and longitudinal force is now required for fast friction estimation, the force observer has been updated. This update consists of a higher sampling rate, 1000 Hz instead of 50 Hz, giving room for more aggressive pole placement. The optimization algorithm still runs at 2 Hz. With the lower sample rate, the force observer would become unstable with the new poles.

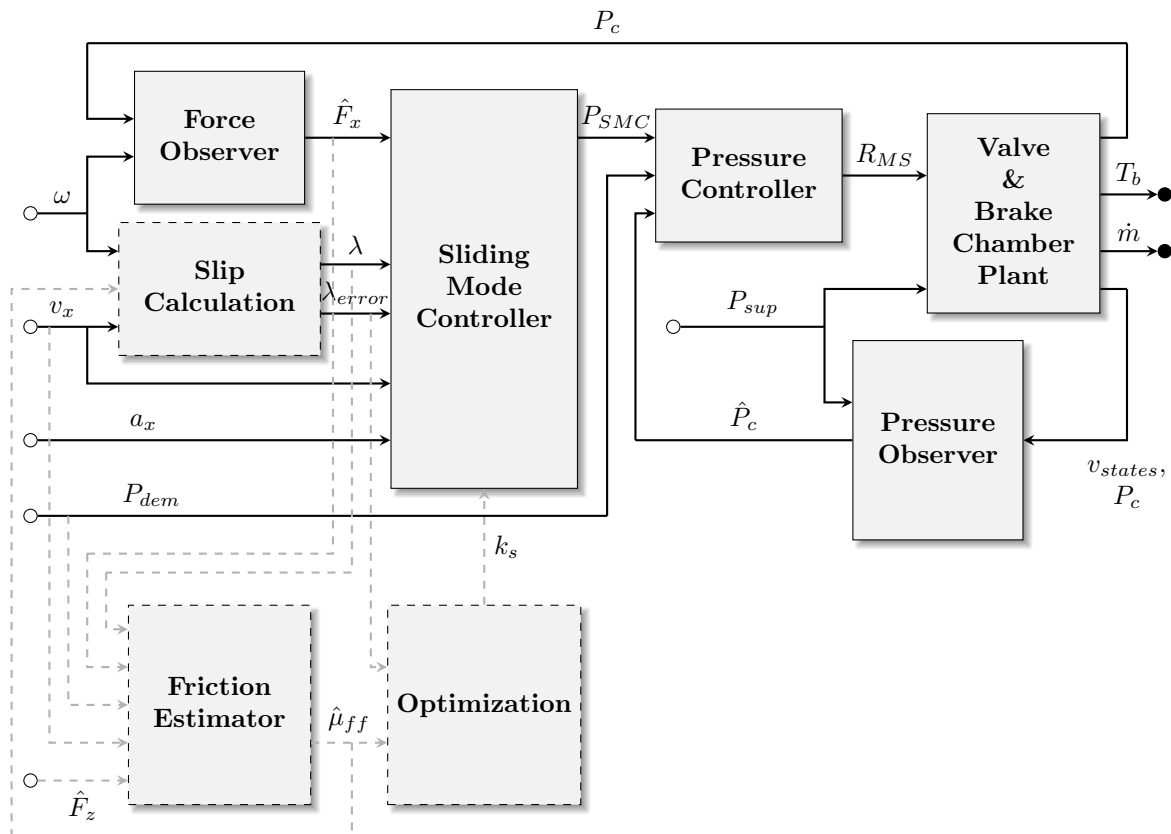


Figure 4.7: Updated local brake controller. The dashed lines show what has been changed since Figure 3.7. The white and black circles are system inputs and outputs respectively.

5 Results

In this chapter the results of the models developed during the progress of this thesis project are going to be presented. More specifically, in the first subsection of this chapter, the friction estimator block is going to be tested against winter test data. Subsection 5.2 presents the simulation results of the wheel slip control braking VTM model with the incorporated friction estimator sub-block for different kinds of driving cycle and surface. The last subsection of this chapter illustrates the simulation results of the model, described in subsection 5.2, with adaptive wheel slip controller gain and slip reference signal, according to the output of the friction estimator block. Then, a comparison between this model and the validated model, presented in section 3.3, is going to be depicted.

In appendix E, results from both the friction estimation as well as the adaptive reference slip algorithms implemented on the real truck are shown.

5.1 Friction Estimator Testing

In this section the friction estimator sub-block, created in section 4.1 is going to be individually tested against winter test data. The procedure of testing the friction estimator sub-block is similar to the one of the partial validation, described in subsection 3.4.1. More specifically, the input signals of the friction estimator block are taken by the correspondent available signals from the experimental data. At this point it should be mentioned that the experimental data did not involve signals about the estimation of the normal forces acting on the wheels of the vehicle. Therefore, the normal force estimator sub-block, presented in subsection 4.1.4, is going to be used for the estimation of the necessary normal forces. Obviously, the inputs to the normal force estimator sub-block are going to be the correspondent necessary signals, taken by the experimental data as well. Both RLS methods, i.e. forgetting factor and Kalman filter, are going to be tested using winter test data. The forgetting factor has been tuned to be 0.995 and the noise covariance matrix of the Kalman filter 0.001.

5.1.1 Testing Results

The friction coefficient estimation for all wheels of the friction estimator sub-block using the winter test data, concerning straight-line braking test from 60-0 km/h on dry asphalt, is presented below.

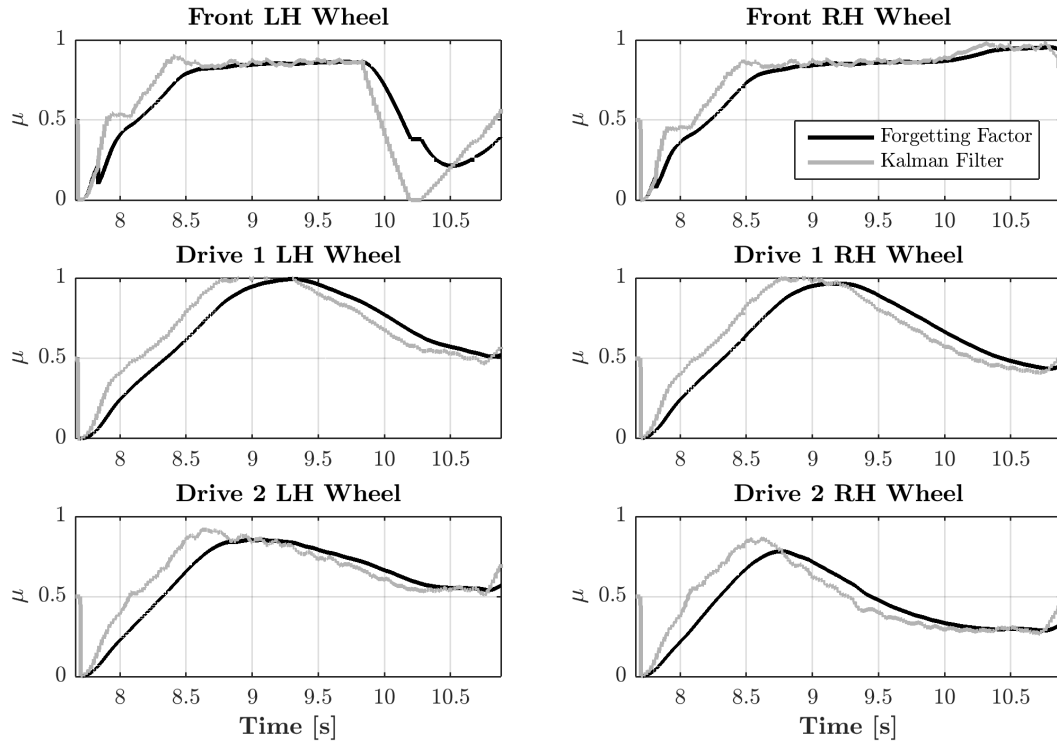


Figure 5.1: *Friction coefficient estimation using the test data from winter testing - Dry Asphalt. Braking starts at 7.5 s.*

Figure 5.1 presents the friction coefficient estimation individually for the six wheels of the vehicle. Since data from the real experiment on dry road is being used, the friction coefficient estimation for each individual wheel is necessary. The friction conditions of the real world vary stochastically, and that is why each of the wheels presents different trend of the friction estimation curve. It is worth mentioning that both RLS methods, i.e. forgetting factor and Kalman filter, perform really well, when it comes to the estimation of the friction coefficient for every wheel. That can be further explained by the fact that the maximum friction coefficient estimation for the wheels varies between 0.8 and 1, which is something reasonable, since the truck is braking on a dry asphalt. Moreover, it can be observed that the Kalman filter method is more spiky in comparison with the forgetting factor method, but that depends mainly on their tuning factors. In addition, when it comes to the wheels 3 and 4 of the driven axle, there is an overestimation of the maximum friction coefficient (i.e. $\mu > 1$). That can be explained by the fact that the points where the maximum coefficient is higher than one, the longitudinal normalized force is higher than one. This is happening because the normal force estimator signal can not be taken directly by the test data, and it comes indirectly via the normal force estimator block. For that reason, it could be possible that sometimes the longitudinal force of the test data is higher than the estimated normal force. For the Drive 1 and 2 wheel, after 9.5 seconds the reference slip is easily tracked, after which the brake pressure goes down, which play an important role in the force observer. Consequently, the estimated longitudinal force goes down, which leads to an underestimation of the friction coefficient.

The friction coefficient estimation of each of the wheels of the vehicle, when it comes to the winter test data for straight-line braking on packed snow from 80-0 km/h, is illustrated below.

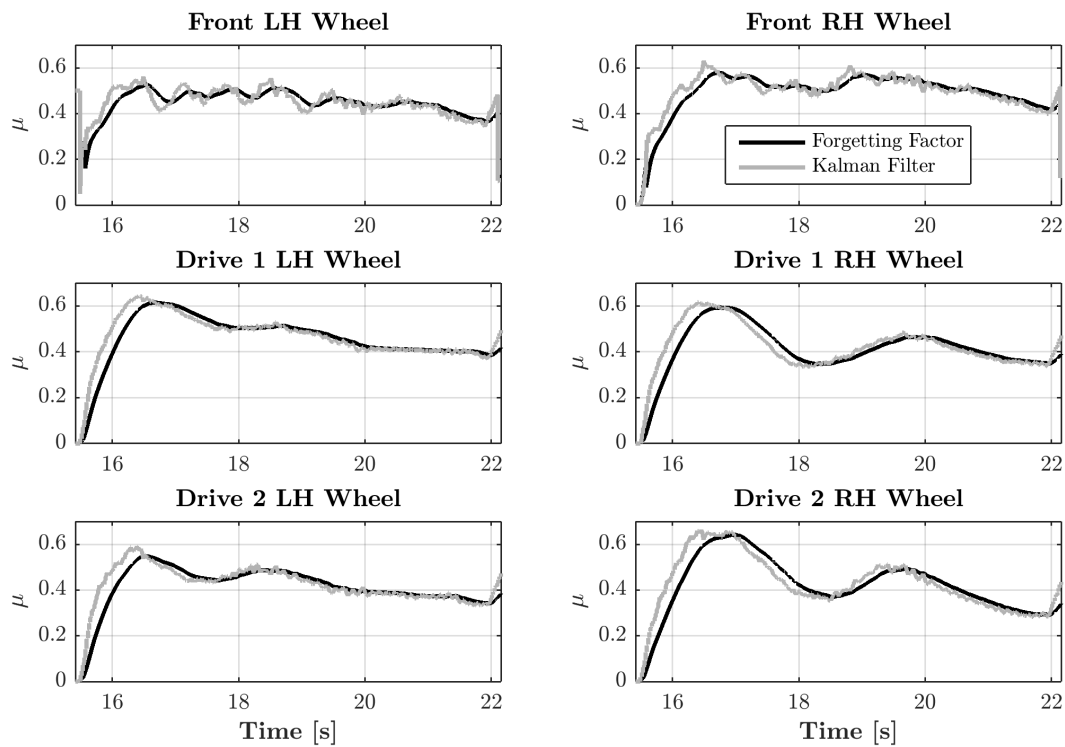


Figure 5.2: Friction coefficient estimation using the test data from winter testing - Packed Snow

Figure 5.2 shows that the friction estimator sub-block performs really good even using the winter test data from packed snow, since it can be seen that for all the wheels and methods the friction coefficient estimation varies between 0.4 and 0.6. Again, the behavior of the Kalman filter algorithm is more spiky than the forgetting factor algorithm, as a result of their tuning factors.

Next figure to be shown is the friction coefficient estimation of the friction estimator block using the data from straight-braking test from 60-0 km/h on polished ice.

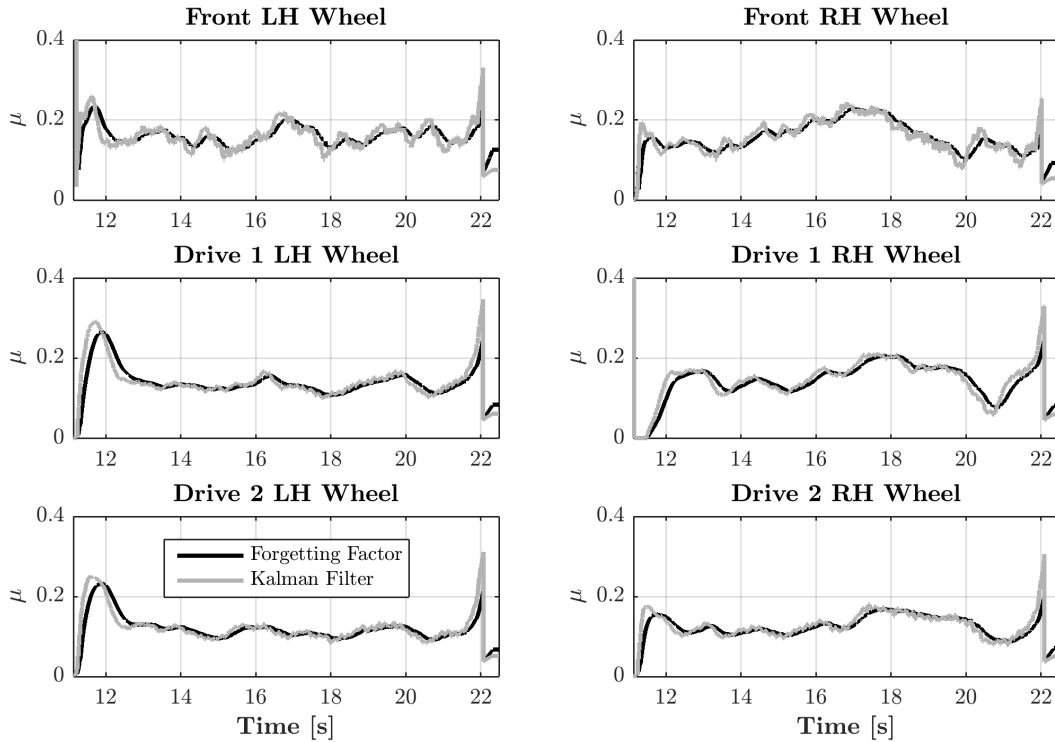


Figure 5.3: *Friction coefficient estimation using the test data from winter testing - Polished Ice*

As it can be seen in figure 5.3 the friction coefficient prediction using both RLS methods varies between 0.19 and 0.3. That is really promising, when it comes to the performance of the RLS methods, since both algorithms produce reasonable friction coefficient estimates for the ice surface as well. Both algorithms have similar curving behavior for all the wheels using their aforementioned tuning factors.

5.1.2 Discussion - Conclusion

Comparing figures 5.1, 5.2 and 5.3, it can be observed that the average value of the friction coefficient estimation for each different surface is representative to the kind of surface that the vehicle is assumed to be on. The strange non-symmetric behavior of the friction estimation curves of the front axle (wheel 1 and wheel 2), presented in the figure 5.1, is caused due to the behavior of the longitudinal force signal, taken by the test data of the dry asphalt case. The behavior of both the estimated longitudinal and normal forces, which are being fed to the friction estimator block, determine the behavior of the RLS methods and the range of the friction coefficients. The smooth or spiky behavior of the RLS methods depends on their tuning parameters. The forgetting factor and the noise covariance matrix have been chosen to be 0.995 and 0.001 respectively for reasons that have been explained in 4.1.3.

To conclude, the friction estimator sub-block seems to perform really good, when it comes to the estimation of the friction coefficient, provided that the tuning factors have been chosen appropriately. However, the quality/availability of the input signals plays a paramount role concerning the quality of the prediction of the friction coefficient.

5.2 Friction Estimation Model Integration

In this section, the friction estimator block has been incorporated to the validated VTM model. Different kinds of simulations are going to be done in order to illustrate the performance of the friction estimator sub-block. More specifically, different kinds of driving cycles (i.e. mild and hard braking), along with different kinds of surfaces have been created, in order to test the response of the friction estimator sub-block.

5.2.1 Surface with Constant Friction Level

In this subsection, the validated VTM model with the incorporated friction estimator sub-block is going to be tested for three different kinds of surfaces and two different driving cycles. More specifically, the values of reference friction coefficient that have been given to the simulation environment in order to correspond to different kinds of surfaces are $\mu = 0.63$ for dry asphalt, $\mu = 0.36$ for packed snow and $\mu = 0.18$ for polished ice. The two driving cycles that have been created in order to show the performance of the friction estimator sub-block on each of the aforementioned three surfaces can be separated into two main categories of straight-line braking tests. These are a hard braking test and a combined mild and hard braking test.

Hard Braking Simulation

During the straight-line hard braking test the vehicle brakes from 60 km/h to 0 km/h on dry asphalt and on polished ice, and from 80 km/h to 0 km/h on packed snow, utilizing its maximum braking force. Plots of the estimated friction coefficient of both RLS methods, longitudinal velocity and filtered slip of the front LH wheel are going to be depicted for each different kind of surface. The response of the friction estimator sub-block for the rest of the wheels of the vehicle is illustrated in Appendix D. The tuning factors of the forgetting factor and Kalman filter methods have been set to be 0.995 and 0.001 respectively, for reasons that have been explained in subsection 4.1.3.

The response of the friction estimator sub-block of the front LH wheel, when it comes to the straight-line hard braking test on dry asphalt, is presented in figure 5.4.

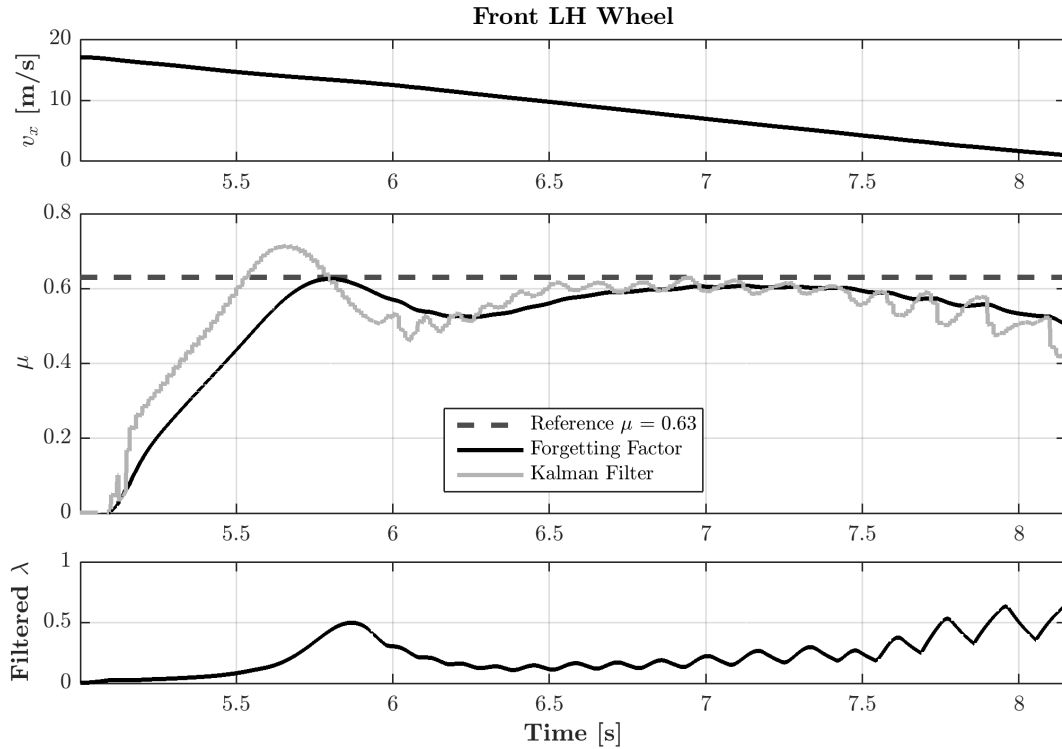


Figure 5.4: *Friction coefficient estimation of the Front LH wheel of the validated model on dry asphalt*

Figure 5.4 shows, as long as the longitudinal velocity of the vehicle is declining and the average filtered slip is above the threshold level of 0.005, the algorithms work and both RLS methods are able to predict the friction coefficient. However, as a result of their tuning, the Kalman filter method is faster, more spiky (precise) and presents higher overshoot than the smoother forgetting factor method. The trend of the behavior of both RLS methods are not that stable, as a result of the estimated longitudinal and normal forces.

The response of the friction estimator sub-block of the front LH wheel, when it comes to the straight-line hard braking test on packed snow, is presented in figure 5.5.

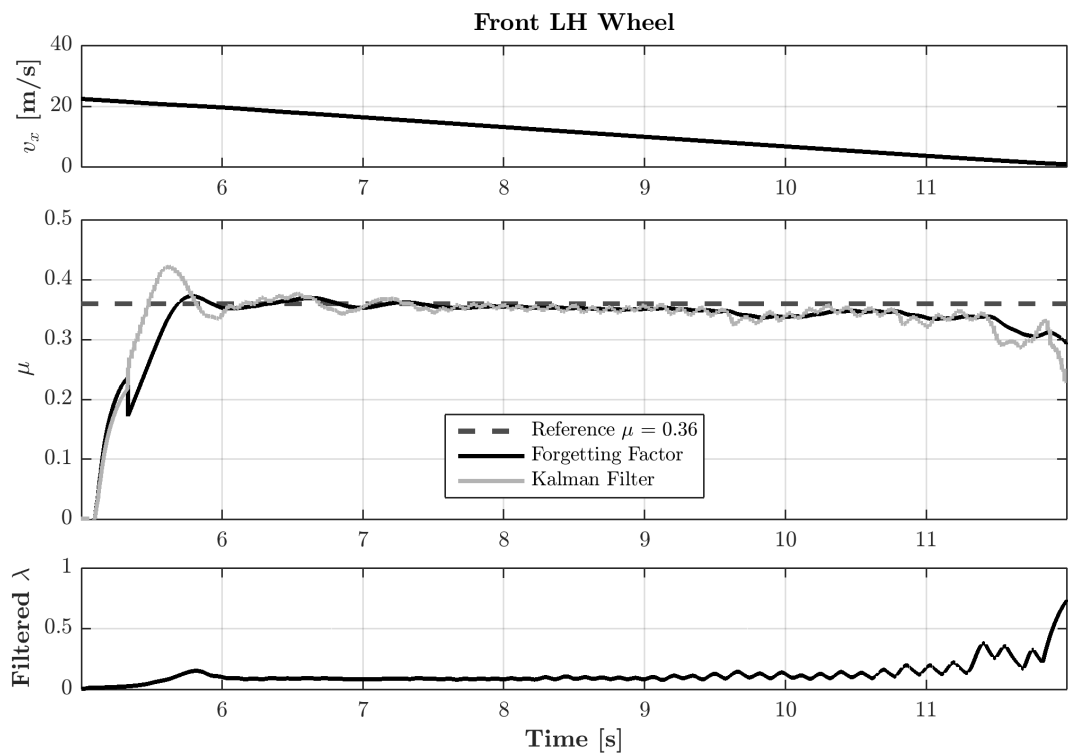


Figure 5.5: Friction coefficient estimation of the Front LH wheel of the validated model on packed snow

Figure 5.5 shows that the reference friction coefficient is captured correctly by both RLS methods. Again, the behavior of the Kalman filter is more oscillatory and it presents higher overshoot than the forgetting factor method. It can also be observed that using the forgetting factor method at $t = 5.3s$ the estimated rising μ drops abruptly from 0.23 to 0.18 and then starts to rise again until its maximum value. This happens due to the condition that has been set inside the friction estimator block, which states that the way of estimating the friction will change when the filtered slip is higher than 0.025. Hence, in this case, the forgetting factor algorithm switches from the slip-slope based friction estimation to the normalized-force based friction estimation.

The response of the friction estimator sub-block of the front LH wheel, when it comes to the straight-line hard braking test on polished ice, is presented in figure 5.6.

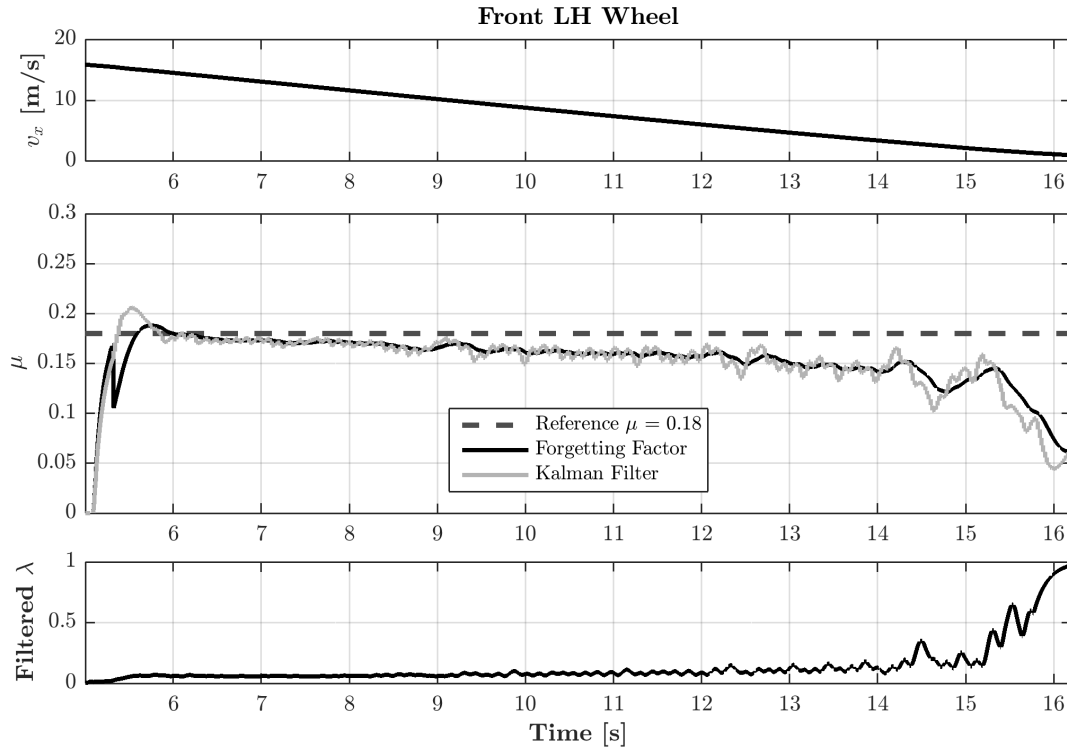


Figure 5.6: Friction coefficient estimation of the Front LH wheel of the validated model on polished ice

Figure 5.6 shows that both methods perform good and appear to behave the same way like it was described earlier, when it comes to the dry asphalt and packed snow case. The switching condition of the friction estimation algorithm is illustrated also in this figure by this sudden decrease of the estimated μ at $t = 5.3s$. Overall, both methods are really able to capture the reference μ value.

Discussion - Conclusion

Comparing the results of the friction estimator output, presented in figures 5.4, 5.5 and 5.6, it can be observed that during straight line braking tests of the front LH wheel and having different initial velocity values, the estimation of the friction coefficient is really precise. Both RLS methods perform well and can capture the reference μ . However, as a result of their tuning factors, the Kalman filter response is more spiky than the forgetting factor response. In addition, the abrupt decrease of the estimated μ , due to the friction estimation switching condition, is illustrated in all of the aforementioned figures, however it is more clear for the packed snow and polished ice case. A short conclusion of these hard braking tests on different surfaces could be that when the braking forces are high enough, then the estimation of the friction coefficient can be really accurate.

Combined Mild and Hard Braking Simulation

During the combined mild and hard braking driving cycle, the vehicle is going to use initially ($t = 5s$) low and after 3 seconds high braking forces in order to brake from different initial velocities on three different surfaces. The tuning factor of the forgetting factor method, the conditions of the friction estimator and the reference friction coefficients (friction surfaces), along with their correspondent initial velocities have been kept the same, like the ones that had been set for the hard braking case. Moreover, the plot of the slip slope of the front LH wheel is going to be presented here, as well, since it is used for the estimation of the friction coefficient during the procedure of the mild braking. At this point, it should be also mentioned that only the forgetting factor friction estimation is going to be presented, when it comes to the combined mild and hard braking results. The reason is that the purpose of this driving cycle is to show that the slip-slope based friction estimation method works properly, when it uses the already developed and verified against experimental results forgetting factor method, introduced by [73], [65] and [66].

The response of the friction estimator sub-block of the front LH wheel, when it comes to the combined mild and hard straight-line braking test on dry asphalt, is presented in figure 5.7.

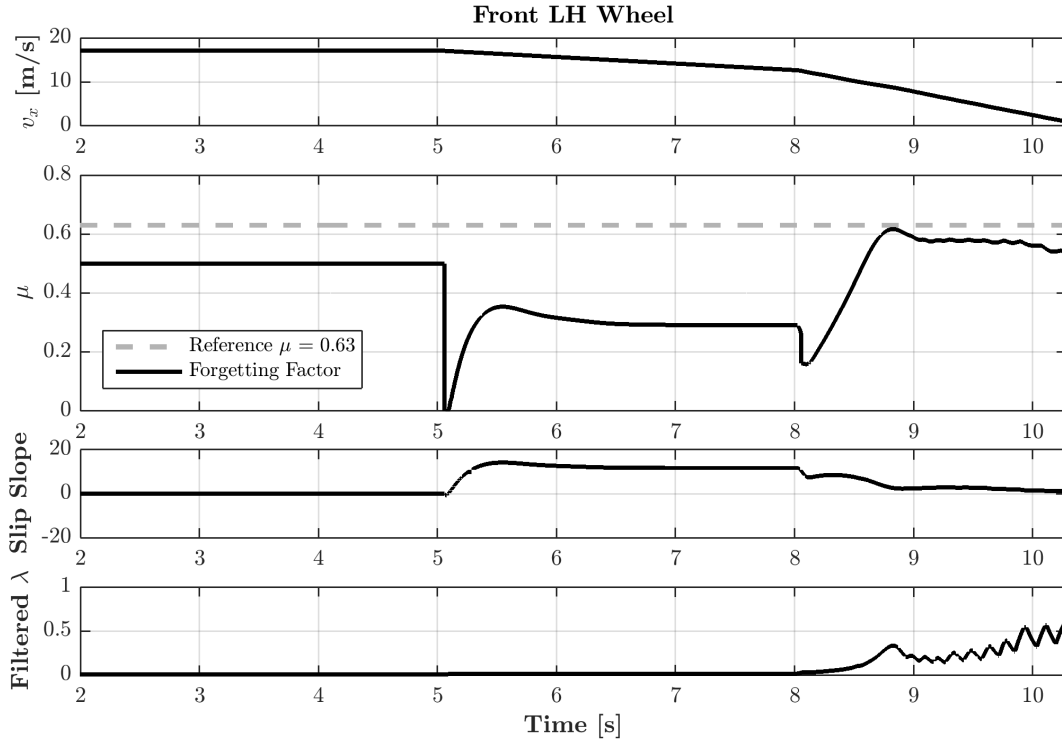


Figure 5.7: Friction coefficient and slip slope estimation of the Front LH wheel of the validated model on dry asphalt

Figure 5.7 shows that during the mild braking driving cycle, where the slip-slope based method is used for the estimation of the friction coefficient, i.e. $5s < t < 8s$, the average slip-slope value is almost 17. The prediction of the friction coefficient during this period is almost on average 0.3, which means that the estimated friction coefficient using the slip-slope forgetting factor method is underestimated, in comparison with the reference friction coefficient of 0.63. This can be explained by comparing the figures 4.1 and 4.3. Figure 4.1 has been used during the formulation of the friction estimator block of the model. More specifically, a condition that has been set to the friction estimator block is that the slip-slope based estimation method is used when the slip is lower than 0.025, according to figure 4.1. It can be easily seen in this figure that for slip values less than 0.025, there is a clear distinction of the slip-slope. However, the friction curves of the tire model that it used for simulation can not provide a clear distinction of the slip-slope of the curves, when slip is lower than 0.025, according to figure 4.3. The slip slope estimation multiplied with the A constant (from equation 4.22), described in subsection 4.1.3, produces the underestimation of the friction coefficient, when it comes to the period of mild braking. On the other hand, during the hard braking part of this driving cycle, i.e. $t > 8s$, the friction coefficient estimation is closer to the reference $\mu = 0.63$, since in that case the normalized longitudinal force, instead of the slip-slope is utilized.

The response of the friction estimator sub-block of the front LH wheel, when it comes to the combined mild and hard straight-line braking test on packed snow, is presented in figure 5.8.

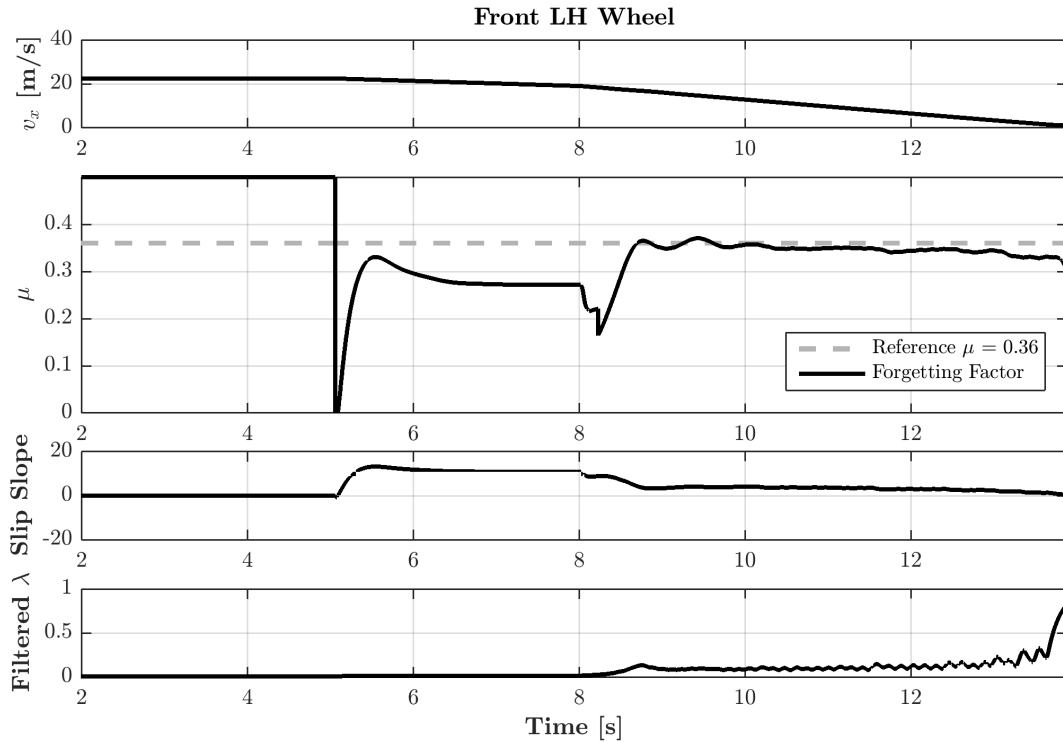


Figure 5.8: *Friction coefficient and slip slope estimation of the Front LH wheel of the validated model on packed snow*

Similar results, like the ones of the dry asphalt case can be seen in figure 5.8, which shows that during the mild braking driving cycle, where the slip-slope based method is used for the estimation of the friction coefficient, i.e. $5s < t < 8s$, the prediction of the friction coefficient during this period is almost on average 0.28, which means that the estimated friction coefficient using the slip-slope forgetting factor method is underestimated, in comparison with the reference friction coefficient of 0.36. As it has already been explained earlier, the underestimation of the friction coefficient occurs, because of the difficulty to distinct the slip-slope of the friction curves of the tire model for low slip values, used in the simulations (figure 4.3). Hence, the combination of the estimated slip slope, along with the constant A (from equation 4.22) produce the underestimated value of the friction coefficient. On the other hand, during the hard braking part of this driving cycle, i.e. $t > 8s$, the friction coefficient estimation is closer to the reference $\mu = 0.36$, since in that case the normalized longitudinal force, instead of the slip-slope is utilized.

The response of the friction estimator sub-block of the front LH wheel, when it comes to the combined mild and hard straight-line braking test on polished ice, is presented in figure 5.9.

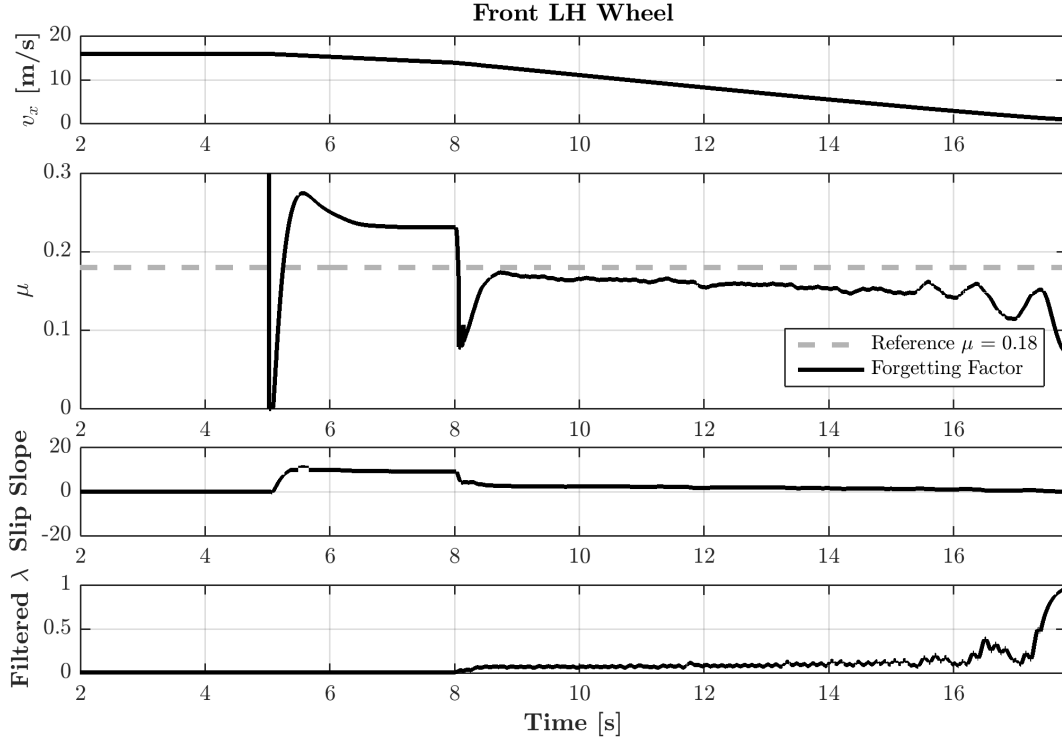


Figure 5.9: *Friction coefficient and slip slope estimation of the Front LH wheel of the validated model on polished ice*

Figure 5.9 shows that during the mild braking driving cycle, where the slip-slope based method is used for the estimation of the friction coefficient, i.e. $5s < t < 8s$, the prediction of the friction coefficient during this period is almost on average 0.25, which means that the estimated friction coefficient using the slip-slope forgetting factor method is overestimated, in comparison with the reference friction coefficient of 0.18. The reason behind this overestimation of the friction coefficient is the same like in the case of mild braking on dry asphalt and packed snow (i.e. difficulty to get the right slip-slope of the tire model for low slip values, used in simulations). The trend is different (overestimation of μ instead of underestimation), as a result of the product between the slip slope estimation 4.3 and A constant (equation 4.22). On the other hand, during the hard braking part of this driving cycle, i.e. $t > 8s$, the friction coefficient estimation is closer to the reference $\mu = 0.18$, since in that case the normalized longitudinal force, instead of the slip-slope is utilized.

Discussion - Conclusion

Comparing the figures 5.7, 5.8 and 5.9, it can be said that the slip-slope based friction estimation method works during the procedure of mild braking for all the different kinds of surfaces. However, due to the inability of the tire model to give correct slip-slope estimation values, when slip is lower than 0.025, the friction coefficient estimation using this method underestimates (dry asphalt, packed snow) or overestimates the friction coefficient (polished ice). When it comes to the periods of the hard braking (i.e. slip is higher than 0.025), the algorithm seems to give reasonable friction coefficient estimates (i.e. really close to the correspondent reference friction coefficient estimates) for all the three different kinds of surfaces. However, this something that it has already been confirmed by the previous subsection, as well.

5.2.2 Surface with Variable Friction Level

In this subsection surfaces with variable friction levels are going to be examined, in terms of prediction of the friction coefficient. Three different friction scenarios are presented in this subsection. Step change of the reference friction coefficient three seconds after the initialization of the braking procedure. More specifically, the first step change of the reference friction coefficient is from dry asphalt ($\mu = 0.63$) to polished ice ($\mu = 0.18$),

the second one is from polished ice ($\mu = 0.18$) to packed snow ($\mu = 0.36$) and the third one is from packed snow ($\mu = 0.36$) to dry asphalt ($\mu = 0.63$). As a result of the conclusion of the previous subsection only the hard braking driving cycle is going to be used, since in that case the friction estimator sub-block gives reasonable friction coefficient estimates. The tuning factors of both RLS methods and the conditions of the friction estimator block, described in previous subsection are going to be kept the same. However, the initial velocities for all the tests have been set to be 80 km/h. The controller gains, as well as the offsets of the reference slip levels are going to be determined by the initial surface that the vehicle is braking on. Therefore, if the vehicle is braking from dry asphalt to polished ice, the controller gains and the offsets of the reference slip that are going to be used are the ones that are being used for hard braking on dry asphalt (presented on the table 3.1), and they are not going to change until the end of the simulation. The correspondent friction estimation plots for all the wheels are attached to Appendix D of this thesis project.

The response of both RLS methods as a result of the step change of the reference friction coefficient from dry asphalt to polished ice, three seconds after the initialization of the hard braking procedure, is illustrated in figure 5.10.

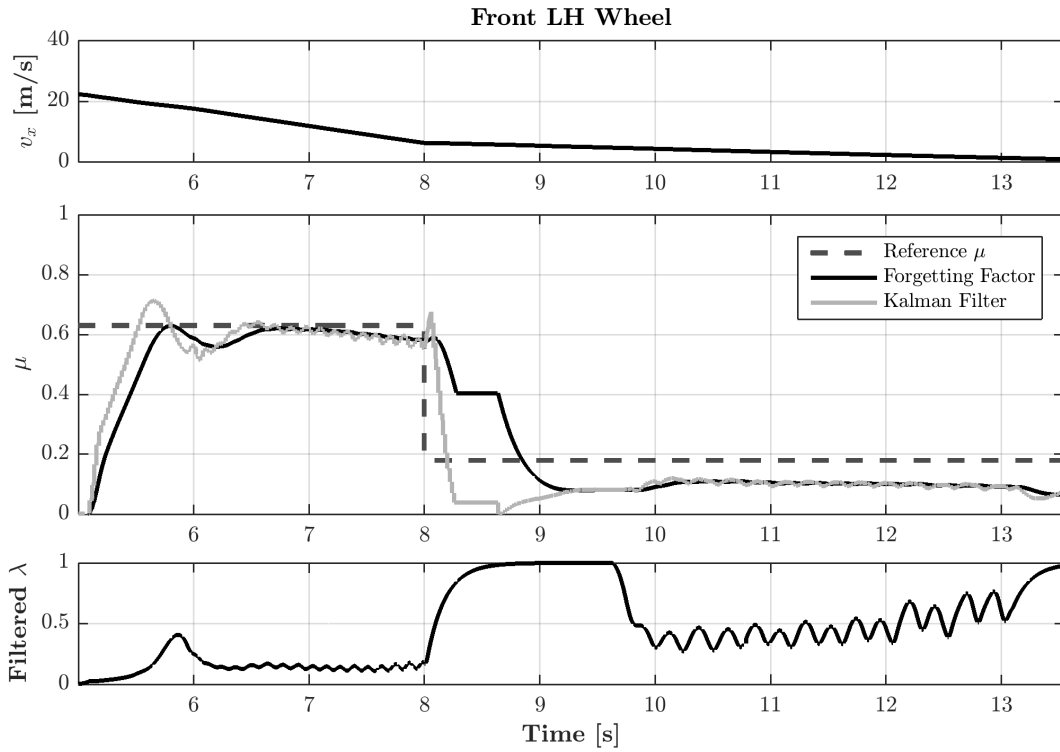


Figure 5.10: *Friction coefficient estimation of the Front LH wheel of the validated model from dry asphalt to polished ice*

As can be seen in figure 5.10, during the step change of the reference friction coefficient, both RLS methods are able to keep track of this change. The Kalman filter method appears to change quicker to the new reference μ value, in comparison with the forgetting factor method. However, as a result of its tuning, it appears to have a lot of noise. In addition, both methods converge to the same new reference μ value after 9 seconds. The reason why it takes more than 1 second in order for the two methods to predict the new reference μ value is that the controller gains and slip reference offset that are used after the step change of the μ value are the same like the ones of the dry asphalt case (table 3.1). That is also the main reason, why initially ($t < 8s$) the friction coefficient estimation is really accurate in comparison with the reference μ , while after the step change of the μ , where the predicted friction coefficient is slightly lower than the reference one for both RLS methods.

The response of both RLS methods as a result of the step change of the reference friction coefficient from

polished ice to packed snow, three seconds after the initialization of the hard braking procedure is illustrated in figure 5.11.

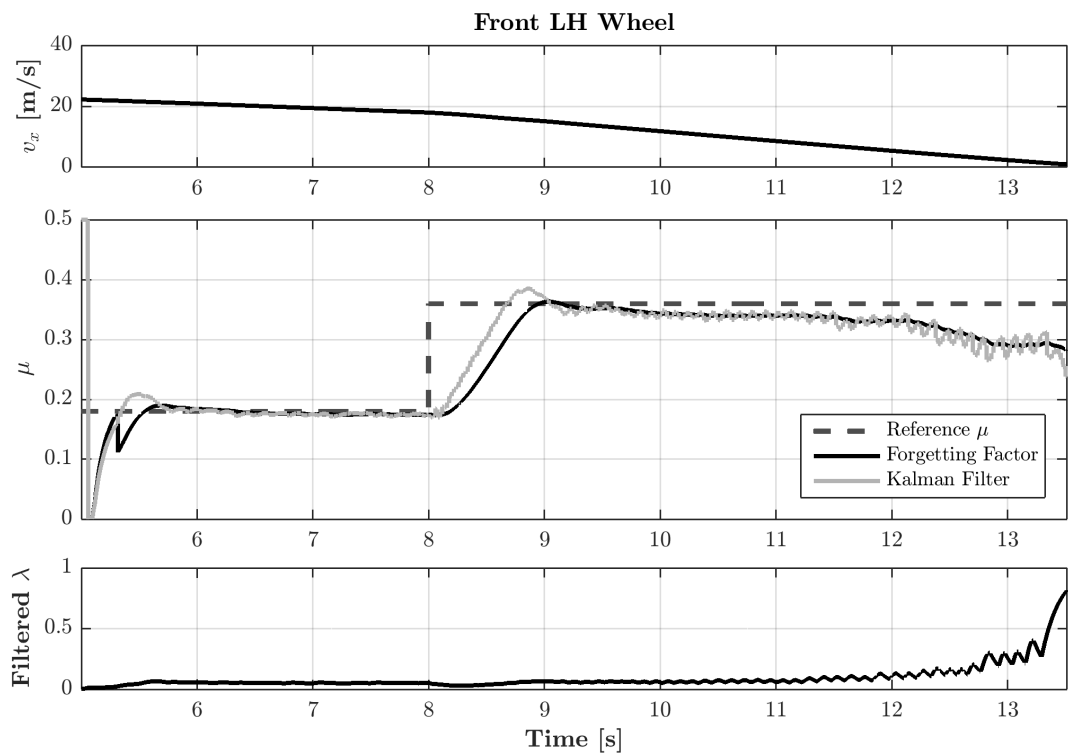


Figure 5.11: Friction coefficient estimation of the Front LH wheel of the validated model from polished ice to packed snow

As it can be seen in figure 5.11, during the step change of the reference friction coefficient, both RLS methods are able to keep track of this change. The Kalman filter method appears to change quicker to the new reference μ value, in comparison with the forgetting factor method. However, as a result of its tuning appears to have a lot of noise and high overshoot. In addition, both methods converge to the same new reference μ value after 9 seconds, but the forgetting factor method appears smoother behavior in comparison with the Kalman filter one. Again, the reason why it takes more than 1 second in order for the two methods to predict the new reference μ value is that the controller gains and slip reference offset that are used after the step change of the μ value are the same like the ones of the polished ice case (table 3.1). That is also the main reason, why initially ($t < 8s$) the friction coefficient estimation is really accurate in comparison with the reference μ , while after the step change of the μ , where the predicted friction coefficient is slightly lower than the reference one for both RLS methods.

The response of both RLS methods as a result of the step change of the reference friction coefficient from packed snow to dry asphalt, three seconds after the initialization of the hard braking procedure is illustrated in figure 5.12.

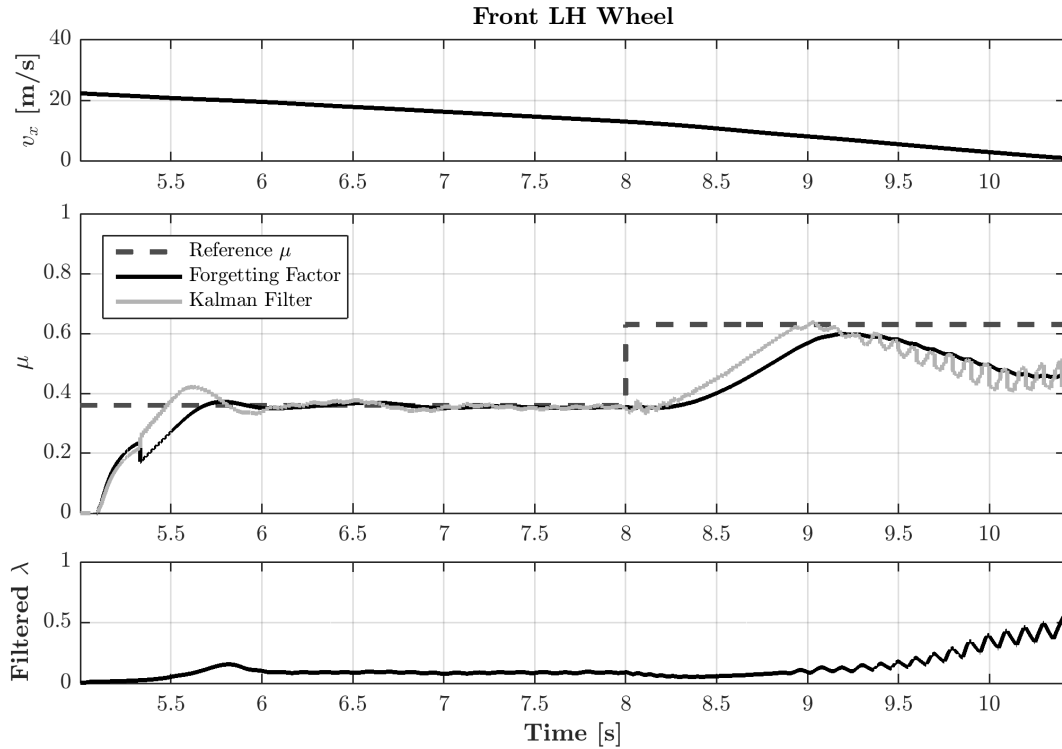


Figure 5.12: Friction coefficient estimation of the Front LH wheel of the validated model from packed snow to dry asphalt

As it can be seen in figure 5.12, during the step change of the reference friction coefficient, both RLS methods are able to keep track of this change. The Kalman filter method appears to change quicker to the new reference μ value, in comparison with the forgetting factor method. However, as a result of its tuning appears to have a lot of noise. In addition, both methods cannot converge to the same new reference μ value after 9 seconds, but the forgetting factor method appears smoother behavior in comparison with the Kalman filter one. Again, the reason why it takes more than 1 second in order for the two methods to predict the new reference μ value is that the controller gains and slip reference offset that are used after the step change of the μ value are the same like the ones of the polished ice case (table 3.1). That is also the main reason, why initially ($t < 8s$) the friction coefficient estimation is really accurate in comparison with the reference μ , while after the step change of the μ , where the predicted friction coefficient is slightly lower than the reference one for both RLS methods. It is worth mentioning that the predicted friction coefficient for both RLS methods after the step change of the reference μ can not remain stable. That occurs due to the lower controller gains of the packed snow case, as well as the different slip reference offsets that need to be used for the dry asphalt case.

Discussion - Conclusion

Comparing the friction estimation plots of the figures 5.10, 5.11 and 5.12, it can be said that both RLS methods can predict the new reference friction coefficients. Since the controller gains and the slip reference offsets remain independent on the new conditions (i.e. step change of the μ), it is reasonable that they cannot accurately estimate the new reference μ value, after the step μ change. The forgetting factor method appears to be smoother than the Kalman filter method, hence it is an ideal method for using it for controller gain optimization and slip reference offset adjustment, according to the kind of the braking surface. Provided that the model could change the controller gains and the slip reference offset in order for them to be adapted to the kind of the braking surface, then faster response of the forgetting factor method, better prediction of the new reference friction coefficient, less air usage, less braking distance and less slip error are expected.

5.3 Gain optimization with friction estimation

Now, since information about the friction coefficient is available, the optimization method described in subsection 4.2.2 can be used. For all friction bins, the optimization method is run for 500 seconds to collect data. During this time, the tank pressure will be kept constant at 10 bars as no depletion is assumed. The driving cycle consists of driving up to speed, followed by heavy braking until 20 percent of the maximum speed, and then the cycle repeats again. During each heavy braking cycle, data is collected and the optimization is active.

Figure 5.13 shows how the values for k_s converge over time. It becomes evident that for the lower friction bins, more data is collected. This results in the observed convergence for the lower friction bins. At the higher friction bins, this convergence is not yet observed. It can be seen that the values for k_s still vary erratically as expected, since too little data is available.

An interesting observation can be made about the peaks in the low friction surface bins after a steady state value is already obtained. These peaks are created due to a guess of k_s for a given μ at $t - 1$, while at t , it appears that the friction over that period was actually different, and the results for that specific value of k_s are saved for that specific friction bin.

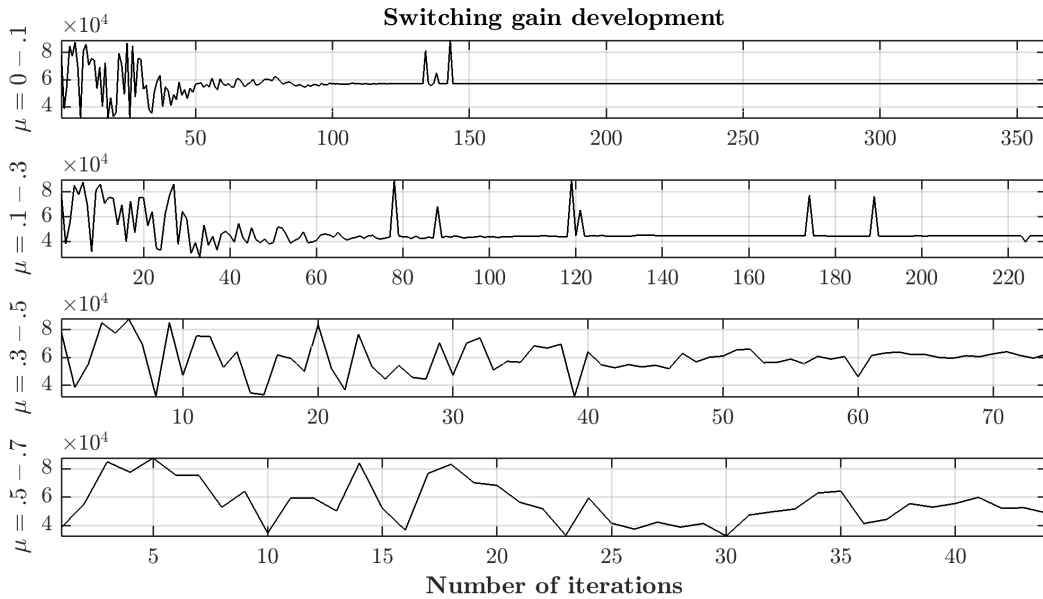


Figure 5.13: *Development of the switching gain during optimization.*

Figure 5.14 shows the optimized k_s for the first four friction bins, as there is not enough data collected during 500 seconds of simulation for the higher friction bins. Put simply, on high friction surface, braking takes too little time for the optimization running at 2 Hz to collect enough data samples.

It is hard to spot a trend in the optimized switching gains k_s as only four friction bins are represented, but it appears that for all axles the following holds: bin1 > bin2 < bin3 > bin 4. Some caution has to be taken with respect to the higher friction bins, as also here not many data samples are available and it is very possible that the optimal value is not yet found.

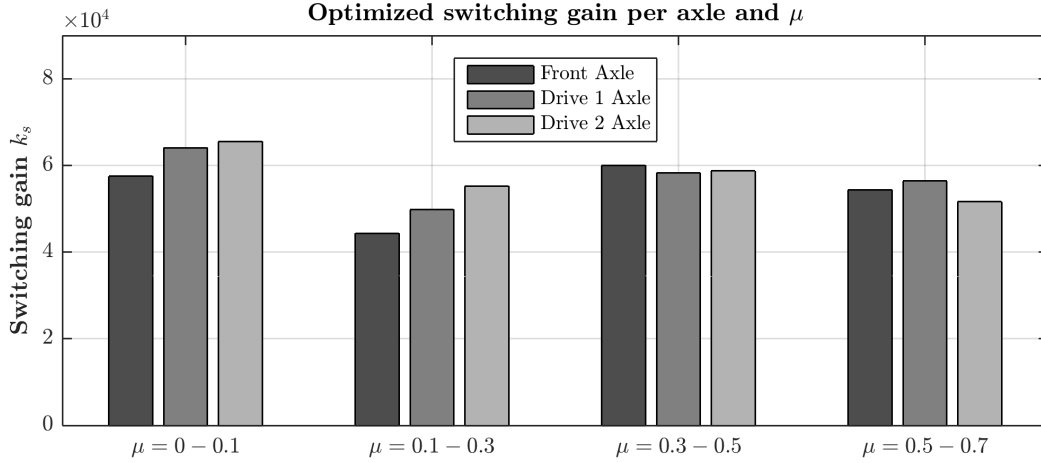


Figure 5.14: Optimized switching gains for each axle, for each friction bin.

5.4 Optimized System Results

Four tests are used to compare the performance of the optimized slip controller with respect to the original system. Similar to the reference slip, the found optimal control gains are used in a lookup table from which they are extracted according to the friction information. The four tests consist of the following situations:

1	2	3	4
$\mu = 0.4 \rightarrow 0.2$	$\mu = 0.2 \rightarrow 0.4$	$\mu = 0.7 \rightarrow 0.2$	$\mu = 0.2 \rightarrow 0.7$
Snow to Ice	Ice to Snow	Asphalt to Ice	Asphalt to Snow

For the original system, the used gains were based on the ones of the asphalt case, as can be seen in table 3.1.

Figure 5.15 shows the first two situations, where after three seconds of braking, the surface conditions change. Figure 5.16 shows the third and fourth situation, where the friction surface changes from ice to asphalt and vice versa. For all four velocity plots, it can be seen that the optimized model comes to a standstill before the default model. Only when going from ice to snow, it can be observed that the air usage is higher for the optimized model. For all other situations, the air usage is also better for the optimized model.

The performance is further illustrated by table 5.1. It can be seen that for all scenarios, the braking distance is improved with at minimum six percent and at maximum 20 percent. The slip error and air usage however are not that unanimous, as only the slip error has increased for driving from ice to asphalt, while the air usage shows an increase for going from ice to snow.

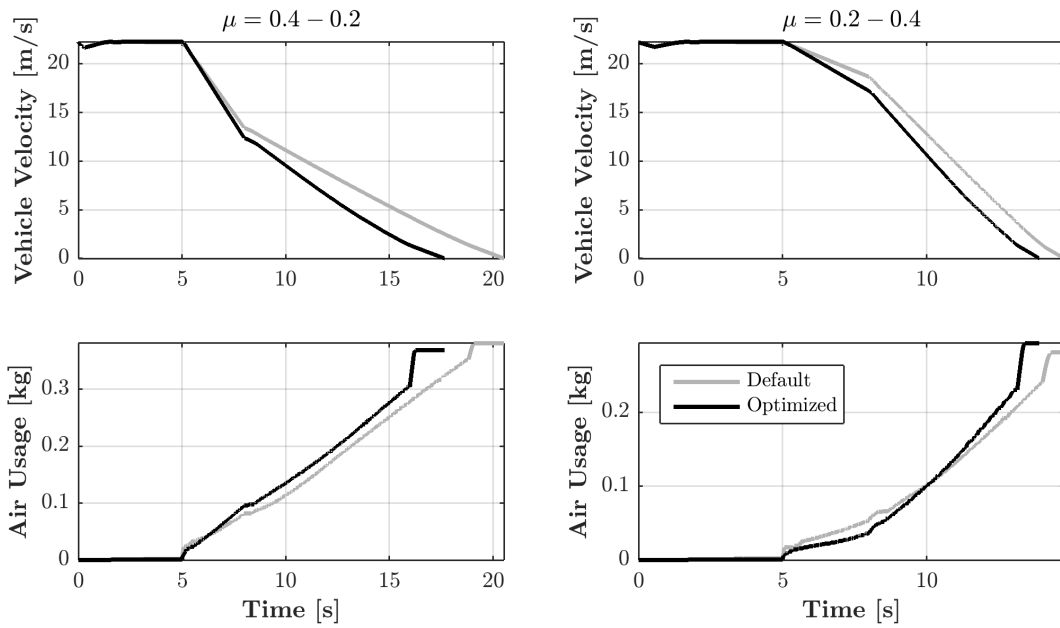


Figure 5.15: Vehicle velocity and air usage for the original and optimized model during surface with a change of surface at 3 seconds into braking. Braking starts at 5 seconds.

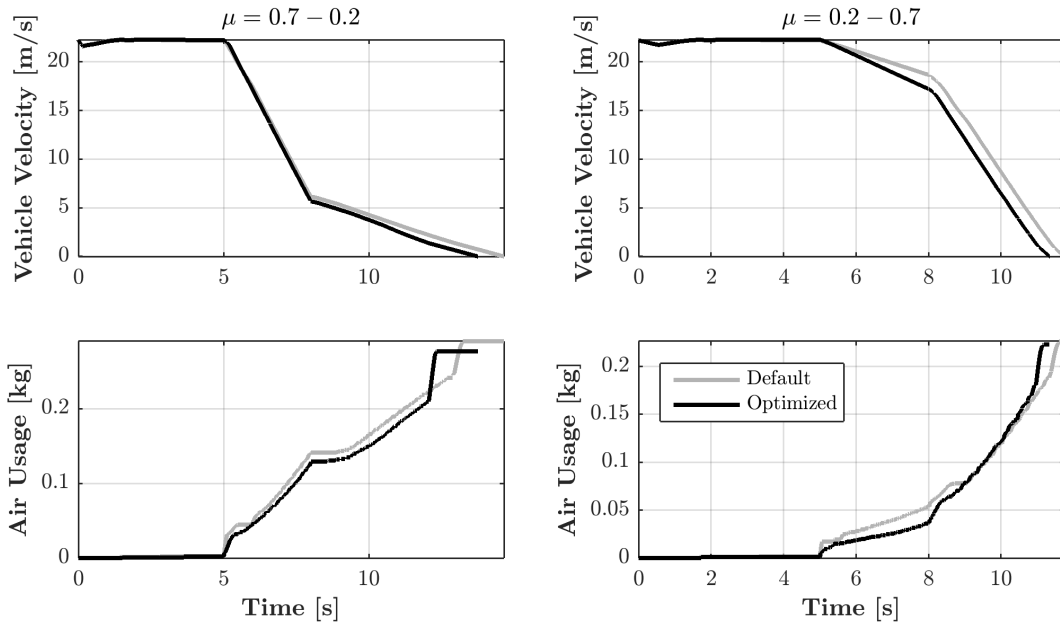


Figure 5.16: Vehicle velocity and air usage for the original and optimized model during surface with a change of surface at 3 seconds into braking. Braking starts at 5 seconds.

Table 5.1: Performance increase of the optimized (opt.) model with respect to the default (def.) model. The percentual difference is denoted by (diff.).

		$\mu = 0.4 \rightarrow 0.2$			$\mu = 0.2 \rightarrow 0.4$			$\mu = 0.7 \rightarrow 0.2$			$\mu = 0.2 \rightarrow 0.7$		
		Def.	Opt.	Diff. %									
Braking		133	107	-20	121	106	-12	63	59	-6	97	87	-10
Distance													
	[m]												
Slip Error		0.14	0.17	+21	0.08	0.11	+38	0.37	0.42	+14	0.15	0.07	-53
	[-]												
Air Usage		0.38	0.37	-3	0.28	0.29	+4	0.29	0.28	-3	0.23	0.22	-4
	[kg]												

As the optimization algorithm has tried to minimize the slip error, the results from table 5.1 with respect to the slip error might seem that good. However, as the controller now obtains a better estimation about the peak friction reference slip, it might prove harder to exactly control towards this value. The fact that the controller is closer to the peak reference slip is illustrated by the decrease in braking distance. On the other hand, it might also be that the values found for the switching gains are not as good as they could be. This has both to do with the parameters set for the optimization, as well as the amount of available data from the optimization. Figure 5.13 illustrates that for the higher friction bins, no steady-state value is found yet.

Nevertheless, the most important brake metrics, braking distance and air usage, show improvement with respect to the default model. Even though the situation from driving from ice to snow shows that the air usage has gone up with four percent, the braking distance has gone down with twelve percent, which is a very worthwhile trade off.

6 Discussion

Using test data acquired during the winter tests, chapter 3 has shown that the integration of the slip controller in the VTM has succeeded, and that the behavior of the updated VTM is sufficiently similar to the one of the truck used in the tests. As mentioned however, there are several points for which the VTM presents different behavior. Especially on dry asphalt and for low speeds, the VTM seems to diverge more with respect to wheel slip. The lateral dynamics showed good overall performance from the VTM, while here also differences in wheel slip, yaw rate and sideslip were observed. Either way, in all cases, the Pacejka tire model is the most probable culprit for discrepancies. With a large number of parameters to tune, and limited knowledge about the tire parameters of the actual tires used on the truck, it was virtually impossible to get it exactly right. Nonetheless, a good enough approximation was reached for the goals of this thesis project.

The slip-slope friction estimation algorithm has shown to give good results for different friction surfaces and driving cycles. With the chosen tuning parameters, it has become evident that the recursive least squares identification method using the forgetting factor outperformed the Kalman filter. For heavy braking, most of the time normalized force was used as a measure of the friction surface. For the mild braking however, slip-slope estimation has been used. Unfortunately, due to the limitations of the Pacejka Tire model, slip-slope estimation did not show good results for all different surface conditions, as the estimated slip-slope was roughly the same for every surface. When a change in friction is concerned, the friction estimation algorithm still showed good results and fast enough convergence.

The optimization algorithm has proven to work properly with the difficult environment it had to work in. For the lower friction bins, where more data was available, convergence could be observed. It is however impossible to say whether the found value actually is the optimal point or at least close to the optimal point, as both the algorithm is relatively untested and the initial conditions might need to be tuned to provide better results.

Ultimately, using the optimized controller with friction estimation has resulted in a reduction of braking distance for all four driving tests, and only for one case air consumption has increased. To what extent this should be contributed to the optimization of the switching gain k_s or the reference slip level remains unknown. As mentioned earlier, it could very well be that the slip level for the peak friction coefficient is approximated better resulting in the improved stopping distance, where the optimization of the switching gain only limited the slip error around that point. As it might be harder to control the slip at this slip peak, the increase in slip error could be explained. Nevertheless, performance of the complete system has been improved.

7 Conclusion

By improving the brake performance of a truck, both the stopping distance and air-usage can be decreased, resulting in increased active safety and better fuel consumption due to smaller air tanks and compressors. This thesis project has set out to increase the performance of the slip control braking even further. By integrating the VTM, Volvo's vehicle dynamics model, with a model of FABV braking and slip control, a platform has been created to develop and test new wheel-based functions using slip control braking. The updated vehicle model has been validated against test data and has shown to be adequate for further function development.

With the validated vehicle model, three new wheel-based functions have been created to improve the braking performance. The first and most important function was the on-line friction estimation during braking. Using recursive least squares algorithms and force observers, it has been shown that the friction can be estimated quickly and correctly. The second one relied on the friction estimation to produce a reference signal for the ideal wheel slip using a pre-defined lookup table. The third function was able to optimize the switching gain of the sliding mode controller during operation to minimize the error between the reference slip and the actual wheel slip.

With the real-time friction estimation and optimization of the controller working in parallel, results of up to twenty percent in braking distance were obtained, where in most cases, also a reduction in air usage could be observed.

The FABV braking system with optimized slip control proves to be a great improvement for the active safety of the vehicle. But not only braking performance can benefit from the information about friction that has become available. Also other systems could be improved, as well by the knowledge of the friction coefficient. To conclude, a new step has been set in the realization of slip control braking using FABV on trucks, and the braking performance of heavy vehicles will be increased drastically.

8 Future Work

As mentioned in the introduction, some limitations have been set to determine the scope of this thesis work. With the newly acquired knowledge, some recommendations can be done regarding future work on slip control braking using the FABV.

From the modeling point of view, the tire model is the key for accurate modeling of the vehicle. The Pacejka tire model could be improved by better tire parameters, or being updated to a newer version or using a different tire model which captures the dynamics better. As VTM includes more truck configurations than the one used in this thesis project, behavior of other trucks with slip control braking could be assessed in simulation too.

Regarding friction estimation, more complex methods are available which are supposed to capture the tire-road friction even better, utilizing also lateral dynamics. More complex models have, for example, more tire models to be estimated. That also requires more sophisticated filtering and identification algorithms to be used. Having better information about the tire-road friction will not only improve the slip-control braking performance, but also other systems throughout the vehicle, such as stability control systems, roll-over prevention systems and collision avoidance systems for autonomous driving.

Next to controller optimization, other wheel-based functions can be incorporated to obtain even better braking performance. These include brake gain estimation, brake capability monitoring and brake torque control.

The optimization method used in this thesis could be investigated further on or even replaced by one more efficient or accurate.

The simulations and test data were limited to straight-line braking and brake-in-turn maneuvers. To validate the model even further, other tests could be also devised and more data could be gathered. Examples of other tests could be steady state cornering, step steer test, or the standardized sine-with-dwell. Gathering more test data like air-usage and wheel normal loads could provide important information for better validation of the vehicle model.

Finally, with improved braking performance of the local brake controllers, also vehicle wide algorithms can be improved. Using peak friction for example, AEBS and ACC can be improved. Knowing the optimal slip, stability control could be improved. This again will lead to increased safety of the vehicle.

References

- [1] Changsun Ahn, Hwei Peng, and H Eric Tseng. Estimation of road friction for enhanced active safety systems: Algebraic approach. In *American Control Conference, 2009. ACC'09.*, pages 1104–1109. IEEE, 2009.
- [2] Changsun Ahn, Hwei Peng, and H Eric Tseng. Estimation of road friction for enhanced active safety systems: Dynamic approach. In *American Control Conference, 2009. ACC'09.*, pages 1110–1115. IEEE, 2009.
- [3] Anton Albinsson, Fredrik Bruzelius, Mats Jonasson, and Bengt Jacobson. Tire force estimation utilizing wheel torque measurements and validation in simulations and experiments. In *12th International Symposium on Advanced Vehicle Control (AVEC'14), Tokyo Japan*, pages 294–299, 2014.
- [4] Luis Alvarez, Jingang Yi, Roberto Horowitz, and Luis Olmos. Dynamic friction model-based tire-road friction estimation and emergency braking control. *Journal of dynamic systems, measurement, and control*, 127(1):22–32, 2005.
- [5] E Baker, L Nyborg, and H Pacejka. Tire modeling for use in vehicle dynamic studies. *Society of Automotive Engineers Paper# 870421*, 1987.
- [6] Egbert Bakker, Lars Nyborg, and Hans B Pacejka. Tyre modelling for use in vehicle dynamics studies. Technical report, SAE Technical Paper, 1987.
- [7] Egbert Bakker, Hans B Pacejka, and Lars Lidner. A new tire model with an application in vehicle dynamics studies. Technical report, SAE Technical Paper, 1989.
- [8] Horst Bauer. *Automotive handbook*. Society of Automotive Engineers, 2000.
- [9] Derek Bowman. Assessment of 'r' ratio on slwg surface. Technical report, MIRA Ltd, 2013.
- [10] Carlos Canudas-De-Wit and Roberto Horowitz. Observers for tire/road contact friction using only wheel angular velocity information. In *Decision and Control, 1999. Proceedings of the 38th IEEE Conference on*, volume 4, pages 3932–3937. IEEE, 1999.
- [11] Neal A Carlson. Fast triangular formulation of the square root filter. *AIAA journal*, 11(9):1259–1265, 1973.
- [12] Long Chen, Mingyuan Bian, Yugong Luo, and Keqiang Li. Real-time identification of the tyre-road friction coefficient using an unscented kalman filter and mean-square-error-weighted fusion. *Proceedings of the Institution of Mechanical Engineers, Part D: Journal of Automobile Engineering*, 230(6):788–802, 2016.
- [13] Wanki Cho, Jangyeol Yoon, Seongjin Yim, Bongyeong Koo, and Kyongsu Yi. Estimation of tire forces for application to vehicle stability control. *IEEE Transactions on Vehicular Technology*, 59(2):638–649, 2010.
- [14] Phil R Dahl. A solid friction model. Technical report, DTIC Document, 1968.
- [15] Phil R Dahl. Measurement of solid friction parameters of ball bearings. Technical report, DTIC Document, 1977.
- [16] C Canudas De Wit, Hans Olsson, Karl Johan Astrom, and Pablo Lischinsky. A new model for control of systems with friction. *IEEE Transactions on automatic control*, 40(3):419–425, 1995.
- [17] C Canudas De Wit and Panagiotis Tsiotras. Dynamic tire friction models for vehicle traction control. In *Decision and Control, 1999. Proceedings of the 38th IEEE Conference on*, volume 4, pages 3746–3751. IEEE, 1999.
- [18] A Dunn and R Hoover. Class 8 truck tractor braking performance improvement study. *Report, Department of Transportation, USA*, 2004.
- [19] B. Thorvald E. Wennerstroem, S. Nordmark. *Vehicle Dynamics*. KTH Royal Institute of Technology, KTH Vehicle Dynamics, Aeronautical and Vehicle Engineering, Stockholm 2011.

- [20] Economic Commission for Europe of the United Nations (UN/ECE). *Uniform provisions concerning the approval of vehicles of categories M, N and O with regards to braking [2016/194]*, regulation no 13 edition, 2015.
- [21] Okwuchi Chigoziri Emereole. *Antilock performance comparison between hydraulic and electromechanical brake systems*. University of Melbourne, Department of Mechanical and Manufacturing Engineering, 2004.
- [22] Paul S Fancher. Generic data for representing truck tire characteristics in simulations of braking and braking-in-a-turn maneuvers. Technical report, 1995.
- [23] PS Fancher. Integrating anti-lock braking systems with the directional control properties of heavy trucks. *Anti-Lock Braking Systems for Road Vehicles.—London: IMechE.—1985*, 1985.
- [24] Brian Feeny, Ardshir Guran, Nikolaus Hinrichs, and Karl Popp. A historical review on dry friction and stick-slip phenomena. *Applied Mechanics Reviews*, 51:321–342, 1998.
- [25] Garrick Forkenbrock, Mark Flick, and W Riley Garrott. A comprehensive light vehicle antilock brake system test track performance evaluation. Technical report, SAE Technical Paper, 1999.
- [26] J Fox, R Roberts, C Baier-Welt, Lok Man Ho, L Lacraru, and B Gombert. Modeling and control of a single motor electronic wedge brake. Technical report, SAE Technical Paper, 2007.
- [27] Tom French. *Tyre technology*. 1989.
- [28] R Garrott and A Dunn. Nhtsa research efforts to significantly improve braking performance of medium and heavy trucks. In *20th international technical conference on the enhanced safety of vehicles conference*, 2007.
- [29] Fredrik Gustafsson. Slip-based tire-road friction estimation. *Automatica*, 33(6):1087–1099, 1997.
- [30] Fredrik Gustafsson and Fredrik Gustafsson. *Adaptive filtering and change detection*, volume 1. Citeseer, 2000.
- [31] MSA Hardy and D Cebon. An investigation of anti-lock braking systems for heavy goods vehicles. *Cambridge University Engineering Department*, 1995.
- [32] Leon Henderson. *Improving emergency braking performance of heavy goods vehicles*. PhD thesis, University of Cambridge, 2014.
- [33] Leon Henderson and David Cebon. Full-scale testing of a novel slip control braking system for heavy vehicles. *Proceedings of the Institution of Mechanical Engineers, Part D: Journal of Automobile Engineering*, 230(9):1221–1238, 2016.
- [34] Leon Henderson, David Cebon, and Leo Laine. Brake system design for future heavy goods vehicles. In *International Symposium on Heavy Vehicle Transport Technology (HVTT14)*, 2016.
- [35] Lok Man Ho, Richard Roberts, Henry Hartmann, and Bernd Gombert. The electronic wedge brake-ewb. Technical report, SAE Technical Paper, 2006.
- [36] Tesheng Hsiao, Nien-Chi Liu, and Syuan-Yi Chen. Robust estimation of the friction forces generated by each tire of a vehicle. In *American Control Conference (ACC), 2011*, pages 5261–5266. IEEE, 2011.
- [37] Jessica S Jermakian. Crash avoidance potential of four large truck technologies. *Accident Analysis & Prevention*, 49:338–346, 2012.
- [38] Fangjun Jiang and Zhiqiang Gao. An application of nonlinear pid control to a class of truck abs problems. In *Decision and Control, 2001. Proceedings of the 40th IEEE Conference on*, volume 1, pages 516–521. IEEE, 2001.
- [39] Thomas Kailath, Ali H Sayed, and Babak Hassibi. *Linear estimation*, volume 1. Prentice Hall Upper Saddle River, NJ, 2000.
- [40] Uwe Kiencke and Lars Nielsen. *Automotive control systems*, volume 2. Springer, 2005.

- [41] FW Kienhöfer and D Cebon. An investigation of abs strategies for articulated vehicles. In *Proc. of the 8th International Symposium on Heavy Vehicle Weights and Dimensions, Misty Hills Conference Centre, Gauteng, South Africa*, pages 1–15, 2004.
- [42] FW Kienhöfer and D Cebon. Improving abs on heavy vehicles using slip control. In *Proceedings of the 9th international symposium on heavy vehicle weights and dimensions*, pages 892–903, 2006.
- [43] Emir Kutluay and Hermann Winner. Validation of vehicle dynamics simulation models—a review. *Vehicle System Dynamics*, 52(2):186–200, 2014.
- [44] Jon Lawes. *jon lawes Car Brakes: A Guide to Upgrading, Repair and Maintenance*.
- [45] Chankyu Lee, Karl Hedrick, and Kyongsu Yi. Real-time slip-based estimation of maximum tire-road friction coefficient. *IEEE/ASME Transactions on mechatronics*, 9(2):454–458, 2004.
- [46] Li Li, Fei-Yue Wang, and Qunzhi Zhou. Integrated longitudinal and lateral tire/road friction modeling and monitoring for vehicle motion control. *IEEE Transactions on intelligent transportation systems*, 7(1):1–19, 2006.
- [47] Lennart Ljung. *System identification*. Wiley Online Library, 1999.
- [48] Anil Kunnappillil Madhusudhanan, Matteo Corno, Mustafa Ali Arat, and Edward Holweg. Load sensing bearing based road-tyre friction estimation considering combined tyre slip. *Mechatronics*, 39:136–146, 2016.
- [49] Anil Kunnappillil Madhusudhanan, Matteo Corno, and Edward Holweg. Vehicle yaw rate control using tyre force measurements. In *Control Conference (ECC), 2015 European*, pages 2577–2582. IEEE, 2015.
- [50] JI Miller, FW Kienhofer, and David Cebon. Design concept for an alternative heavy vehicle slip control brake actuator. In *Proc. of the 10th International Symposium on Heavy Vehicle Transport Technology, ENPC, Marne-la-Vallee, France*, pages 429–442, 2008.
- [51] Jonathan I Miller. *Advanced braking systems for heavy vehicles*. PhD thesis, University of Cambridge, 2010.
- [52] Jonathan I Miller and David Cebon. A high performance pneumatic braking system for heavy vehicles. *Vehicle System Dynamics*, 48(S1):373–392, 2010.
- [53] Jonathan I Miller and David Cebon. An investigation of the effects of pneumatic actuator design on slip control for heavy vehicles. *Vehicle System Dynamics*, 51(1):139–164, 2013.
- [54] Jonathan I Miller, Leon M Henderson, and David Cebon. Designing and testing an advanced pneumatic braking system for heavy vehicles. *Proceedings of the Institution of Mechanical Engineers, Part C: Journal of mechanical engineering science*, 227(8):1715–1729, 2013.
- [55] Desmond F Moore. The friction of pneumatic tyres. 1975.
- [56] Steffen Müller, Michael Uchanski, and Karl Hedrick. Slip-based tire-road friction estimation during braking. In *Proceedings of 2001 ASME International Mechanical Engineering Congress and Exposition*, pages 213–220, 2001.
- [57] National Highway Traffic Safety Administration, Washington. *Light Vehicle Brake Systems*, laboratory test procedure for fmvs 135 edition, 2005.
- [58] Malcolm James Nunney. *Light and heavy vehicle technology*. Newnes, 2013.
- [59] U.S. Department of Transportation. Traffic safety facts 2014, 2014.
- [60] U.S. Department of Transportation. Freight facts and figures, 2015.
- [61] OICA. Vehicles in use. <http://www.oica.net/category/vehicles-in-use/>, 2017.
- [62] Hans B Pacejka and Robin S Sharp. Shear force development by pneumatic tyres in steady state conditions: a review of modelling aspects. *Vehicle system dynamics*, 20(3-4):121–175, 1991.

- [63] JAKUB PROKEŠ. Realtime estimation of tyre-road friction for vehicle state estimator.
- [64] D Radlinski. Mechanics of heavy duty truck systems course notes—braking capabilities of heavy-duty trucks. *UMTRI Course on Heavy Vehicle Systems, Cambridge University Engineering Department, Cambridge, UK*, 2007.
- [65] Rajesh Rajamani. *Vehicle dynamics and control*. Springer Science & Business Media, 2011.
- [66] Rajesh Rajamani, Gridsada Phanomchoeng, Damrongrit Piyabongkarn, and Jae Y Lew. Algorithms for real-time estimation of individual wheel tire-road friction coefficients. *IEEE/ASME Transactions on Mechatronics*, 17(6):1183–1195, 2012.
- [67] Laura R Ray. Nonlinear tire force estimation and road friction identification: Simulation and experiments. *Automatica*, 33(10):1819–1833, 1997.
- [68] Shankar Sastry and Marc Bodson. *Adaptive control: stability, convergence and robustness*. Courier Corporation, 2011.
- [69] Jean-Jacques E Slotine, Weiping Li, et al. *Applied nonlinear control*, volume 199. prentice-Hall Englewood Cliffs, NJ, 1991.
- [70] Jacob Svendenius. Tire modeling and friction estimation. *PhD Theses*, 2007.
- [71] Michael Uchanski, Karl Hedrick, et al. Estimation of the maximum tire-road friction coefficient. *Journal of Dynamic System, Measurement, and Control*, 125(12):607–617, 2003.
- [72] Tom van den Boom and Bart de Schutter. *Optimization in systems and control*. MicroWeb Edu, 2015.
- [73] Junmin Wang, Lee Alexander, and Rajesh Rajamani. Friction estimation on highway vehicles using longitudinal measurements. *Journal of dynamic systems, measurement, and control*, 126(2):265–275, 2004.
- [74] R. Wescott. New hgv braking could save lives with quicker stops. <http://www.bbc.com/news/business-32845386>, BBC, May 2015.
- [75] Jo Yung Wong. *Theory of ground vehicles*. John Wiley & Sons, 2008.
- [76] Jingang Yi, Luis Alvarez, Xavier Claeys, and Roberto Horowitz. Emergency braking control with an observer-based dynamic tire/road friction model and wheel angular velocity measurement. *Vehicle system dynamics*, 39(2):81–97, 2003.

A Vehicle Parameters

The public version of the report does not have this data available.

B Model Modifications

The public version of the report does not have this data available.

C Parameter Changes

The public version of the report does not have this data available.

D Friction Estimation

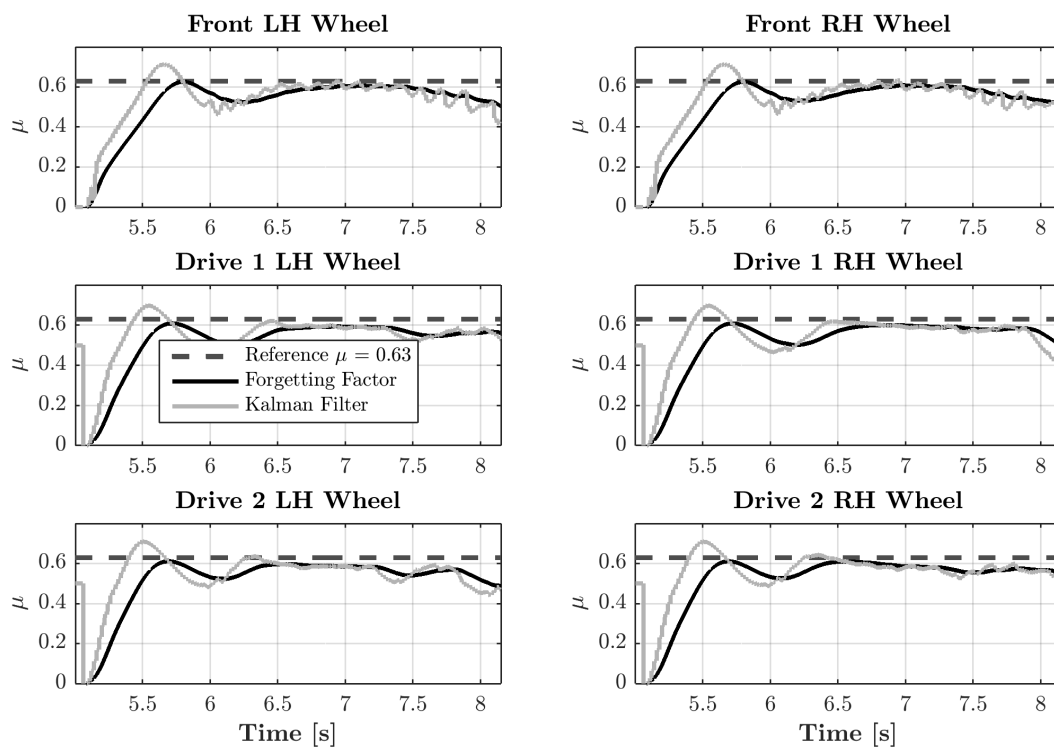


Figure D.1: Friction coefficient estimation of all wheels of the validated model on dry asphalt

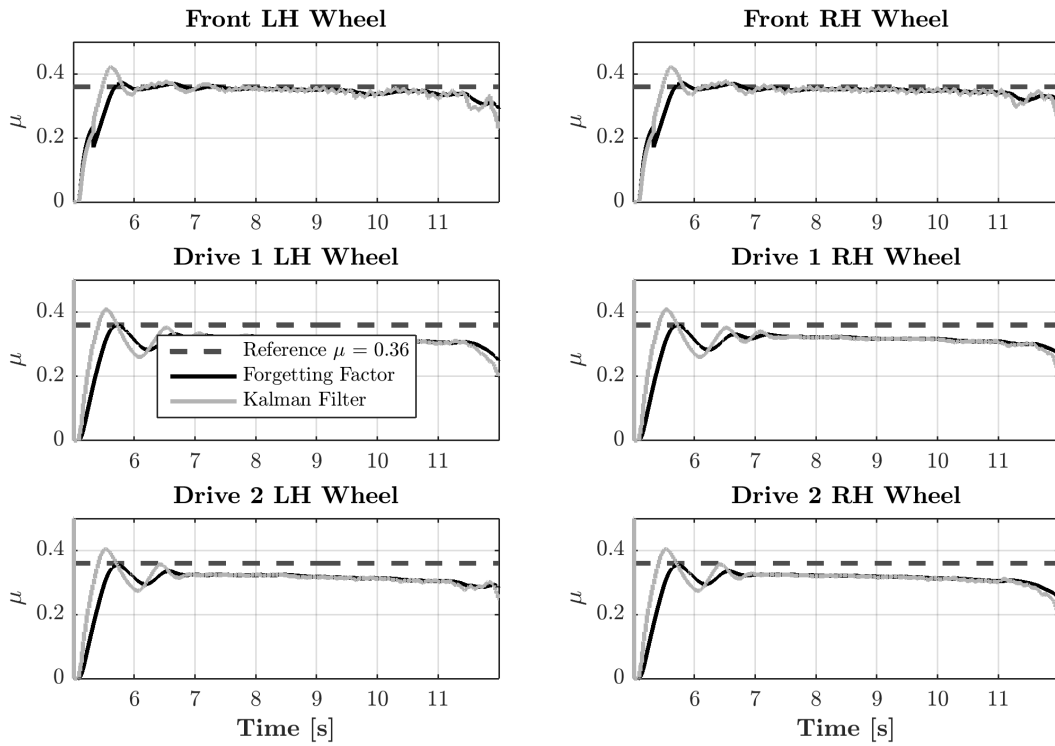


Figure D.2: Friction coefficient estimation of all wheels of the validated model on packed snow

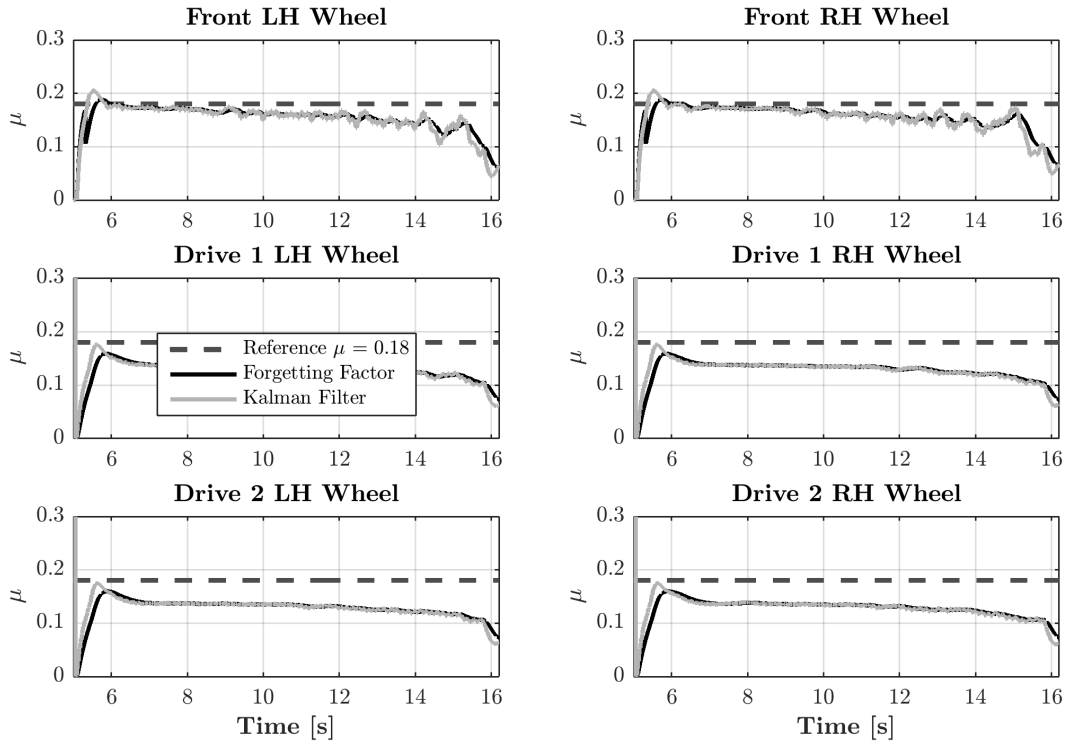


Figure D.3: Friction coefficient estimation of wheels of the validated model on polished ice

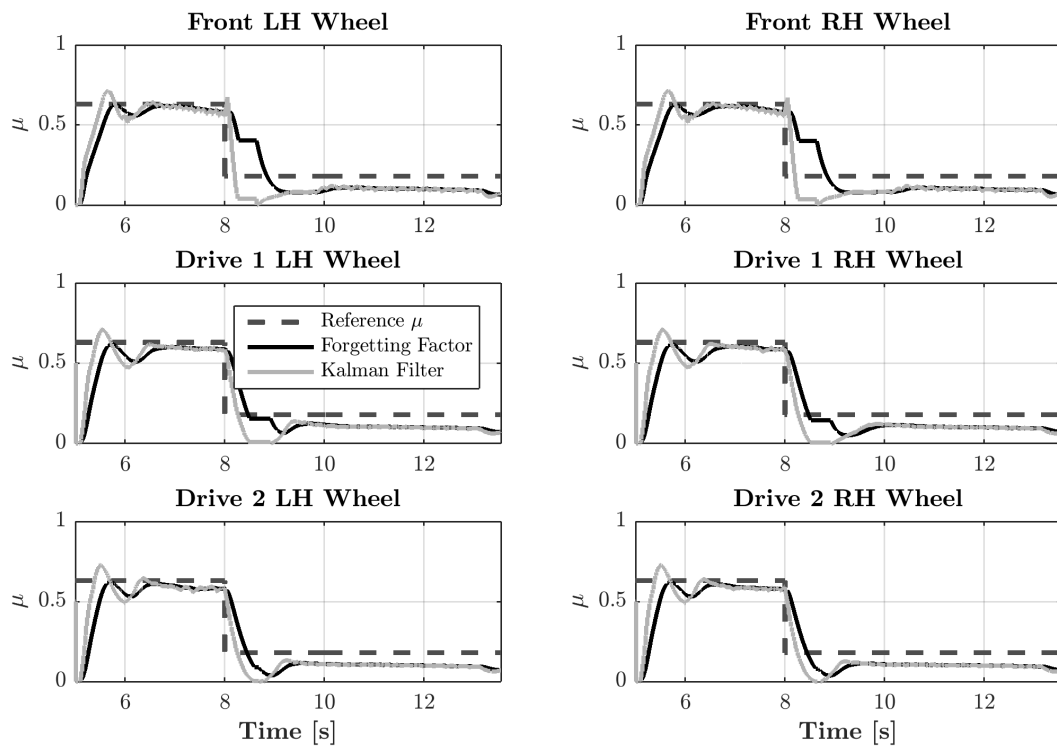


Figure D.4: Friction coefficient estimation of all wheels of the validated model from dry asphalt to polished ice

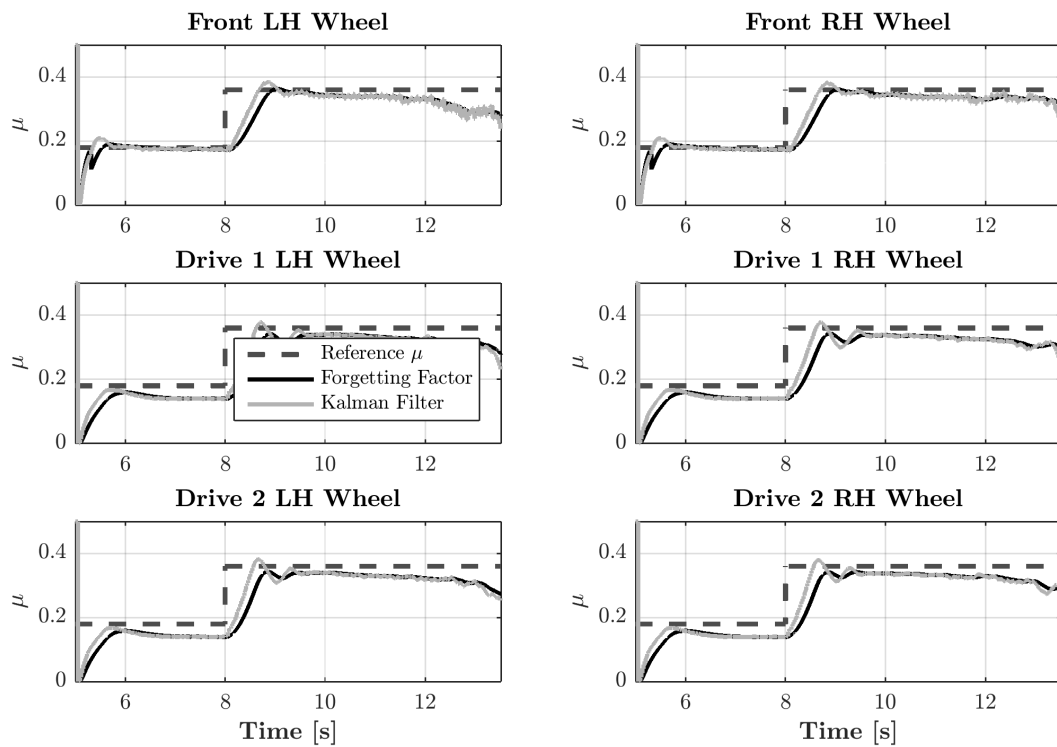


Figure D.5: Friction coefficient estimation of all wheels of the validated model from polished ice to packed snow

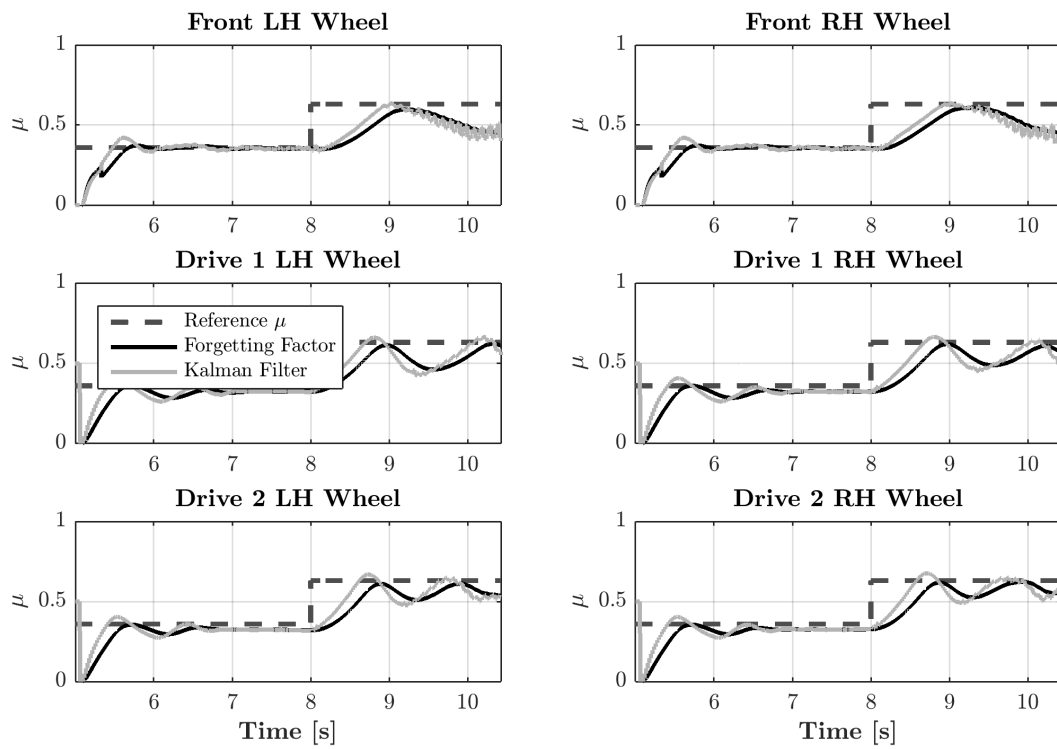


Figure D.6: Friction coefficient estimation of all wheels of the validated model from packed snow to dry asphalt

E Vehicle Testing Addendum

The last part of the thesis consisted of testing the developed functions on a test vehicle. The test vehicle has a prototype FABV installed at each wheel, controlled by an individual ECU. These individual ECUs are controlled by a central dSPACE Autobox ECU.

The first step of implementing the functions on the ECU was converting the developed function in MATLAB and Simulink to C-code which can be compiled for execution on the ECU. Via Matlab's auto-code generation, the necessary C-files could be created with ease.

The next step consisted of testing the input and output of the ECU. To reach this goal, the CAN communication protocol is used to send the ECU the required information and receive the ECU's output. Side by side simulations in Simulink showed that the output of the ECU corresponded to that of the previously created models.

The final step of preparations was setting up dSPACE to communicate with the respective ECUs via the Autobox. Now, during the experiment, parameter changes could be easily made at the ECU. Figure E.1 gives a graphical representation of the method.

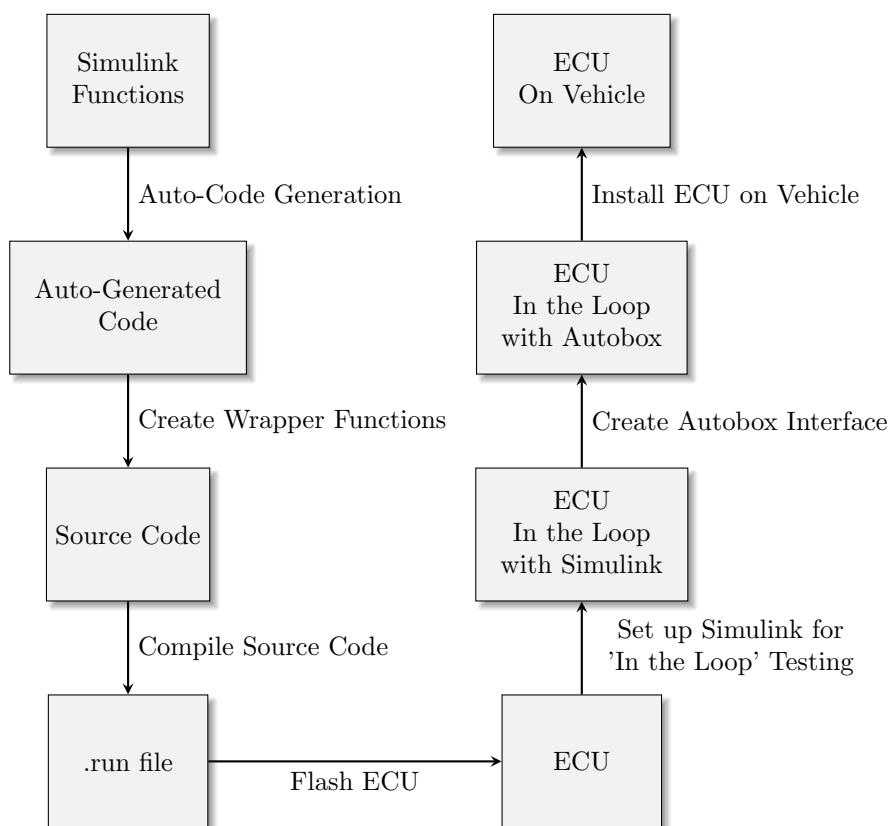


Figure E.1: Graphical representation of the method for testing the developed functions in Simulink on the ECU at vehicle wheel base.

The two functions that were tested on the ECU were the friction estimation algorithm and the adaptive reference slip algorithm. The ECU updated with the two functions was mounted on the drive-1 axle of the 8x4 Volvo truck on the left hand side. Hence, only results of the left hand wheel of the drive-1 axle are going to be presented.

Tests were performed at the Volvo test track in Hällered, Sweden. The friction coefficient of this test track, when it comes to the wet basalt surface, had been estimated to be approximately 0.13 [9] The tests consisted of:

- Hard braking on wet basalt
- Mild braking on wet basalt
- Hard braking from wet basalt to dry asphalt
- Hard braking from dry asphalt to wet basalt

E.1 Results

The first test which was carried out with the vehicle was straight-line hard braking on wet basalt from 60-0 km/h. Plots of longitudinal and wheel speed, estimated friction coefficient and wheel slip are illustrated in the figure below.

In Figure E.2 it can be seen that when the vehicle starts to brake (almost when $t = 21s$), then the friction estimation algorithm start to work. More specifically, on the wet basalt the friction estimation algorithm seems to have fast response and after two seconds it is able to predict a reasonable value of the friction coefficient.

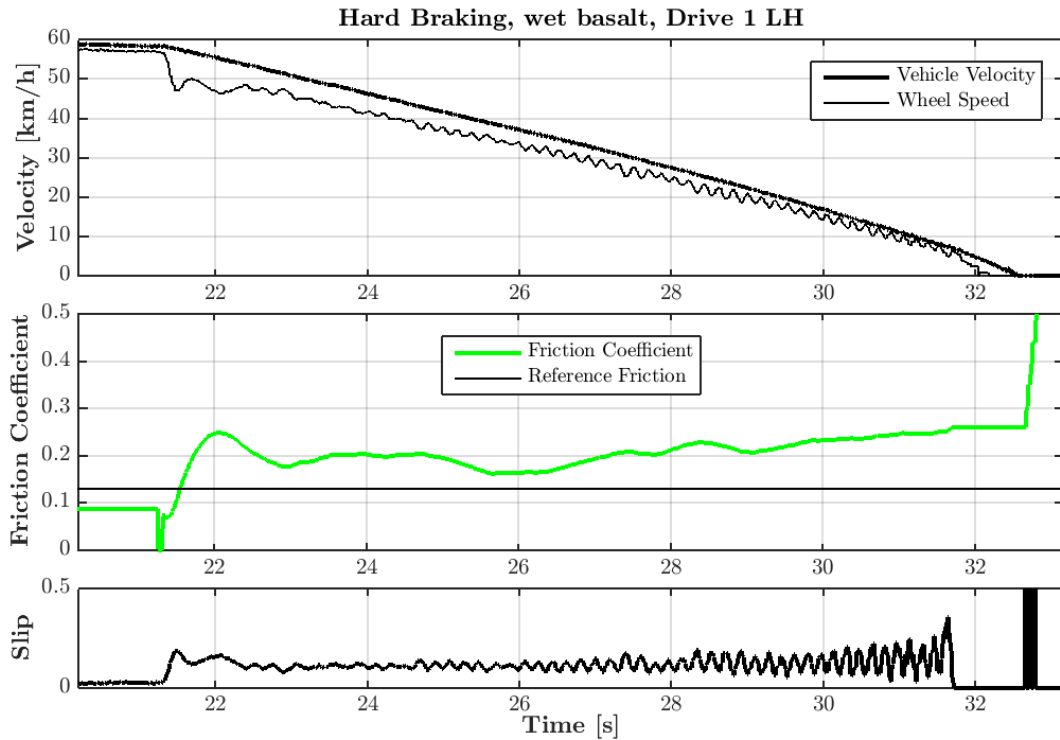


Figure E.2: In the top plot of the figure the longitudinal vehicle speed and wheel speed of the left hand wheel of the drive-1 axle are presented. In the second plot of the figure the estimated friction coefficient, along with the reference friction coefficient are illustrated. In the third plot of the figure it is depicted the longitudinal wheel slip of the the left hand wheel of the drive-1 axle.

The second test which was carried out with the vehicle was straight-line mild braking (brake pressure was set to be 1.2 bar) on wet basalt from 38-0 km/h. Plots of longitudinal and wheel speed, estimated friction coefficient and wheel slip are illustrated in the figure below.

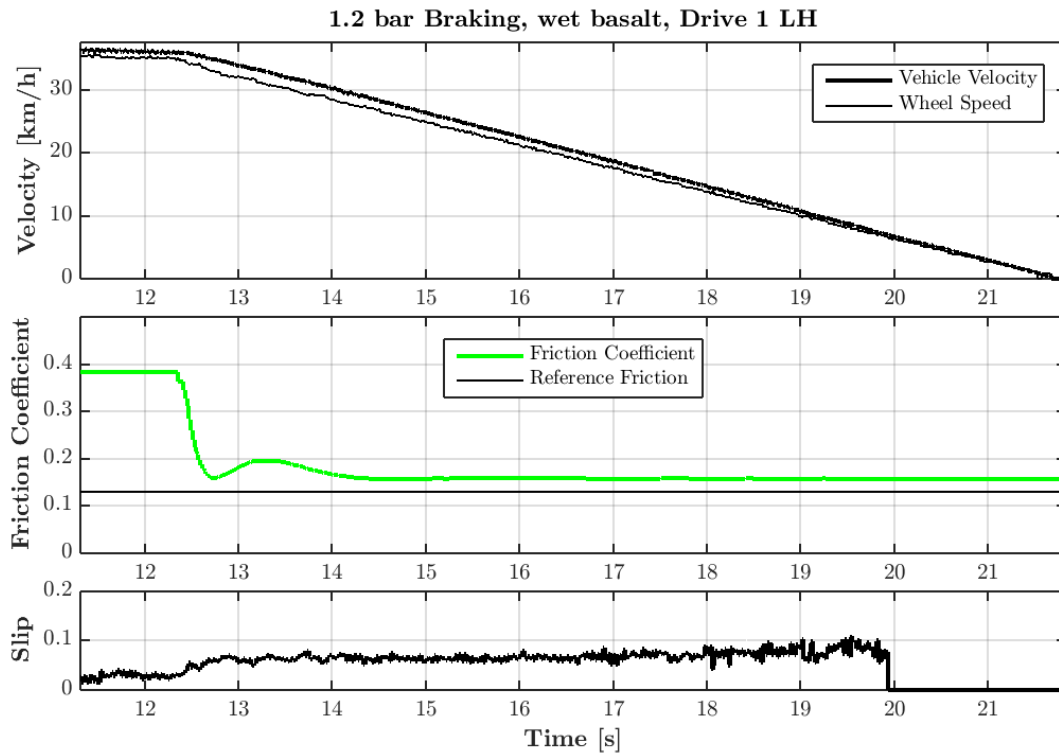


Figure E.3: In the top plot of the figure the longitudinal vehicle speed and wheel speed of the left hand wheel of the drive-1 axle are presented. In the second plot of the figure the estimated friction coefficient, along with the reference friction coefficient are illustrated. In the third plot of the figure it is depicted the longitudinal wheel slip of the the left hand wheel of the drive-1 axle.

In Figure E.3 it can be seen that when the vehicle starts to brake (almost when $t = 12.5s$), then the friction estimation algorithm start to work. More specifically, the friction estimation algorithm on wet basalt seems to have fast response and after one and a half seconds it is able to predict a reasonable value of the friction coefficient. The interesting part on this kind of test is that the friction estimation algorithm works properly and produces reasonable friction coefficient values, even when the brake pressure is not that high.

The third test which was carried out with the vehicle was straight-line hard braking on wet basalt from 39-0 km/h. In this test, apart from the operation of the friction estimation algorithm, also the performance of the reference slip signal algorithm (lookup table) was examined, according to the kind of surface that the vehicle is braking on. The initial implementation of the lookup table provided a too low reference slip value. Using global control, an increased reference slip signal using the lookup table was sent to the ECU of the brake valve of the drive-1 axle on the left-hand wheel. Plots of longitudinal and wheel speed, estimated friction coefficient, wheel slip and adaptive reference slip signal are illustrated in the figure below.

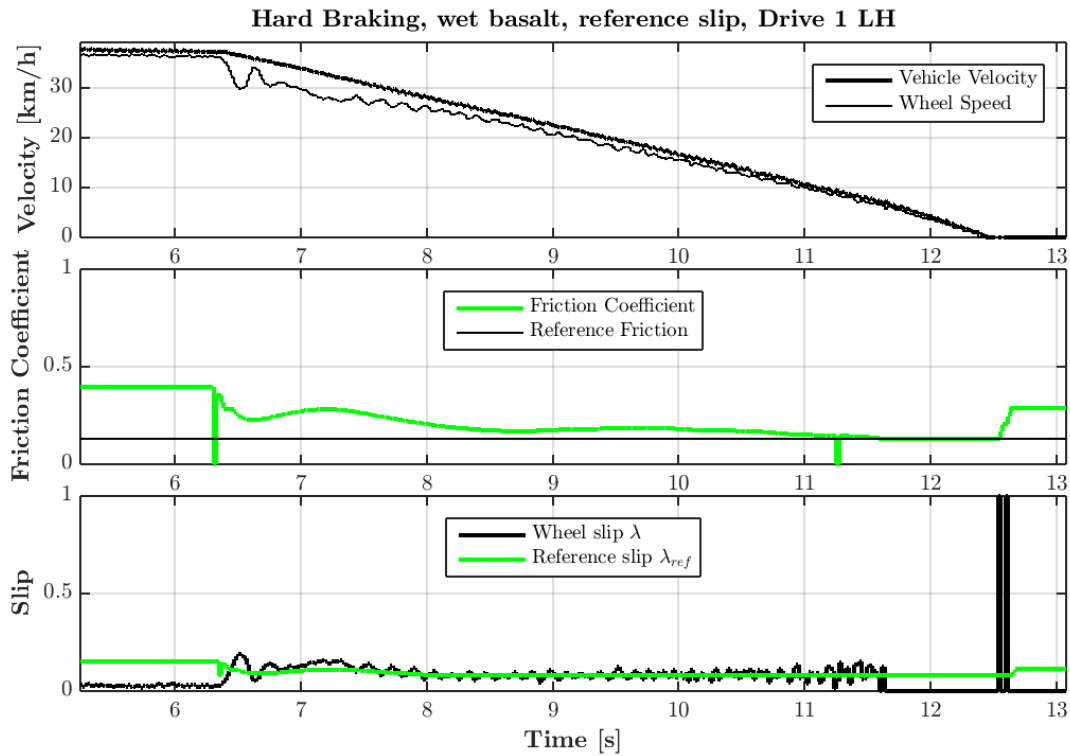


Figure E.4: In the top plot of the figure the longitudinal vehicle speed and wheel speed of the left hand wheel of the drive-1 axle are presented. In the second plot of the figure the estimated friction coefficient, along with the reference friction coefficient are illustrated. In the third plot of the figure both the longitudinal wheel slip of the the left hand wheel of the drive-1 axle and the corresponding adaptive reference slip signal are depicted.

In Figure E.4 it can be seen that when the vehicle starts to brake (almost when $t = 6.5s$), then the friction estimation algorithm start to work. More specifically, the friction estimation algorithm seems to have fast response and after one and a half seconds it is able to predict a reasonable value of the friction coefficient. In the last plot of this figure the performance of the adaptive reference slip signal can be seen. The linear connection between the friction estimation algorithm and the adaptive reference slip signal algorithm is clearly illustrated in this figure, observing the general trend of these two signals. In addition, by looking at the last plot of this figure, it can be seen that the wheel slip follows the adaptive reference slip signal properly.

The fourth test which was carried out with the vehicle was straight-line hard braking from wet basalt to dry asphalt from 50-0 km/h. In this test, apart of the operation of the friction estimation algorithm, and the performance of the reference slip signal algorithm, also the ability of the friction estimation algorithm to estimate the friction coefficient was examined for a changing friction surface. Plots of longitudinal and wheel speed, estimated friction coefficient, wheel slip and adaptive reference slip signal are illustrated in the figure below.

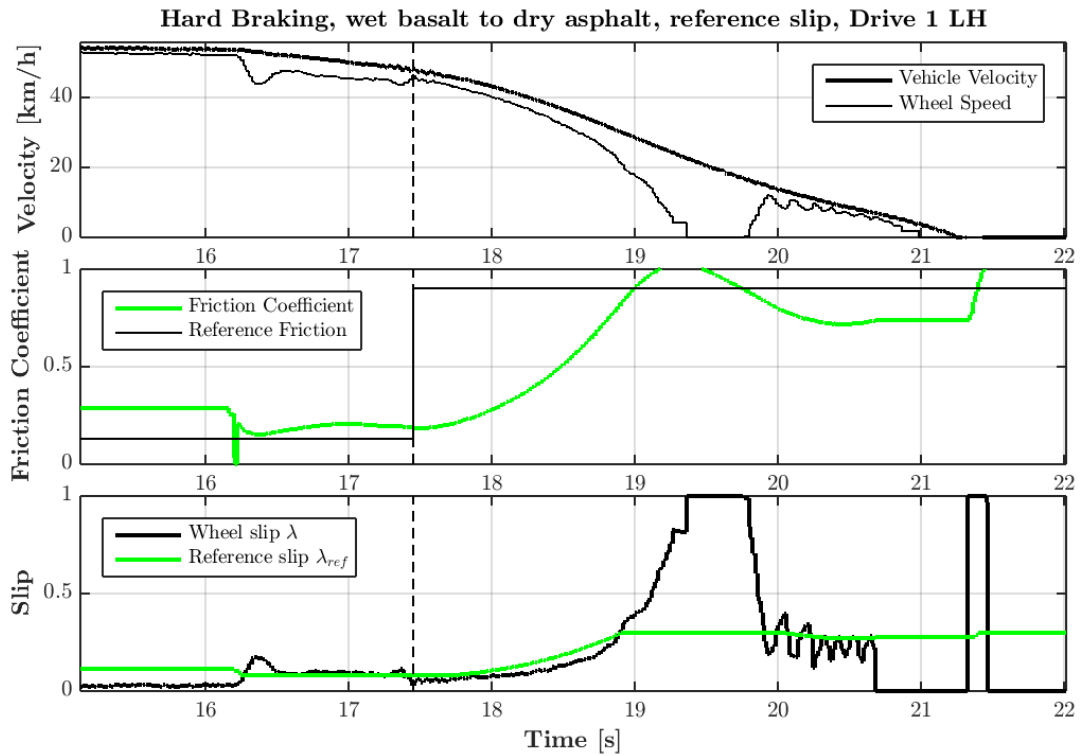


Figure E.5: In the top plot of the figure the longitudinal vehicle speed and wheel speed of the left hand wheel of the drive-1 axle, along with the point of changing of the friction surface (dashed line), are presented. In the second plot of the figure the estimated friction coefficient, along with the reference friction coefficient are illustrated. In the third plot of the figure both the longitudinal wheel slip of the the left hand wheel of the drive-1 axle and the corresponding adaptive reference slip signal, along with the point of changing of the friction surface (dashed line), are depicted.

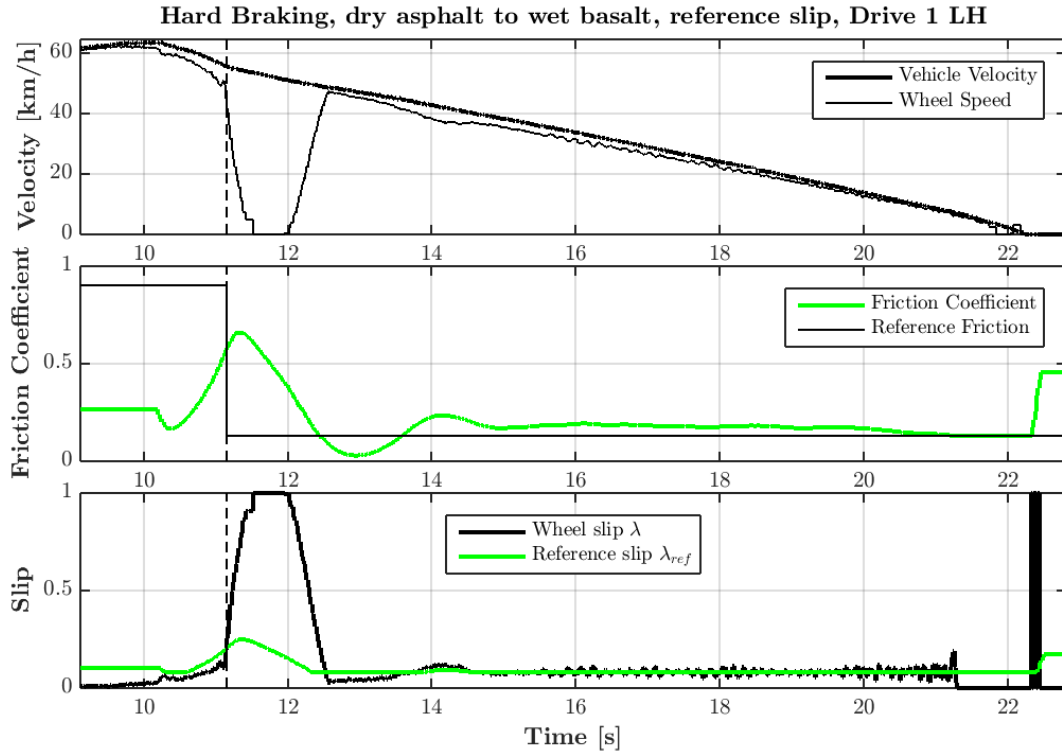


Figure E.6: In the top plot of the figure the longitudinal vehicle speed and wheel speed of the left hand wheel of the drive-1 axle, along with the point of changing of the friction surface (dashed line), are presented. In the second plot of the figure the estimated friction coefficient, along with the reference friction coefficient are illustrated. In the third plot of the figure both the longitudinal wheel slip of the the left hand wheel of the drive-1 axle and the corresponding adaptive reference slip signal, along with the point of changing of the friction surface (dashed line), are depicted.

In Figure E.5, it can be seen that the vehicle starts to brake from 50 km/h on wet basalt at almost $t = 16.5s$. The vehicle continues to brake and after one second (i.e. when $t = 17.5s$), the surface changes from wet basalt to dry asphalt. At $t = 19.5s$ a wheel lock can be observed. The friction coefficient algorithm is able to give reasonable friction coefficient estimate on wet basalt. The same also holds for the estimated friction coefficient on dry asphalt. However, the algorithm can track the change on the friction surface and give a reasonable estimate after three seconds.

Figure E.6 shows the opposite situation where braking occurs on asphalt first and then on the wet basalt. Braking starts at roughly $t = 10s$, and very quickly the surface changes, at $t = 11s$. The friction estimation algorithm tries to estimate the level of friction coefficient for the dry asphalt, but before it is able to do so, the change to wet basalt has been made. Again, after three seconds from changing the surface, the friction coefficient on wet basalt is estimated correctly.

This slow response of the friction estimation algorithm, as well as the wheel lock that occurs at $t = 19.5s$ for Figure E.5 and $t = 11s$ for Figure E.6 can be caused due to the controller gains of the sliding mode controller. More specifically, the controller gains that were used on this test were the ones of the wet basalt surface, which are less aggressive than the correspondent ones of the dry asphalt surface. Also, the pole placement of the force observer was set to be not too aggressive. More aggressive pole placement could lead to faster response of the longitudinal force observer, increasing the response of the friction estimation. In the last plot of this figure, it can be seen that the reference slip signal is dependent on the estimated friction coefficient, and hence on the surface that the vehicle is braking on. Therefore, even the wheel slip is able to follow the adaptive reference slip signal according to the surface on which the vehicle is braking. After $t = 19s$ the wheel slip cannot follow the reference slip signal due to lower controller gains, and hence it is increasing up to one, where the wheel lock occurs.

E.2 Discussion and Conclusion

To conclude, the complete vehicle testing showed that the friction estimation algorithm works properly independent of the kind of surface that the vehicle is braking on. However, where in the simulation convergence only took around 1 second, in real life this was closer to three seconds. The importance of having good force signals as inputs to the friction estimator block shows to be of paramount importance. More specifically, the estimation of the friction coefficient on surfaces with low friction is more precise and stable in comparison with the correspondent one on surfaces with high friction. This estimation depends a lot on the trend of longitudinal and normal forces, where in high friction surfaces the changes of these forces are more severe in comparison with the correspondent ones on surfaces with low friction. Hence, on surfaces with low friction, the predictability of the friction estimation algorithm is better without better information about the load transfer. Another important aspect is the adaptability of the reference slip signal according to the surface which the vehicle is braking on. The linear relationship between the friction coefficient and the reference slip signal can influence the performance of the sliding mode controller, in terms of better braking distance and/or better air usage, as it was showed on this thesis project.

The only function not tested during the vehicle testing is the switching gain optimization, as this would require a large number of consecutive runs. Testing this function will be needed to confirm the conclusions made in this report based on the results obtained with the simulations.